2012

FINITE ELEMENT ANALYSIS OF THE CONTACT DEFORMATION OF PIEZOELECTRIC MATERIALS

Ming Liu
University of Kentucky, mingliuUK@gmail.com

STUDENT AGREEMENT:

I represent that my thesis or dissertation and abstract are my original work. Proper attribution has been given to all outside sources. I understand that I am solely responsible for obtaining any needed copyright permissions. I have obtained and attached hereto needed written permission statements(s) from the owner(s) of each third-party copyrighted matter to be included in my work, allowing electronic distribution (if such use is not permitted by the fair use doctrine).

I hereby grant to The University of Kentucky and its agents the non-exclusive license to archive and make accessible my work in whole or in part in all forms of media, now or hereafter known. I agree that the document mentioned above may be made available immediately for worldwide access unless a preapproved embargo applies.

I retain all other ownership rights to the copyright of my work. I also retain the right to use in future works (such as articles or books) all or part of my work. I understand that I am free to register the copyright to my work.

REVIEW, APPROVAL AND ACCEPTANCE

The document mentioned above has been reviewed and accepted by the student's advisor, on behalf of the advisory committee, and by the Director of Graduate Studies (DGS), on behalf of the program; we verify that this is the final, approved version of the student's dissertation including all changes required by the advisory committee. The undersigned agree to abide by the statements above.

Ming Liu, Student

Dr. Fuqian Yang, Major Professor

Dr. Fuqian Yang, Director of Graduate Studies

FINITE ELEMENT ANALYSIS OF THE CONTACT DEFORMATION OF PIEZOELECTRIC MATERIALS

DISSERTATION

A dissertation submitted in partial fulfillment of the requirements for the degree of Doctor of Philosophy in the College of Engineering at the University of Kentucky

By
Ming Liu

Lexington, Kentucky

Director: Dr. Fuqian Yang, Professor of Materials Engineering, University of Kentucky, Lexington, Kentucky

2012

ABSTRACT OF DISSERTATION

FINITE ELEMENT ANALYSIS OF THE CONTACT DEFORMATION OF PIEZOELECTRIC MATERIALS

Piezoelectric materials in the forms of both bulk and thin-film have been widely used as actuators and sensors due to their electromechanical coupling. The characterization of piezoelectric materials plays an important role in determining device performance and reliability. Instrumented indentation is a promising method for probing mechanical as well as electrical properties of piezoelectric materials.

The use of instrumented indentation to characterize the properties of piezoelectric materials requires analytical relations. Finite element methods are used to analyze the indentation of piezoelectric materials under different mechanical and electrical boundary conditions.

For indentation of a piezoelectric half space, a three-dimensional finite element model is used due to the anisotropy and geometric nonlinearity. The analysis is focused on the effect of angle between poling direction and indentation-loading direction on indentation responses.

For the indentation by a flat-ended cylindrical indenter, both insulating indenter and conducting indenter without a prescribed electric potential are considered. The results reveal that both the indentation load and the magnitude of the indentation-induced potential at the contact center increase linearly with the indentation depth.

For the indentation by an insulating Berkovich indenter, both frictionless and frictional contact between the indenter and indented surface are considered. The results show the indentation load is proportional to the square of the indentation depth, while the indentation-induced potential at the contact center is proportional to the indentation depth.

Spherical indentation of piezoelectric thin films is analyzed in an axisymmetric finite element model, in which the poling direction is anti-parallel to the indentation-loading direction.

Six different combinations of electrical boundary conditions are considered for a thin film perfectly bonded to a rigid substrate under the condition of the contact radius being much larger than the film thickness. The indentation load is found to be proportional to the square of the indentation depth.

To analyze the decohesion problem between a piezoelectric film and an elastic substrate, a traction-separation law is used to control the interfacial behavior between a thin film and an electrically grounded elastic substrate. The discontinuous responses at the initiation of interfacial decohesion are found to depend on interface and substrate properties.

KEYWORDS: Indentation, Anisotropy, Piezoelectric Materials, Finite Element Analysis, Mechanical and Electrical Boundary Conditions

Ming Liu

Student's Signature

12/12/2012

Date

FINITE ELEMENT ANALYSIS OF THE CONTACT DEFORMATION OF PIEZOELECTRIC MATERIALS

By

Ming Liu

Dr. Fuqian Yang

Director of Dissertation

Dr. Fuqian Yang

Director of Graduate Studies

12/12/2012

This dissertation is lovingly dedicated to my parents, Yongde Liu (father) and Guiling Tian (mother), for making it possible to embark on this journey. Their support, encouragement, and constant love have sustained me throughout my life.

ACKNOWLEDGEMENTS

I am most grateful to the members of my committee, Dr. Fuqian Yang, Dr. Yang-Tse Cheng, Dr. Thomas John Balk, and Dr. Haluk Ersin Karaca, and my outside examiner Dr. Changyou Wang, for their time, inspiration, and expertise throughout my doctoral research. Special thanks to my supervisor Dr. Fuqian Yang, to whom I am deeply indebted, for his perseverance as a graduate advisor, his enlightenment when doing research, his exquisite attention to detail, his demand for excellence, his guidance in preparing me as a researcher, and the invaluable hours he spent in revising my writings, which have enabled me to complete my doctoral study and dissertation effectively.

My deepest gratitude is to my parents, whose unselfish devotion has nourished and kept me healthy and strong, whose unwavering support has helped me overcome many crisis situations, whose constant encouragement has stimulated my future efforts, and whose never-ending love always gives me strength and hope. I owe every achievement of mine to my parents, who form the rock and origin of my happiness.

My gratitude also goes to my instructors: Dr. Yang-Tse Cheng, Dr. Thomas John Balk, Dr. Tongguang (Tony) Zhai, Dr. Bruce J. Hinds, Dr. Matthew J. Beck, Dr. Richard E. Eitel, Dr. Jimmie Joe Cathey, and Dr. Ingrid St. Omer for their teachings and the high quality scholarship, to which I aspire. I would also like to thank Bruce Cole, Chelsea Hansing, Nancy Miller, Ge Zhang, Vikram Gazula, Jerry Grooms, Krishna Prabhala, Adam Jundt, Guangfeng Zhao and Ding Li for their assistant during my doctoral study.

TABLE OF CONTENTS

LIST OF TABLES

LIST OF FIGURES

Chapter - 1 Motivation and summary

1.1 Introduction

Piezoelectric materials are functional materials with mechanical and electrical coupling, and they are extensively used as actuators and sensors in many branches of modern technologies (e.g., aerospace, automotive, medical, and electronic industries). Measurement of piezoelectric materials including both mechanical and electrical properties is vital for their performance assessment and reliability prediction. Lack of easy and inexpensive means of the characterization of mass-produced piezoelectric materials adds largely to their production cost [1]. In addition, piezoelectric actuators, sensors, and other piezoelectric components are generally in either bulk forms or thin-film forms (e.g., thin films, beams, and plates), and become smaller due to the increasing miniaturization in the microelectromechanical systems (MEMS) [1, 2]. Characterization of piezoelectric materials, especially in small volumes, is a challenge, while there is an increasing need for probing material properties of piezoelectric materials of small volume [3].

Indentation techniques including micro- and nano-indentation (of high-resolution ~ 3-10 nm [4]) are especially suitable for characterizing materials of small volume at micro- and nano-length scales, and can be the only method in many cases [1]. Measurement of piezoelectric coefficients, especially for thin films, with high accuracy is challenging [5,6]. Instrumented indentation, in which indentation load and displacement can be measured simultaneously, offers a powerful tool for the characterization of brittle materials such as piezoelectric materials. It has been recognized that the indentation response of piezoelectric materials can be used to characterize the properties of piezoelectric materials [6]. Moreover, the contact loading during indentation provides a viable and attractive method for investigating the contact behavior of piezoelectric materials, which plays an important role in the functional behaviors of piezoelectric

materials, since piezoelectric components are prone to contact in applications such as random access memory, and actuators that control structural deformation.

In spite of simplicity and the ease of use of the indentation test, deciphering indentation results is nontrivial due to the non-uniform distributions of stress and strain beneath the indenter, and gets even more complicated for piezoelectric materials due to the intrinsic coupling between mechanical and electrical fields. Successful application of indentation technique relies on the corresponding contact mechanics [7,8,9], such as deformable-rigid contact and elastic contact, which can be used to measure piezoelectric constants [10,11].

1.2 Motivation

The purpose of this dissertation is to study the contact mechanics of piezoelectric materials since piezoelectric materials are often used in some "contact-prone" applications [12]. The knowledge of electromechanical interaction between piezoelectric materials and other components is essential to understanding the performance of piezoelectric components, and has stimulated the interest in the indentation experiment of piezoelectric materials as an effective technique for characterizing electromechanical properties of piezoelectric materials.

The contact deformation behavior of piezoelectric materials is complex due to the coupled mechanical and electrical properties of piezoelectric materials. There are only limited cases that can be solved analytically. Thus, finite element method (FEM) is used, especially for three-dimensional (3D) problems of anisotropic material.

The indentation behavior of piezoelectric materials is a function of material properties, mechanical and electrical boundary conditions. It is necessary to study the roles of material orientation and mechanical as well as electrical boundary conditions in the indentation of piezoelectric materials. Accordingly, three propositions are made in this dissertation with objective of investigating effects of crystallographic orientation and

boundary conditions on the indentation of piezoelectric materials in both half-space and film forms.

1.3 Summary

Although analytical solutions of the indentation of isotropic, elastic semi-infinite materials have been well established [13,14,15,16,17], directional dependence of material properties has complicated the contact behavior of anisotropic materials. Effects of material anisotropy on the contact deformation requires further study [18] for the applications of indentation in anisotropic materials. For example, shear stresses, pop-in load and displacement varied with crystallographic orientation of Cr_3Si single crystals [19]. Deviation of effective elastic modulus from elastic isotropy to anisotropy could be about 6%, and the physical meaning of the contact modulus calculated from load-displacement curves still remains unsolved for anisotropic materials [20].

Most of the literature on the indentation response of piezoelectric materials has focused on the problem of transversely isotropic materials with axisymmetric axis (the poling direction) being parallel to the indentation-loading direction [3,12,21,22,23,24,25,26,27]. However, it is possible for the indentation-loading direction not to be parallel to the poling direction, and the polarization direction is not necessarily perpendicular to the sample due to bias- or stress-induced polarization switching.

Although some results suggested that the effect of the poling direction (with respect to the indentation-loading direction) on the strength of the material could be neglected [2], more work is needed to verify their conclusion.

1.3.1 Effects of material orientation on contact behavior of a piezoelectric half space

3D finite element analysis was used to study the effect of the angle between the loading direction and the axisymmetric direction on the indentation behavior of a transversely isotropic piezoelectric half-space by a cylindrical indenter of a flat end. Two cases were considered, which included (a) the indentation by an insulating indenter, and (b) the indentation by a conducting indenter. Both the indentation load and the

indentation-induced potential were found to be proportional to the indentation depth. Using the simulation results and the analytical relationship for the indentation by a rigid, insulating indenter, semi-analytical relationships were developed between the indentation load and the indentation depth and between the indentation-induced potential on the indenter and the indentation depth, respectively, for the conducting indenter. The proportionality between the indentation-induced potential and the indentation depth is only a function of the angle between the loading direction and the poling direction, independent of the type of indenters, which may be used to measure the relative direction of the loading axis to the axisymmetric axis of transversely isotropic piezoelectric materials from the indentation test.

Also, a 3D finite element simulation was used to study the effect of the indentation direction related to the axisymmetric axis of a transversely isotropic piezoelectric half space on the indentation behavior of the piezoelectric material by a rigid insulating Berkovich indenter. The finite element results showed that the indentation load was proportional to the square of the indentation depth with the pre-factor depending on the relative direction and the piezoelectric properties of the material. The indentation-induced potential at the contact center was found to be proportional to the indentation depth with the proportionality only a function of the angle between the indentation direction and the poling direction. These relationships may be used in the sharp-instrumented indentation to measure the relative direction of the loading axis to the poling direction (axisymmetric axis) of transversely isotropic piezoelectric materials.

1.3.2 Effects of electrical boundary conditions on contact behavior of thin films

Electrical boundary conditions can either aid or decrease the indentation strength of piezoelectric materials [2] because electric field can either enhance or suppress indentation deformation and influence loading-unloading curves, depending on the direction of the electric field [3,28]. Electrical boundary conditions such as electric charge and electric potential on the deformed surface play important roles in controlling the contact behavior of piezoelectric materials.

Finite element simulation was used to analyze the effect of electric boundary

conditions on the indentation deformation of a transversely isotropic piezoelectric film with the contact radius much larger than the film thickness. Six different combinations of electric boundary conditions were used. The simulation results showed that the indentation load is proportional to the square of the indentation depth and the indentation-induced electric potential at the contact center is a linear function of the ratio of the indentation depth to the film thickness for all six cases. The contact stiffness is proportional to the contact area and inversely proportional to the film thickness. The nominal piezoelectric charge coefficient d_{33} is inversely proportional to the derivative of the electric potential with respect to the indentation depth for the indentation of piezoelectric films by a conducting indenter with a grounded rigid substrate.

1.3.3 Indentation-induced decohesion of piezoelectric films

Thin films have been widely used to protect the underlying substrates against wear, damage, impact and thermal degradation in the applications of microelectronics, optoelectronics and semiconductor devices [29,30,31]. The interface strength between film and substrate is of practical importance and plays a critical role in determining the reliability and durability of the film/substrate systems [32]. The instrumented indentation technique including microindentation and nanoindentation has provided a unique method to characterize the interaction between a film and the associated substrate due to its simplicity and efficiency.

FEM was used to study the indentation-induced interfacial decohesion between a transversely isotropic piezoelectric thin film weakly bonded to an elastic substrate, under the condition that both the indenter and substrate are electrically grounded. It is found that the traction-separation law for interfacial failure provides a feasible way to investigate interfacial decohesion, and the discontinuities of the indentation response curves can be used to characterize interface and material properties. The simulation results show that the dominant parameters in the traction-separation law are cohesive energy and strength. Films of a larger thickness, substrates of a large elastic modulus as well as a larger Poisson's ratio, are desirable for preventing the interfacial decohesion.

1.4 Outline of this dissertation

This dissertation is organized in seven chapters.

Chapter - 1 introduces the motivation and summary.

Chapter - 2 is dedicated to the literature review.

Chapter - 3 focuses on the finite element analysis of the indentation of a piezoelectric half space by a flat-ended cylindrical indenter. The indenter is either insulating or conducting without a prescribed electric potential.

Chapter - 4 analyzes the Berkovich indentation of a piezoelectric half space. An insulating indenter is considered. The contact between the indenter and the sample is either frictionless or frictional.

Chapter - 5 studies the effects of different electrical boundary conditions on the indentation responses of a piezoelectric film perfectly bonded to a rigid substrate under the condition that the contact radius is much larger than the film thickness.

Chapter - 6 investigates the indentation-induced interfacial decohesion of a piezoelectric film weakly bonded to an elastic and electrically grounded substrate. The indenter is considered to be rigid and electrically grounded.

Chapter - 7 contains the conclusion and prospects of future work.

Chapter - 2 Literature review

2.1 Introduction

This chapter is divided into four parts. In the first section, the background knowledge of piezoelectric materials is presented. The second section discusses the application of indentation techniques in characterizing piezoelectric materials. A brief review on indentation-induced interfacial failure is given in the third section. The last section is the summary.

2.2 Piezoelectric materials

Piezoelectric materials represent a broad class of materials whose electromechanical coupling has led to important applications. The first application of piezoelectricity appeared in sonar, in which piezoelectric quartz was used to produce ultrasonic waves during World War I [33]. Since World War I, applications of piezoelectric materials have been expanded to many branches of science and technology such as flexible structures, electronics, navigation, and biology. A major drawback of piezoelectric ceramics (piezoceramics) is the brittleness.

Many important achievements on piezoelectric materials have been made in last several decades. The manufacture technology of piezoceramics has become mature with large-scale commercialization of piezoceramics of low cost and improved performance (such as high dielectric and coupling constants), while the study of the contact behavior between electrodes and piezoelectric materials is still at an early age [23], and needs to be investigated.

Multilayer structures consisting of piezoelectric materials have recently received the most attention because of high energy density, relatively high generative forces, and quick responses (1-10μs) [34,35,36]. In these multilayer structures, piezoelectric materials, which are usually hard, are attached to or sandwiched between metals [37] and electrodes [38]. In an arranged way, they can respond to mechanical loading intelligently.

Because of intrinsic anisotropy, piezoceramics in the multilayer structures experience inharmonious contacts (such as elliptical contact between piezoceramics and other components including electrodes) [39,40,41]. The stress and electric field concentrations near the contact regions between the ceramics and the structure could occur and result in crack initiation and propagation, even failure of components during operation with mechanical or electrical loading [42,43]. Improvement of performance and reliability of piezoelectric materials and piezoelectric-based structures necessitate the analysis of the contact deformation of piezoelectric materials [44].

2.2.1 Piezoelectric effect and piezoelectricity

The direct piezoelectric effect, discovered by Pierre Curie and Jacques Curie [33], describes induction of electric variables, such as electric potential, electric polarization, and current and electric charges of either positive or negative value on certain corresponding surfaces by mechanical deformation or strain. This effect has been used in sensing applications to measure variables such as displacements, strains, accelerations, or other mechanical changes of structure.

The converse piezoelectric effect, predicted mathematically by Gabriel Lippmann and verified by the Curies, describes induction of mechanical deformation with strain, stress, or change in volume by externally electric loading such as an electric potential and electric field. This effect has been used in actuator applications to control mechanical change, since structures made from piezoelectric materials can bend, expand, or contract when an electrical loading is applied.

Piezoelectric effect can be used for energy conversion between electrical and mechanical forms, which is essential for the realization of electromechanical devices in microelectromechanical systems [3].

2.2.2 Polar axis and polarization

Piezoelectricity is absent in centrosymmetric materials and occurs in crystal classes

with no center of inversion (with the exception of crystal class 432). The lack of a center symmetry results in electric dipoles due to a net stress-induced movement of positive and negative ions with respect to each other. A polar axis exists in some crystals. All the piezoelectric materials used in the form of thin films belong to this material group. Quartz has no polar axis and is only used in single-crystalline form. Before polarization, general ceramics exhibit elastically isotropic, and the average dipole moment over any macroscopic volume is zero due to the random orientation throughout the material; while after polarization, ceramics become piezoelectric. By means of poling, electric forces could move positive and negative charges apart in the direction of the external field so that the centers of positive and negative charges no longer coincide. The application of a high static electric polarization field can switch the polarization or orient the domains of equally oriented polarization vectors. After the field is removed, a large proportion of the polarization still remains, and the material exhibits macroscopically piezoelectric responses. The poling direction (i.e., the direction of polarization) is the direction of the applied electric field that permanently polarizes the initially unpoled material [1].

2.2.3 Finite element analysis of piezoelectric materials

Although modeling of piezoceramics has been studied for over a century, improvement and innovation still persist [45], owing to complexities of the electromechanical interaction between mechanical deformation and electric field in piezoelectric materials. An externally applied voltage can change the shape of a piezoelectric sample (i.e., an electric field creates mechanical strain in piezoelectric materials). The non-uniform strain field will result in stress distribution. The mechanical stress/strain will, in turn, induce an electric field in the material.

Complete constitutive laws for piezoceramics are still lacking [45]. A piezoelectric material is often laminated or adhered to a substrate as a unimorph or bimorph, which makes the modeling of piezoelectric material or structure more complicated [45]. Finite element simulation has been constantly developed in the past 40 years with varying

degrees of success [46,47,48,49]. Modeling of piezoelectricity is a vast area [45]. Finite element packages such as ANSYS [50] and ABAQUS have limitations such as the restriction of linear piezoelectricity without thermal terms. COMSOL has the potential capability for multi-physics analysis, but has not yet been well established. A review of finite element modeling of piezoelectric structures was presented in Piefort [33]. Two and three dimensional finite element models of piezoelectric materials, including shell/planar, beam, solid, have been well formulated [51,52,53]. A finite element model for a laminated composite plate or multilayer structures containing distributed thin piezoelectric sensors and actuators is now available [54,55,56,57]. For the contact between adjacent layers in multilayer structures, the assumption of perfect mechanical and electric contact has been used so that the continuity of displacement and electric potential holds on the interfaces between adjacent layers [58]. An optimization approach, which is to obtain an optimal distribution of piezoelectric material, for the actuator design of multilayer piezoelectric plate and shell structures, so as to provide the maximum displacement in a given direction at a point of the domain, was carried out by the FEM [59]. The existing models usually involved utilizing the entire layer of the piezoelectric materials. Models for distributed piezoelectric materials should be further investigated, and there was more modeling work to do concerning embedded or bonded piezoelectric materials [60]. For large complicated structures with integrated piezoelectric materials, finite element simulation, which has general applicability, is a powerful tool for the design and analysis, and is promising for solving complex geometries and non-uniform electric fields [60]. The rapid advance of computational capacity makes the unsolved formidable problems tractable with the help of FEM and paves the way for measurement of electromechanical properties on the nanoscale.

2.3 Indentation of piezoelectric materials

Indentation techniques originating from hardness measurement have been widely used for measurement of mechanical properties such as elastic modulus, contact stiffness,

fracture, creep parameters, and interface strength of elastic and elastic-plastic materials. New applications of indentation techniques to non-traditional materials with non-mechanical features such as piezoelectric solids with electromechanical coupling have inspired much exploration recently. The use of indentation techniques to characterize piezoelectric materials has been a subject of interest to engineers and scientists since the end of the 20^{th} century. Instrumented indentation techniques are believed to be capable of probing mechanical as well as electrical properties of piezoelectric materials.

Nanoindentation is well known for the measurement of the mechanical properties of materials and thin films. The indentation behavior (force/penetration curve, for example) is related to the material's mechanical properties, which has motivated an increasing number of studies. The successful application of instrumented indentation techniques for characterizing piezoelectric materials depends on the availability of the relationship between indentation responses and material parameters from closed-form solutions and semi-empirical models. The use of indentation techniques has attracted significant attention in the field of characterizing the contact behavior of piezoelectric materials, because indentation can provide the basic foundation for understanding contact mechanics.

A number of researchers have contributed to the theoretical studies of the contact mechanics of piezoelectric materials within the realm of linear piezoelectricity. Generally, quasi-static normal indentation of homogeneous, transversely isotropic, linear elastic, piezoelectric materials was considered [1]. The complex anisotropy makes it hard to obtain analytical solutions for 3D contact problems of piezoelectric materials. Closed-form solutions have been available only for transversely isotropic piezoelectric materials due to the simplicity of transverse isotropy (i.e., the feature of axisymmetry about the poled direction). Although it is believed that the results for PZT-4 are representatives for other piezoelectric materials, the solutions in references [25,26,61,62]

are not applicable for the piezoelectric materials with repeated characteristic roots. Analytical work could be divided into two categories (i.e., half-space case and thin film case), because closed-form solutions for indentation problems can only be obtained for two limiting cases, half space and thin films [62]. Numerical calculations are indispensable for probing indentation of a piezoelectric film of a finite thickness [25,26,62].

2.3.1 Indentation of a piezoelectric half space

Indentation of piezoelectric materials is more complicated than their counterpart of elastic materials due to the directional dependence and mechanical-electrical coupling.

2.3.1.1 Axisymmetric problems

In general, a cylindrical polar coordinate system (r,θ,z) is introduced for the axisymmetric problem, in which the axis of indenter is the axis of revolution (i.e., z-axis), and the transversely isotropic piezoelectric material is isotropic in the (r-θ) plane [2,12,62]. The contact is axisymmetric, nonconforming, monotonically advancing with load, and adhesionless [1]. Rigid indenters with three types of axisymmetric shapes (e.g., flat-ended cylinder, cone, and sphere) have been considered and modeled either as perfect conductor or perfect insulator [1,12,62]. For a conducting indenter, a prescribed electric potential is applied on the indenter [3,12,62]. The contact interaction between indenter and indented surface is frictionless [62].

Matysiak [63] analyzed the axisymmetric contact deformation of a linear piezoelectric half-space by a rigid and perfectly conducting flat-ended indenter using the Hankel transform and derived the relation between contact load and contact area.

Wang and Zheng [64] obtained general solutions for 3D problems in transversely isotropic piezoelectric media by introducing a set of potential functions and gave the expressions of stresses and electric displacements for the case under an in-plane concentrated load.

Ding et al. [65] were concerned with dynamic equations with inertia terms and obtained three general solutions for the boundary-value problem with normal stress and electric displacement on the top surface.

Ding et al. [39] investigated a series of 3D contact problems including spherical indenter, a conical indenter and an upright circular flat punch by extending the Boussinesq and Cerruti solutions for point force and point charge acting on the surface of a transversely isotropic piezoelectric half-space. They obtained the equations for determining the size of the contact region, normal pressure and normal electric displacement inside the contact region and numerically compared their results with those for the corresponding transversely isotropic materials having the same elastic constants.

Saigal et al. [66] investigated the electrical response of a piezoelectric ceramic-polymer 1-3 composite during indentation with a constant cross head velocity and a conductive spherical indenter of zero potential bias. The surface of the specimen opposite to that being indented was coated with silver, and the lower cross head on which the specimen was placed and the indenter were both electrically grounded in order to enforce the zero electrical potential far away from the indenter. They found that the induced current increased with the increase in the indentation load, contact area, indentation velocity, and indenter diameter.

Chen and Ding [61] derived exact solutions for the problem of a rigid sphere, which was conductive and electrically grounded, indenting a transversely isotropic piezoelectric half space by introducing a new potential to take account of piezoelectric effect. Elastoelectric fields were expressed in terms of elementary functions by comparing solutions with pure elasticity. They found the normal stress and electric displacement on the indented surface exhibited singularity at the contact perimeter solely caused by the electric potential imposed over the contact region.

Giannakopoulos and Suresh [12] presented a general theory of a normal,

axisymmetric indentation of transversely isotropic piezoelectric materials under different geometries of indenters (i.e., spherical, conical, and flat-ended cylindrical indenters), and small strain, small electric displacement, and frictionless contact conditions. The rigid indenter was assumed to be either perfectly electric conducting or insulating. The Hankel integral transformations were employed to transform the partial differential equations to a homogeneous system of ordinary differential equations. They derived explicit expressions for contact pressure, electric charge, normal displacement at the contact perimeter, indentation load and induced charge, and found solutions for piezoelectric materials having the same functional forms as those for uncoupled mechanical ones. Their results indicated that a zero net charge under the conducting indenter could be achieved under certain combinations of the indentation load and electric potential applied on the indenter. They checked their analytical solutions by recourse to an axisymmetric finite element model, and found piezoelectric coupling could either stiffen or soften the contact response of piezoelectric materials depending on the material constants. Although good agreement between theoretical predictions and numerical calculations was declared, the zero electric potential applied on the rotational axis is incorrect.

Ramamurty et al. [6] investigated the indentation responses of lead zirconate titanate and barium titanate piezoceramics by a spherical indenter, and obtained force versus (vs.) penetration depth curves revealing the dependence of the indentation stiffness on the material condition (poled or unpoled) and the type of indenter (electrical conductor or insulator). Three types of spherical indentation experiments (i.e., unpoled material, poled material with a conducting indenter and poled material with an insulating indenter) were performed using the displacement control, with a prescribed displacement rate of 2 mm/min. Their experimental results under the condition of zero electric potential far away from the indenter were in good agreement with analytical predictions. They found that the instrumental spherical indentation of piezoelectric materials was a good method for extracting piezoelectric properties and the load-displacement relations were

functionally the same as that of the uncoupled mechanical case. The error analysis showed that the dielectric constants had almost no effect on the indentation stiffness. The parametric analysis showed that both piezoelectric anisotropy and elastic anisotropy had effects on the indentation stiffness, and the indentation stiffness had to be evaluated on a case by case basis.

Sridhar et al. [67] proposed a method for characterizing piezoelectric materials by means of mechanical indentation with a conductive spherical indenter and a constant indentation velocity. They found analytical model could predict experimental behavior of the axisymmetric indentation of linear piezoelectric solids. In their experiment, the cross head on which the specimen was placed and the indenter were both electrically grounded. The surface, which was opposite to the surface being indented, was coated with silver to achieve zero electrical potential condition far away from the indenter. The quasi-static current, which was induced into the punch, was measured by a Keithley-614 electrometer connecting the indenter and the ground. The sign of the induced current for the case of the indentation loading direction being along the poling direction was found to be opposite to that of the indentation loading direction against the poling direction, and the indentation on an unpoled sample resulted in no current. Material constants depending on elastic, dielectric, and piezoelectric constants in a complicated way, were extracted from the measured current vs. time curves.

Giannakopoulos [1] theoretically and computationally dealt with the axisymmetric indentation of a transversely isotropic piezoelectric half space by a rigid spherical indenter. It is noted the definition of the characteristic equation is different from that in reference [12]. Four piezoelectric materials (i.e., PZT-4, PZT-5A, $BaTiO_3$, and 95% $BaTiO_3$-5%$CaTiO_3$) were analyzed. Finite element results indicated the conducting type of indenter together with the material state (i.e., poled or unpoled) influenced the stress and electric flux distributions. It was found: (1) the maximum tensile stress occurred deeper for the conducting indenter than for the insulating indenter; (2) the maximum

magnitude of electric flux occurred at the contact perimeter for the insulating indenter while at the center of the contact area for the conducting indenter; (3) the maximum magnitude of electric flux was higher for the conducting indenter. However, the electrical boundary conditions used were incorrect, because of the zero electrical potential applied on the axisymmetric axis.

Sridhar et al. [68] carried out conical indentation experiments of transversely isotropic piezoelectric materials PZT-4 and $BaTiO_3$ of the poling axis being along the indentation loading direction. In the indenter-velocity controlled experiment, the displacement, indentation force, and quasistatic current were monitored, and the lower cross head, on which the specimen was placed, and the conducting indenter were both electrically grounded. The studies showed that the tip of the indenter behaved as a small sphere during the onset of penetration, and inelastic deformation took place after a certain load, and linear theory was not applicable. They concluded that piezoelectric materials could be characterized by sharp indenters before the occurrence of plastic deformation.

Kalinin et al. [4] derived electroelastic fields for piezoelectric indentation under a conducting spherical indenter of a prescribed electric potential by using the elastic-piezoelectric correspondence principle and presenting the problem as a superposition of two subproblems (i.e., either one with purely mechanical or electrical boundary conditions). Their results were found to be in agreement with those in reference [61], but numerically different from the ones in reference [12]. Indentation elastic stiffness, indentation dielectric constant, and indentation piezocoefficient were defined for piezoelectric materials, because of the linear superposition of solutions for two sub-problems with individual mechanical or electrical contribution, and thus force- and bias-induced phenomena were distinguished. Effects of material constants on the coupling coefficients were investigated and it was found that sensitivity of piezoresponse was dominated by two elastic stiffnesses c_{33} and c_{44}, two piezoelectric constants e_{33} and e_{15}, and two dielectric constants $\in_{11}$ and $\in_{33}$.

Xiong et al. [40] obtained the electro-elastic field around the contact region in a transversely isotropic piezoelectric half-space caused by a circular flat bonded punch under torsion loading by using the general solution of piezoelectric media and the extended-Cerruti solution. Singularity of normal stress and electric displacement was found on the contact edge, and shear stress and electric displacement were approaching zero at the depth of the punch diameter in PZT-4.

Li and Wang [69] investigated the problem of a smooth rigid punch with arbitrary end shape bonded to an anisotropic piezoelectric half-space by the Fourier transform method. The contact pressure, electric displacement, and electric potential were given numerically for an example of flat-ended punch.

Huang et al. [70] analyzed the contact problem of transversely isotropic piezoelectric materials by the potential theory. The solution of the elasto-electric field was obtained by assuming that the electric potential was known under the punch. The punch was assumed to be electrically conductive and connected to a circuit or the bottom surface of the punch was covered with an electrode.

Makagon et al. [71] analyzed the indentation of spherical and conical indenters onto a piezoelectric half-space accompanied by frictional sliding. It was found that the contact area depended noticeably on the tangential effect which is in the form of Coulomb's friction. The solution showed that the tangential displacement and the shear stress reached the maximum magnitude directly under the indenter. The stress distribution in the contact zone was asymmetric due to frictional lateral motion, which was different from the axial symmetric distribution for the normal, frictionless indentation problem alone.

Kalinin et al. [72] analyzed the problem of coupled electromechanical indentation of a transversely isotropic piezoelectric half-space and derived the relationship between the direct and converse piezoelectric effects based on their previous work [4]. The indenter was perfectly conductive with negligible electrostatic field outside the contact area.

Yang [3] revisited the axisymmetric indentation of a transversely isotropic piezoelectric half space by a rigid, conducting indenter of an arbitrary-axisymmetric profile, and derived four different general solutions using the Hanker transform and Yang's results [73]. He defined the contact stiffness, effective piezoelectric constant in indentation and found that for conducting axisymmetric indenters of zero electric potential, the effective piezoelectric coefficient and the ratio of contact stiffness to the square root of contact area are independent of indentation deformation (i.e., the surface profile of indenter), and only dependent on material properties. Effect of electric field and electrical displacement intensity factor were discussed. It was found a contact zone was possible even for zero indentation displacement under a certain electric potential.

Yang [44] summarized the contact mechanics of semi-infinite transversely isotropic piezoelectric materials using the indentation technique. There are three kinds of techniques involved in indentation testing of piezoelectric materials, including charge integration technique, electric current technique, and electrical modulation technique. It was concluded that local piezoelectric response of piezoelectric materials could be examined by the electrical-controlled indentation technique, and 3D numerical simulation was necessary due to the complexity of the directional dependence and mechanical-electrical coupling.

Karapetian et al. [74] derived the stiffness relations for the indentation of a transversely isotropic piezoelectric material by indenters of arbitrary geometries. Relations between the indentation depth, indentation force, electric potential, and electric charge were explicitly solved in terms of the geometry of indenter and material properties.

Kamble et al. [2] performed spherical indentation experiments on a lead zirconate titanate polycrystalline piezoceramic (PZT-4) as well as a complementary axisymmetric finite element simulation to capture distributions of the stress and the electric field under the condition of alignment between the loading axis and the direction of polarization.

Both poled and unpoled samples were tested, and both conducting and insulating indenters were employed. The indentation size effect was observed. To enforce zero electric potential far away from the indenter, the back surface (i.e., the side opposite to that being indented) as well as the side surface of the specimen were coated with gold, and the lower cross head on which the specimen was placed and the upper cross head to which the indenter was attached, were both electrically grounded. Experimental results from the displacement-controlled mode demonstrated that the indentation stiffness and strength depended on the combination of material conditions and electrical boundary conditions as well as the indenter size. Simulation results showed that the difference of the maximum tensile stress and the resultant electric potential fields between unpoled and poled samples. The fractography revealed different fracture behaviors between unpoled and poled samples. In their simulation, zero potential was applied on the symmetric axis, which is incorrect.

Liu and Yang [75] performed an axisymmetric finite element analysis of spherical indentation of a transversely isotropic piezoelectric half space with the poling direction being against the indentation loading direction. They considered four electrical boundary conditions (i.e., insulating indenter, conducting indenter without a prescribed electric potential, electrically grounded conducting indenter, and electrically grounded top surface of the indented sample) and corrected the mistakes in the finite element models in [1,2,12].

2.3.1.2 Two-dimensional problems

Yang [23] obtained closed-form solutions for two-dimensional electroelastic contact problem of a semi-infinite transversely isotropic piezoelectric medium attached with a complaint electrode subjected to uniform displacement and electrical potential, and found four possible different solutions depending on material properties by using Fourier transform and dual integral equations. His numerical results, under the requirement of total electric charge within the contact zone being zero, illustrated distributions of stress,

displacement, electric potential, electric displacement underneath the electrode, and indicated the location of the strongest electromechanical interaction was at the depth approximately equal to the contact radius.

Kirilyuk and Levehuk [76] investigated the contact problems of a transversely isotropic piezoelectric half-plane with free surface perpendicular to the polarization axis for different types of wedge-shaped indenters (flat-ended indenter with rounded one or two edges, half-parabolic indenter, etc.). They compared the indentation response (contact area and contact pressure) of three different materials: purely elastic material, electroded and unelectroded piezoelectric materials.

Wang et al. [43] studied a two-dimensional contact problem of transversely isotropic piezoelectric materials by a single flat-ended punch or two collinear punches. They suggested that the total charge accumulated on the punch surface was zero for the conducting indenter, which is debatable. Both infinite thickness and finite thickness were considered. The results showed the singularity at the punch tip.

Ke et al. [77,78,79] investigated a two-dimensional frictionless or sliding frictional contact problem for a layered half-plane made from functionally graded piezoelectric material whose properties were thickness-dependent. The punch was assumed to be a perfectly rigid electrical insulator with zero electric charge distribution. Different shapes of indenters including flat, triangular, and cylindrical were considered. The friction within the contact region was of the Coulomb type for the case of sliding frictional contact. The contact pressure, contact traction, contact region, maximum indentation depth, normal stress, electric potential, electric displacement and electromechanical fields were determined numerically by using the Fourier transform technique. The singularity behavior at the contact edge for the flat-ended punch was found. Numerical results showed that the contact behavior was noticeably affected by material properties, friction coefficient, and punch geometry. For suppressing the surface contact damage, it was

suggested that the width of the flat punch should be increased, and the slope of the triangular punch should be reduced.

Guo and Jin [80] investigated the two dimensional contact mechanics between a transversely isotropic piezoelectric half space and a rigid conducting cylinder punch with adhesive effect, which included tangential and normal tractions caused by micro-scale contact. In their analysis, the poling direction was perpendicular to indented surface. The assumptions were that the contact region was perfectly bonded without slippage, the contact region was much smaller than the radius of the cylinder, and external force resulted in no bending moment. The punch was subjected to combined mechanical force with inclined angle and electrical loading. They obtained explicit solutions of the stress and electric displacement distributions. The numerical results showed that the electric charge might strengthen or weaken the adhesion depending on the piezoelectric material.

2.3.1.3 Three-dimensional problems

Some progress in the quantitative understanding of the effect of varying poling direction with respect to the indentation direction on the indentation response of piezoelectric materials has been achieved recently. In addition, for non-axisymmetric indenters like Berkovich indenter, the indentation problem is intrinsic 3D even the poling direction is of align with indentation loading direction.

Wong and Zeng [81] investigated the deformation behavior of $[001]^T$- and $[011]^T$-cut single crystal solid solution of $Pb(Zn_{1/3}Nb_{2/3})O_3$–6% $PbTiO_3$ (PZN–6%PT) in both poled and unpoled states by nanoindentation with a standard Berkovich tip of radius 50 nm. The dependence of contact stiffness, elastic modulus and hardness on crystal orientation was found; poling was found to enhance the mechanical property (hardness and modulus) of the crystal compared with the unpoled state; and the strength of the poling field, polarity of the poled surfaces and the variation in poling fields were found to have no influence on the mechanical behavior of the crystals. The pop-in event in the

load-displacement curve revealed the pile-up and local damage around the indentation impressions at ultra-low loads. Plastic deformation was initiated prior to the occurrence of the pop-in. The relationships between the indentation load, displacement and harmonic contact stiffness were studied, and a surface layer of approximately 300 nm thickness with different mechanical properties from the interior, which was possibly due to crystal fabrication processes, was found.

Zhao [82] used an axisymmetric finite element model to study indentation responses of Lead Zirconate Titanate-5H (PZT-5H) for three different cases including uncoupled mechanical case (i.e., only a transversely isotropic material), poled sample with conducting or insulating indenter cases. A 3D model was built to investigate the effect of poling direction. However, only one case of the indentation loading along non-poling direction was studied with no detailed information. He investigated the effect of elastic modulus in the poling direction on the indentation load-displacement curve. His results for a flat-ended cylindrical indenter showed: (1) the distributions of von-Mises stress were almost the same for the three cases, while the magnitude of stress concentration was influenced by the polarization and electrical boundary conditions; (2) electric potential distribution was greatly influenced by electrical condition of indenter; (3) poled samples were more easily damaged than uncoupled ones due to the higher von-Mises stress concentration for the poled sample, and the indentation load was highest for the poled sample/insulating indenter case, and lowest for the uncoupled one under the same indentation displacement; (4) a linear relationship existed between the elastic modulus (or the piezoelectric coefficient d_{33}) in the poling direction and the ratio of load to displacement (or charge to force).

Cheng and Venkatesh [83] established a 3D finite element model to investigate the indentation responses of anisotropic piezoelectric materials of four different crystal symmetries. They considered three different indenters (i.e., spherical, conical, and flat-ended cylindrical indenters), two different electrical boundary conditions (i.e.,

insulating indenter and conducting indenter of zero electric potential), and different material orientations (i.e., poling direction against the indentation loading direction, poling direction perpendicular to the indentation loading direction). Significant effects of different material properties on stress and electric flux fields were found. Their results revealed the difference of the indentation responses under different material orientations and mechanical and electrical boundary conditions.

2.3.2 Indentation of piezoelectric thin films

Piezoelectric materials of low dimensions, such as nanowires [84,85,86], nanobelts [87,88], thin films [89,90,91], and nanotube arrays [92], have been widely used in various engineering applications such as sensors [93] and actuators [36] in smart structures and systems, and have the potential in the applications of energy scavenging [84,94,95], transportation [96], and aerospace [97,98].

Most theoretical studies on the indentation of piezoelectric materials focused on the half-space case, since the indentation responses of film/substrate systems are more complicated. Closed-form solutions for indentation of thin films of a finite thickness cannot be obtained and can only be studied numerically. There are only a few studies on the contact mechanics of piezoelectric thin films in contact with a substrate. A rigid substrate was considered by Wang et al. [62], and elastic substrate was considered by Wang and Cheng [25], and Wu et al. [26]. A perfectly bonding interface between film and substrate is usually assumed.

2.3.2.1 Indentation of piezoelectric films on a rigid substrate

Koval et al. [99] investigated the electromechanical response of piezoelectric materials under nanoindentation. The materials used were pure lead tetragonal structured zirconate titanate (PZT) and Mn-doped PZT, which were films of different thicknesses. The indentation force was 500 mN, and was applied parallel to the poling direction. The conductive indenter was a spherical WC-Co cement with 500 μm nominal radius. The

electrodes and the nanoindentation measuring system were electrically grounded. The stress-induced quasi-static electrical current generated due to the direct piezoelectric effect was measured with an electrometer during the loading/unloading cycle. The piezoelectric coefficient could be obtained from the slope of charge vs. load curves. Their results demonstrated the film thickness dependency of the electric current, and the significant effect of nanoindentation on the domain rearrangement of the local polarization state of the films. It showed that the sign of the electrical current would change upon unloading, and the effective piezoelectric coefficient was dependent on the force.

Wang et al. [42] investigated the contact problem of a piezoelectric layer with a rigid conducting or insulating circular indenter on its surface. They obtained the displacement, stress, electric displacement and electric potential distribution, and the dependence of the indentation load and electric charge on the indentation depth of the indenter for both half space and finite thickness. Their results showed negligible effect of the permittivity of the air, and singularity in the mechanical and electric fields. For the piezoelectric medium of a finite thickness, the normal displacement, friction and electric potential were all zero on the bottom surface.

Wang et al. [62] obtained closed-form solutions for the axisymmetric indentation problem of a transversely isotropic piezoelectric half space by flat-ended cylindrical, conical and spherical indenters using the Hankel integral transformation. Both insulating and conducting indenters were considered. They found their results were consistent with those by Chen and Ding [61] and Kalinin et al. [4], but numerically different from those given by Giannakopoulos and Suresh [12]. They also obtained closed-from solutions for indentation of an infinitely thin film made of a transversely isotropic piezoelectric material ideally bonded to a rigid and conducting substrate of zero electric potential, using the Taylor series expansion method and the extended Johnson's assumption (i.e., the radial displacement is zero). They found solutions for transversely isotropic

piezoelectric films reduced to those of elastic transversely isotropic thin films [100] by setting piezoelectric coefficients to be zero. Numerical analysis was conducted for a piezoelectric film of a finite thickness by utilizing the Abel inverse transformation method to investigate the effect of film thickness. It was found the ratio of contact radius to film thickness played an important role in gauging the transition between the two asymptotes (i.e. half space and infinitely thin film), while the ratio of the indentation depth to the film thickness had no effect on the normalized indentation response. Their results obtained under a constant ratio (i.e., 0.1) of the indentation depth to the film thickness implied that different materials, electrical boundary conditions, semi-apex angle of conical indenter, and radius of spherical indenter had little effect on the normalized indentation responses. They proposed two two-parameters, semi-empirical models accounting for the effect of the film thickness: the first one for the normalized responses of indentation force and electric charge; the second one for electric potential and contact radius. It was found that the first model was insensitive to different piezoelectric materials, while the second model was material-dependent, which implies ambiguity of the semi-empirical models.

2.3.2.2 Indentation of piezoelectric films on elastic substrate

Recently, a systematic research on the effects of elastic substrate on the indentation responses of piezoelectric films has been carried out.

Wang and Chen [25] investigated the influences of elastic substrate and thickness of films on the axisymmetric indentation of piezoelectric films ideally bonded to an isotropic elastic half space of zero electric potential using the integral transform method, and conducted numerical calculations for various Young’s moduli and Poisson’s ratios of the substrate under three axisymmetric indenters (i.e., punch, cone and sphere) and two electrical boundary conditions (i.e., insulating and conducting indenters). The prescribed electric voltage on the indenter was proportional to the film thickness for the case of a conducting indenter. The calculation results under a constant ratio (i.e., 0.1) of the

indentation depth to the film thickness implied that whether the indenter was ideally insulating or conducting had little effect on the mechanical responses, but had prominent effect on the electric responses. For the three types of indenters, normalized results were found to be almost the same; the case of a hard film on a soft substrate behaved differently from the case of a soft film on a hard substrate; and mechanical responses could be expected very well from the half space results under the conditions that Young's modulus and Poisson's ratio of substrate were close to those in the isotropic plane of the transversely isotropic piezoelectric film. Their analytical calculations were validated by recourse to an axisymmetric finite element analysis by using ABAQUS FEM package for the insulating spherical indenter case.

Wu et al. [26] studied the indentation problems of a transversely isotropic piezoelectric layer on an elastic half space by using the Hankel transform and the Green's functions with the theorem of superposition. Different types of indenters (i.e., flat-ended cylindrical, conical and spherical indenters), electrical boundary conditions (i.e., insulating and conducting indenters), and film/substrate bonding conditions (i.e., frictionless contact and perfectly bonding) were considered. Their results showed that increasing substrate modulus increased indentation load, electric charge and contact radius under the same indentation displacement; substrate effect could be ignored when the ratio of film thickness to contact radius is no less than 10. The contact response for the stiffer substrate behaves differently from that for the softer substrate; the effect of electric potential applied on the conducting indenter was prominent, and the variations of normalized responses, which depended on interface conditions, were similar for all three indenter shapes. Although it was found that increasing Poisson's ratio of substrate increased the indentation load and contact radius, the effect of Poisson's ratio on the indentation-induced charge was not illustrated.

Song et al. [101] performed extensive two-dimensional axisymmetric finite element simulations of conical indentation of a transversely isotropic piezoelectric thin films

perfectly bonded to an elastic substrate in order to probe effects of elastic and piezoelectric coefficients on the indentation responses. They proposed empirical equations relating the maximum indentation load and the power exponent of loading curve to the elastic and piezoelectric coefficients, based on dimensional analysis and the numerical results of the indentation loading at a broad spectrum of possible material combinations. Their forward analysis based on numerical simulation was verified by the reverse analysis in the nanoindentation tests. Elastic and piezoelectric coefficients of piezoelectric thin films were extracted from the indentation experiment with the indentation depth of one-fifth of film thickness.

2.4 Indentation-induced interfacial failure

Interfacial failure between adjacent layers due to inter-laminar stresses is becoming a critical area for predicting the reliability of multilayer thin film structures. Multilayer structures (or smart structures) possess a better compromise performance (better displacement/voltage sensitivity, for example) for actuators. A singularity of electric and stress/strain fields due to the electromechanical interaction between electrode layer and piezoelectric layer could introduce mechanical and electric instability and cause nucleation and propagation of cracks for relaxing the incompatible strains [23]. Interfacial normal stress is believed to control the delamination initiation [102]. To improve the reliability of multilayer structures, it is necessary to quantitatively understand the fracture process by the contact-induced interfacial decohesion.

Indentation experiments, analytical analyses and numerical analyses have been used to study the interfacial failure between films and substrates in multilayer structures [103,104,105,106,107,108,109,110]. However, there are only a few sources like reference [111] addressing the interfacial adhesion analysis of piezoelectric thin films by nanoindentation test, which is still at its early stage.

2.4.1 Experimental studies on indentation-induced interfacial failure

Kriese et al. [105] used indentation to cause the delamination of copper and tungsten films from silicon wafer by indentation testing and observed: (1) delaminations were circular and geometrically similar to craters with an easily identifiable radius; and (2) unloading was uniform. Huang et al. [112] conducted Vickers indentation tests on ZnO/Si systems, and measured the delamination radius, the radial crack length and the delamination profile. They observed: (1) the indentation-induced radial cracks was smaller than the delamination size; and (2) film thickness and indentation load had prominent effects on the delamination behaviors. Borrero-López et al. [106] studied lateral, transverse, radial, and ring cracks in a Ta-C/Si system under different film thicknesses and indentation loads by cross-sectional observations and spherical nanoindentation. They found: (1) fracture is generic for thin film/substrate brittle structures; and (2) lateral cracks, which lead to delamination of thick films and to spallation of thin films, occurred during unloading.

2.4.2 Theoretical studies on indentation-induced interfacial failure

Using elastic fracture mechanics and the post-buckling behavior of circular plate, Evans and Hutchinson [113] analyzed the indentation-induced delamination of pre-compressed coatings, in which they used the energy release rate and the critical stress as the buckling condition to describe the incidence of delamination. Following the same approach, Marshall and Evans [114] developed a plate model to analyze the indentation-induced delamination of an elastic coating from the substrate by considering the effect of indentation stress and lateral residual stress on the equilibrium crack length and the onset of the plate buckling..

2.4.3 Numerical studies on indentation-induced interfacial failure

To quantitatively understand the indentation-induced delamination, finite element methods have been used to describe the interface delamination. Baqi and Giessen [107]

developed a finite element model to simulate the indentation-induced delamination of a thin film from a ductile substrate by a spherical indenter, in which a cohesive model was used for the interface between the coating and the substrate. Their results showed that the interfacial delamination occurred during the unloading stage and initiated at a location away from the loading axis. Li and Siegmund [108] studied the indentation-induced delamination of a coating system consisting of a ductile film and an elastic substrate. They used a cohesive zone model in the simulation and observed the delamination-induced buckling of the surface coating. She et al. [109] performed a three–dimensional finite element analysis of the interface delamination created by the microwedge indentation using a traction-separation law [110] for the cohesion and failure behavior of the interface between the film and the substrate. They concluded that a sudden drop of the indentation load is always accompanied by the occurrence of the interface delamination. Liu and Yang [115] carried out finite element analysis of indentation-induced delamination in a film/substrate structure with both film and substrate being elasto-perfectly plastic and a simple criterion for interfacial failure (i.e., a critical tensile stress).

2.5 Summary

Existing literatures about the indentation of piezoelectric materials are mainly concerned with transversely isotropic piezoelectric materials with the poling direction being either parallel or anti-parallel to the indentation loading direction. It is desirable to carry out a systematic research on the indentation of transversely isotropic piezoelectric materials with the poling direction being misaligned with the indentation loading direction and to explore the effects of material orientations (i.e., the angle between the polarization direction and the indentation loading direction) on the indentation responses of piezoelectric materials. A pre-determined electric potential is usually prescribed on the conducting indenter [62]; few works have dealt with the conducting indenter without a pre-determined electric potential, for which case the closed-from solution has been

unavailable. The knowledge of the electromechanical interaction between the electrode layer and the piezoelectric layer is essential to improving the reliability of multilayer smart structures. Research on interfaces concerning the integration of dissimilar materials in piezoelectric multilayer structures will impact a variety of structural applications. The finite element simulation of the contact deformation of piezoelectric material is indispensable for the three dimensional analysis due to anisotropy and nonlinearity from both material and geometry.

Chapter - 3 Boussinesq indentation of a piezoelectric half space

3.1 Introduction

With the extensive applications of piezoelectric materials used as sensors, actuators, transducers in aerospace, bioengineering, automobile, flexible structures and smart systems of small volume, there is a great need to understand the electromechanical behavior of piezoelectric materials for quality control and performance prediction in recent years. Various techniques have been developed to characterize mechanical properties (e.g., elastic modulus, yield stress, and hardness) of materials, which include indentation technique [6,44,56,63,70,116,117,118,119], piezoresponse force microscopy [4,44,120,121], and atomic force microscopy [98,120,122]. In the heart of the contact technique is the relationship between the indentation load and the indentation depth, which depends on the properties of materials.

Matysiak [22] was the first to analyze the axisymmetric contact of a transversely isotropic piezoelectric half-space. Giannakopoulos and Suresh [12] used Matysiak's approach [22] to present a general solution for the axisymmetric indentation of a piezoelectric half-space. Using the potential theory, Ding et al. [39] obtained analytical solutions of the stress and electric fields for the indentation of a transversely isotropic piezoelectric half-space by axisymmetric indenters. Yang [23] studied the electromechanical coupling between a compliant surface electrode and a transversely isotropic piezoelectric half-space. Yang [3] obtained the contact stiffness, effective piezoelectric constant and electric displacement intensity factor for the axisymmetric indentation of a semi-infinite piezoelectric material by a rigid, conducting indenter of an arbitrary-axisymmetric profile. Wang and Chen [25] considered the indentation of a piezoelectric film bonded to an elastic substrate by an axisymmetric indenter and reduced the indentation problem to the solution of a dual integral equation. Wu et al. [26] reduced the solution for the indentation of a piezoelectric film on an elastic film to a Fredholm integral equation of the second kind and solved the problems numerically.

Due to the complexity of electromechanical interaction, finite element methods have been used to analyze the contact deformation of piezoelectric materials. Wang and Han [42] analyzed the indentation of a piezoelectric layer by a flat-ended cylindrical indenter and numerically simulated the deformation of the piezoelectric layer being indented. Giannakopoulos [1] misused zero electric potential on the axisymmetric axis in the finite element analysis of the spherical indentation of piezoelectric materials. Kamble et al. [2] applied the same condition used by Giannakopoulos [1] in the finite element analysis of the spherical indentation of polycrystalline PZT-4. Liu and Yang [75] used the FEM to examine the effect of surface electric conditions on the spherical indentation of transversely isotropic piezoelectric materials without applying electric condition to the axisymmetric axis. Using axisymmetric and 3-D finite element simulations, Zhao [82] recently studied the effect of poling direction and indenter size on the indentation of PZT-5H by a flat-ended cylindrical indenter in which only one case with the indentation direction being un-parallel to the poling direction was shown. No detailed study was given to the effect of crystal orientation.

Piezoelectric interaction depends on crystal orientation, and the effect of material anisotropy on indentation response requires detailed study. When the direction of indentation loading is not aligned with the poling direction, axisymmetric analysis cannot suffice. Asymmetric analysis is needed to understand the effect of material anisotropy including stiffness and piezoelectric responses associated with crystal orientation. Three-dimensional finite element analysis has been widely used for investigating anisotropic structures [83,123,124] in which analytical solutions are deficient. In this work, three-dimensional finite element analysis of the Boussinesq indentation of transversely isotropic piezoelectric materials is performed. The study is aimed at analyzing the effect of material anisotropy on the relationship between indentation load and indentation depth and that between indentation-induced potential and indentation depth.

3.2 Problem formulation

Consider a rigid, cylindrical indenter of flat end that is normally pressed into a linear piezoelectric half-space (z>0). The loading direction is parallel to the surface normal of the piezoelectric material; let the angle between the loading direction and the poling direction (axisymmetric axis) be θ.

The mechanical boundary conditions for the indentation are:

$$\sigma_{rz}(r,0)=0 \tag{3.1}$$

$$\sigma_{zz}(r,0)=0 \text{ for } r>a \tag{3.2}$$

$$u_z(r,0)=\delta \text{ for } r<a \tag{3.3}$$

where σ_{ij} $(i,j=r,\theta,z)$ are the components of the stress tensor, u_i are the components of the displacement vector, δ is the indentation depth, and a is the contact radius, which is the same as the radius of the indenter. Equation (3.1) represents frictionless contact between the indenter and the piezoelectric material, and Equation (3.2) indicates stress-free condition outside the contact zone. The indentation load, F, can be calculated from the force balance on the indenter as

$$F=-\int_0^{2\pi}\int_0^a \sigma_{zz}(r,0)rdrd\theta \tag{3.4}$$

where θ is the azimuth angle between a reference line and the r-axis.

The conditions at infinity require

$$u_r(r,z)=u_z(r,z)=0 \text{ and } \phi(r,z)=0 \text{ for } \sqrt{r^2+z^2}\to\infty \tag{3.5}$$

in which $\phi(r,z)$ is electrical potential.

Two types of indenters are used in the analysis: one is a perfectly electrical insulating indenter; the other is a perfectly conducting indenter, as follows.

Case I. Insulating indenter

The electric boundary condition on the surface of the piezoelectric material for the

indentation by an insulating indenter is

$$D_z(r,0) = 0 \text{ for } r \geq 0 \tag{3.6}$$

where D_z is the normal component of the electric displacement vector.

Case II. Conducting indenter

According to the direct piezoelectric effect, the indentation deformation will create an electric field in the piezoelectric material and a uniform electric potential over the contact zone by a conducting indenter [23]. The electric potential is dependent on the indentation depth to be determined from solving the indentation deformation. The electric boundary conditions on the surface of the piezoelectric material are

$$D_z(r,0) = 0 \text{ for } r > a \tag{3.7}$$

$$\phi(r,0) = \phi_c \text{ for } r < a \tag{3.8}$$

with ϕ_c being the indentation-induced electric potential on the indenter, which is to be determined from solving the contact deformation.

3.3 Finite element modeling

In the simulation, transversely isotropic piezoelectric materials are used since most polycrystalline and poled piezoelectric materials conform to this symmetry group [6]. Table 3.1 lists the material properties used in the simulation, which are referenced to the intrinsic material coordinate with the poling direction the same as the axisymmetric axis of the materials.

The indenter is modeled as a rigid surface, and the contact between the indenter and the piezoelectric material is assumed as frictionless. The bottom surface of the piezoelectric material is fixed and electrically grounded. Displacement-controlled indentation is used in the simulation. The indenter is gradually pushed onto the surface of the piezoelectric material to a preset depth, and then it is withdrawn until the load on the indenter becomes zero

The analysis of the indentation deformation uses the large elastic-plastic feature of the ABAQUS finite element code. The contact radius, *a*, between the indenter and the piezoelectric material is 100 nm. The piezoelectric material is modeled as a cylinder with 1000 nm in height and 1000 nm in radius, which is 10 times the contact radius. Under such a geometrical condition, the piezoelectric material can be approximately treated as semi-infinite. To avoid possible convergence problems arising from the sharp edge of the indenter, a rigid punch with a flat end but a round edge of 0.2 nm in radius is used, whose effect is negligible because of the ratio of the radius of the rounded edge to the diameter of the indenter being less than 1% [125,126]. The finite element mesh, shown in Figure 3.1, consists of 36297 8-node linear piezoelectric bricks with mesh refinement around the contact zone.

3.4 Results and discussion

3.4.1 Load-displacement relationship

From the indentation load-displacement curves, one can determine the contact stiffness and the contact modulus, which depend on the material properties. Figure 3.2 shows the variation of the indentation load with the indentation depth for the indentation of PZT-4 with various angles between the loading direction and the axisymmetric axis (the poling direction). The indentation load increases linearly with increasing the indentation depth, independent of the angle θ, while the ratio of F/δ depends on the angle θ and the type of indenters. It is interesting to note that the ratio of the indentation load to the indentation depth, F/δ, for $\theta=0^{\circ}$ is independent of the type of indenters, i.e. the indentation by a conducting indenter (case II) or by an insulating indenter (case I) produces the same indentation load-displacement curves when the loading direction is parallel to the axisymmetric axis.

Wang et al. [24] had summarized the relationship between the indentation load and the indentation depth for the axisymmetric indentation of transversely isotropic piezoelectric semi-infinite materials by an insulating indenter of flat end, which corresponds to the condition of $\theta=0^{\circ}$. The dependence of the indentation load on the

indentation displacement can be expressed as [12,24]

$$F = 4a\delta \frac{M_6 M_7 - M_5 M_8}{M_1 M_8 - M_2 M_7} \tag{3.9}$$

where M_i (i=1, 2, …, 8) are dependent on the material properties of the piezoelectric material [12,24]. Using the data in Table 3.1, one can obtain the dependence of the indentation load on the indentation depth as $F = 22.864 \times 10^{10} a\delta$ in which the units of a and δ are millimeters and the unit of F is Newton. For the same indentation depth, the percent difference of the indentation load between the results calculated from the finite element analysis and the analytical results is ~7%, suggesting that the finite element mesh is good enough for the 3D analysis of the Boussinesq indentation of a transversely isotropic piezoelectric material.

Figure 3.3 shows the variation of the ratio F/δ with the angle θ for the indentation of PZT-4 by conducting and insulating indenters. Independent of the type of indenters, the ratio starts with a maximum value at θ=0º, decreases to the minimum value at $\theta = 90º$, and then increases to the maximum value at θ=180º. The indentation response, i.e., the ratio of F/δ follows the same behavior for the angle of θ in the range of 180º to 360º. Generally, the ratio for the indentation by an insulating indenter is larger than that by a conducting indenter.

The simulation results for the indentation deformation of $BaTiO_3$ is also included in Figure 3.3 for the variation of F/δ with θ. Obviously, the dependence of F/δ with θ follows a similar trend. Thus, one might suggest that such behavior also applies to other transversely isotropic piezoelectric materials, and the relationship between the ratio F/δ of and θ (in the unit of degree) can be expressed as

$$\frac{F}{\delta} = 4a \frac{M_6 M_7 - M_5 M_8}{M_1 M_8 - M_2 M_7} f(\theta, c_{ij}, e_{ij}, \in_{ij}) \tag{3.10}$$

with $f(\theta, c_{ij}, e_{ij}, \in_{ij})$

$$f(\theta, c_{ij}, e_{ij}, \in_{ij}) = \alpha + \beta \cos\frac{\pi\theta}{90} \tag{3.11}$$

Here, α is a constant related to the indentation response of the piezoelectric material at θ=45˚ and β is a constant dependent on material properties and electric boundary conditions.

From Equation (3.10), the contact stiffness for the indentation of a transversely isotropic piezoelectric half-space by a rigid, cylindrical indenter of flat end can be calculated as

$$\frac{dF}{d\delta} = 4a\frac{M_6M_7 - M_5M_8}{M_1M_8 - M_2M_7}\left(\alpha + \beta\cos\frac{\pi\theta}{90}\right) = 4\sqrt{\frac{A}{\pi}}\frac{M_6M_7 - M_5M_8}{M_1M_8 - M_2M_7}\left(\alpha + \beta\cos\frac{\pi\theta}{90}\right) \tag{3.12}$$

where *A* is the contact area. The contact stiffness is proportional to the square root of the contact area, and the proportionality is dependent on the piezoelectric properties of materials and the electric boundary conditions. Equation (3.12) is the same as that for the indentation by a rigid, spherical indenter when θ=0º [12,127].

3.4.2 Electric potential-displacement relationship

The variation of the indentation-induced electric potential at the contact center with the indentation depth is shown in Figure 3.4 for the indentation of PZT-4 with various angles between the loading direction and the axisymmetric axis (the poling direction). Note that the electric potential within the contact region for the indentation by the conducing indenter is not pre-determined and is the same as the indentation-induced potential on the indenter. The indentation-induced potential linearly increases with increasing the indentation depth. For the same indentation depth, there is no difference between the indentation-induced potential in the contact zone by a rigid, conducting indenter and that at the contact center by a rigid, insulating indenter for all the angles shown in Figure 3.4.

Figure 3.5 shows the variation of the ratio ϕ/δ with the angle θ for the indentation of PZT-4 by conducting and insulating indenters. Obviously, the indentation-induced

potential at the contact center by a rigid, insulating indenter is the same as the indentation-induced potential on the conducting indenter. The reason can be explained by the closed-form solution of the electric potential that an insulating indenter creates a constant electric potential inside the contact area for flat-ended indenter [15,32], which is just the same electric potential constraint as that for conducting indenter. For the indentation of a transversely isotropic piezoelectric half-space by a rigid, insulating indenter, the indentation-induced potential over the contact zone can be expressed as [15, 32]

$$\phi = \delta \frac{M_3 M_8 - M_4 M_7}{M_1 M_8 - M_2 M_7} \tag{3.13}$$

which is independent of the radial variable and satisfies the condition of Equation (3.8). This suggests that the indentation-induced potential by a rigid, cylindrical indenter of flat end is insensitive to the type of indenters. Equation (3.13) can be used to describe the indentation-induced potential on the conducting indenter of flat end for the axisymmetric indentation of a transversely isotropic piezoelectric half-space.

As shown in Figure 3.5, the ratio ϕ/δ starts with a maximum value at $\theta=0^o$, decreases to the minimum value at $\theta=180^o$, and then increases to the maximum value at $\theta=360^o$. The simulation results for the indentation deformation of $BaTiO_3$ is also included in Figure 3.5 for the variation of ϕ/δ with θ. It can be seen that the variation of ϕ/δ with θ follows a similar trend as that for the indentation of PZT-4. Thus, such behavior might also apply to other transversely piezoelectric materials. Note that the sign of the ratio ϕ/δ changes from a positive value to a negative value when the relative direction between the poling direction and the loading direction changes from 0^o to 180°; and the ratio ϕ/δ is zero at $\theta=90^o$ and 270^o. As expected, the indentation-induced potential with the loading direction opposite to the poling direction has the same absolute magnitude as that with the loading direction the same as the poling direction. This is because the piezoelectric constants reverse their sign while the elastic and dielectric constants remain

unaltered due to polarization switching [2]. Based on the discussion, one can express the relationship between the ratio ϕ/δ and θ (in the unit of degree) as

$$\frac{\phi}{\delta} = \frac{M_3 M_8 - M_4 M_7}{M_1 M_8 - M_2 M_7} \cos\frac{\pi\theta}{180} \tag{3.14}$$

which can be used to quantify the relative direction between the loading axis and the poling direction from the indentation test.

3.5 Conclusion

Stress and electric field play an important role in controlling the electromechanical coupling of piezoelectric materials. A 3D finite element model was built to analyze the indentation behavior of a transversely isotropic piezoelectric half-space by a rigid, cylindrical indenter of flat end, aiming at examining the effect of the angle between the loading direction and the poling direction on the indentation response of piezoelectric materials. Two types of indenters were used in the analysis: one was a conducting indenter and the other an insulating indenter.

The finite element results reveal that both the indentation load and the magnitude of the indentation-induced potential linearly increase with increasing the indentation depth. The proportionality for the linear relationship between the indentation load and the indentation depth depends on the angle, type of indenters, and piezoelectric properties of materials. In contrast to the load-displacement relationship, the proportionality for the linear relationship between the indentation-induced potential and the indentation depth is only a function of the angle between the loading direction and the poling direction, independent of the type of indenters. Semi-analytical relationships as a function of the angle were established between the indentation load and the indentation depth and between the indentation-induced potential and the indentation depth. These relationships may be used in the indentation technique to measure the relative direction of the loading axis to the poling direction (axisymmetric axis) of transversely isotropic piezoelectric materials.

Table 3.1 Material properties defined in material coordinate

	PZT-4 [128,129]	$BaTiO_3$ [12]
Elastic coefficients (GPa)		
C_{11}	139	166
C_{12}	77.8	76.6
C_{13}	74.3	77.5
C_{33}	113	162
C_{44}	25.6	42.9
Piezoelectric coefficients (C/m^2)		
e_{31}	-6.98	-4.4
e_{33}	13.84	18.6
e_{15}	13.44	11.6
Dielectric constants (10^{-9} F/m)		
ε_{11}	6.0	11.151
ε_{33}	5.47	15.567

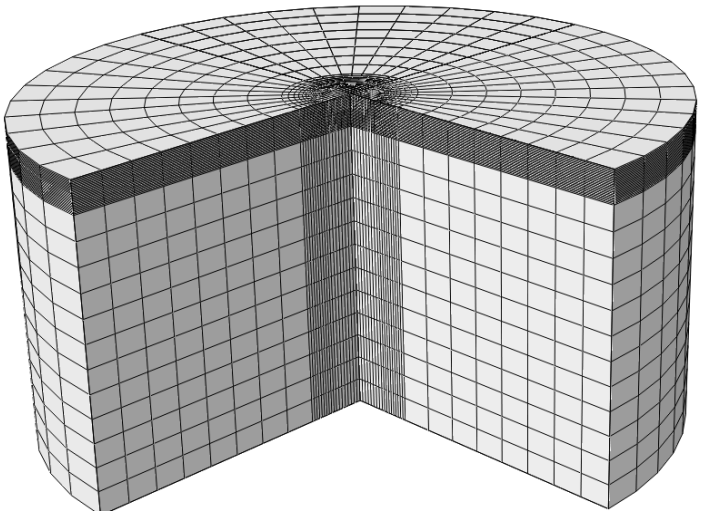

Figure 3.1 Finite element mesh for the indentation of a piezoelectric half-space

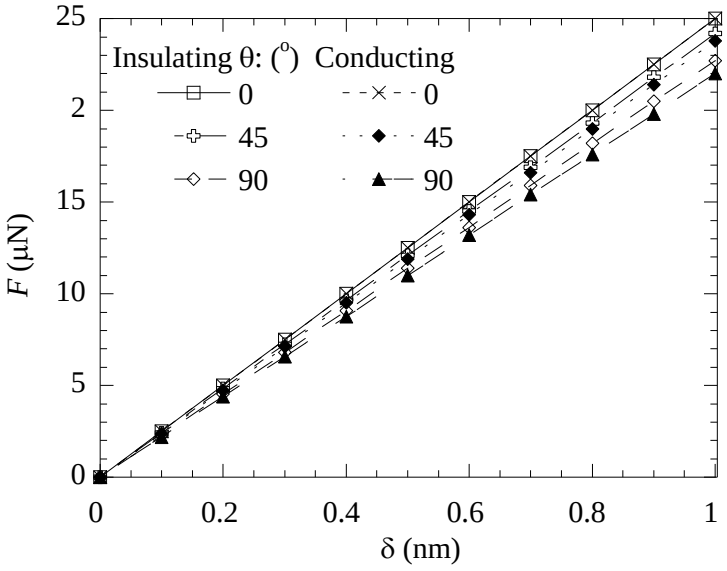

Figure 3.2 Dependence of the indentation load on the indentation depth for the indentation of PZT-4 with various angles between the loading direction and the poling direction

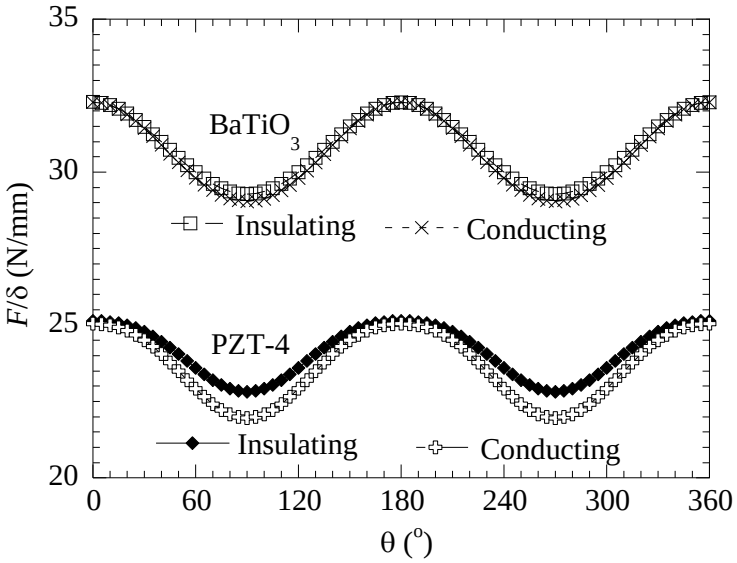

Figure 3.3 Variation of the ratio of F/δ with the angle θ for PZT-4 and $BaTiO_3$

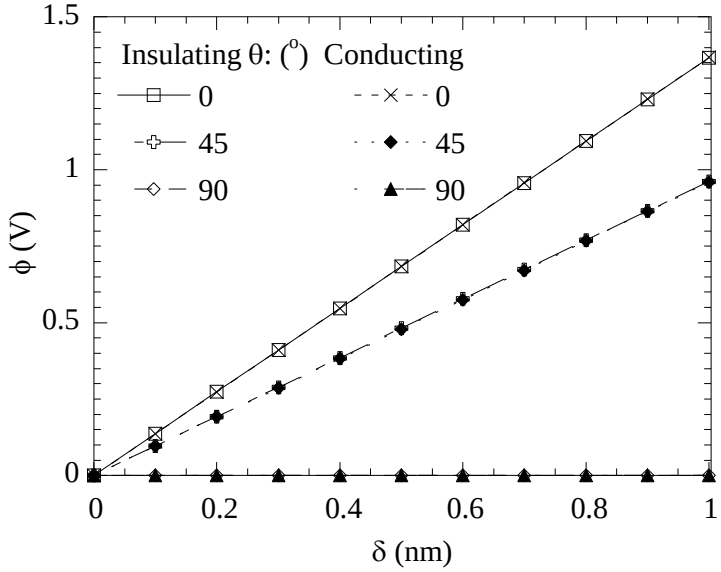

Figure 3.4 Dependence of the indentation-induced electric potential at the contact center on the indentation depth for the indentation of PZT-4 with various angles between the loading direction and the poling direction

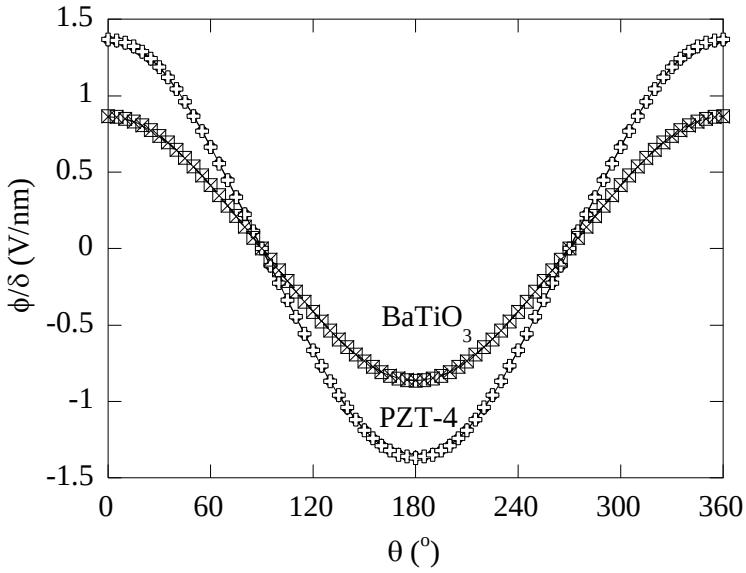

Figure 3.5 Variation of the ratio of ϕ/δ with the angle θ for PZT-4 and $BaTiO_3$

Chapter - 4 Berkovich indentation of a piezoelectric half space

4.1 Introduction

The sharp-instrumented nanoindentation is an effective technique for characterizing the mechanical properties of materials at small scales [6,44,117,118,116,119,130,131], including piezoelectric materials. Successful application of the indentation technique relies on the understanding of the contact mechanics of solids. Although closed-form solutions of the indentation deformation of transversely isotropic piezoelectric materials with the indentation direction being parallel to the axisymmetric axis of the materials have been well established [3,12,23,25,26,39,63], directional dependence of material properties and the coupling between electrical field and mechanical deformation have complicated the contact behavior of piezoelectric materials. This makes it very difficult, if not impossible, to obtain the closed-form solutions of stress and electric fields for the contact deformation of piezoelectric materials when there is an angle between the indentation direction and the axisymmetric axis of the materials. The physical meaning of the contact modulus calculated from the load-displacement curves also remains elusive for anisotropic materials.

There are only limited analytical solutions available for the contact deformation of homogeneous, transversely isotropic piezoelectric materials with the loading direction parallel to the axisymmetric axis of materials. Matysiak [63] used integral transformation to analyze the axisymmetric contact of a transversely isotropic piezoelectric half-space. Giannakopoulos and Suresh [12] followed Matysiak's approach [63] and summarized the load-displacement relationships for the axisymmetric indentation of a transversely isotropic piezoelectric half-space by a flat-ended indenter, a spherical indenter, and a conical indenter. Using the potential theory, Ding et al. [39] obtained analytical solutions of the stress and electric fields for the indentation of a transversely isotropic piezoelectric half-space by a spherical indenter, a conical indenter and an upright circular flat indenter. Yang [23] analyzed the electromechanical coupling between a compliant surface

electrode and a transversely isotropic piezoelectric half-space and discussed the field-induced stress singularity. Yang [3] used integral transformation to solve the deformation and electric fields in a transversely isotropic piezoelectric half-space by a rigid, conducting indenter of arbitrary-axisymmetric profile and obtained the contact stiffness, effective piezoelectric constant and electric displacement intensity factor. Wang and Chen [25] analyzed the indentation response of a piezoelectric film bonded to an elastic substrate by an axisymmetric indenter and reduced the indentation problem to the solution of a dual integral equation. Wu et al. [26] reduced the solution for the indentation of a piezoelectric film on an elastic film to a Fredholm integral equation of the second kind. Wang et al. [24] obtained the asymptotic relationships between the indentation load and the indentation depth for the indentation of a transversely isotropic piezoelectric film on a rigid substrate with the contact size much larger than the film thickness. Wang and Han [42] studied the indentation deformation of a piezoelectric layer by a flat-ended cylindrical indenter and numerically simulated the deformation of the piezoelectric layer indented.

FEM is an efficient technique to analyze the deformation behavior of piezoelectric materials. Giannakopoulos [1] performed the finite element simulation of the spherical indentation of piezoelectric materials while he misused zero electric potential on the axisymmetric axis. Kamble et al. [2] applied the same condition used by Giannakopoulos [1] in the finite element analysis of the spherical indentation of polycrystalline PZT-4. Liu and Yang [75] used the FEM to study the effect of surface electric conditions on the spherical indentation of transversely isotropic piezoelectric materials without applying electric condition to the axisymmetric axis and discussed the limitation of the indentation technique in characterizing the piezoelectric properties of materials. Using axisymmetric and 3-D finite element simulations, Zhao [82] recently studied the effect of poling direction and indenter size on the indentation of PZT-5H by a flat-ended cylindrical indenter in which only one case with the indentation direction being un-parallel to the

poling direction was shown. No detailed study was given to the effect of crystal orientation. Cheng and Venkatesh [83] numerically examined the effect of the indenter surface profile on the indentation response of various piezoelectric materials and the effect of the poling direction, which was limited to two directions (the indentation is either parallel or perpendicular to the axisymmetric axis.)

There is little report on the numerical analysis of the Berkovich indentation of piezoelectric materials. A better understanding of the pertinent issues on the application of the Berkovich indentation in characterizing the piezoelectric properties of materials needs to be elaborated before confident adoption. The purpose of this work is to use the FEM to analyze the Berkovich indentation of a transversely isotropic piezoelectric material in order to provide some insight into the contact deformation of piezoelectric materials. The study aimed to analyze the effect of the indentation direction related to the axisymmetric axis of the material on the relationship between indentation load and indentation depth and that between indentation-induced potential and indentation depth for the sharp-instrumented indentation.

4.2 Problem formulation

Consider the normal indentation of a linear piezoelectric half-space by a rigid, insulating Berkovich indenter. The piezoelectric material considered is transversely isotropic and homogeneous, and the angle between the loading axis (indentation direction) and the axisymmetric axis of the piezoelectric material is θ. The contact between the indenter and the piezoelectric half-space is assumed to follow Coulomb's friction law.

For transversely isotropic piezoelectric materials, the constitutive relations are

$$\sigma_{ij} = C^{E}_{ijkl}\varepsilon_{kl} - e_{ijk}E_k \tag{4.1}$$

$$D_i = e_{ikl}\varepsilon_{kl} + \in^{E}_{ij} E_j \tag{4.2}$$

where σ_{ij} (i, j = 1, 2, 3) are the components of stress tensor, ε_{ij} are the components of

strain tensor, D_i are the components of electric displacement vector, E_i are the components of electric field intensity, C_{ijkl}^{E} are the components of the elastic stiffness tensor measured in a constant electric field intensity, e_{ijk} are the components of the piezoelectric tensor measured in possession of a spontaneous electric field, and $\in_{ij}^{E}$ are the components of dielectric tensor. The relation between the components of the strain tensor ε_{ij} and the components of displacement vector u_i is

$$\varepsilon_{ij} = \frac{1}{2}\left(\frac{\partial u_i}{\partial x_j} + \frac{\partial u_j}{\partial x_i} \right) \tag{4.3}$$

and the relation between the components of the electric field intensity E_i and electric potential ϕ is

$$E_i = -\frac{\partial \phi}{\partial x_i} \tag{4.4}$$

The equilibrium equations are

$$\sum_{j=1}^{3} \frac{\partial \sigma_{ij}}{\partial x_j} = 0 \ \left(i = 1, 2, 3 \right) \tag{4.5}$$

Without any free electric charge in the piezoelectric material, there is

$$\frac{\partial D_1}{\partial x_1} + \frac{\partial D_2}{\partial x_2} + \frac{\partial D_3}{\partial x_3} = 0 \tag{4.6}$$

For the indentation problem of the transversely isotropic piezoelectric material ($x_3 > 0$) by a rigid Berkovich indenter, the mechanical boundary conditions outside the contact zone are

$$\sigma_{13}(x_1, x_2, 0) = \sigma_{23}(x_1, x_2, 0) = 0 \tag{4.7}$$

$$\sigma_{33}(x_1, x_2, 0) = 0 \tag{4.8}$$

Inside the contact zone, there are

$$\sqrt{\sigma_{13}^2(x_1, x_2, 0) + \sigma_{23}^2(x_1, x_2, 0)} = -\mu\sigma_{33}(x_1, x_2, 0) \text{ for } \sigma_{33}(x_1, x_2, 0) < 0 \tag{4.9}$$

$$u_3 = \delta - f(x_1, x_2, 0) \tag{4.10}$$

where μ is the friction coefficient, δ is the indentation depth, and $f(x_1, x_2, 0)$ is the surface profile of the indenter. Equation (4.9) represents the Coulomb friction between the indenter and the piezoelectric material, and Equations (4.7) and (4.8) indicates stress-free condition outside the contact zone. The indentation load can be calculated from the force balance on the indenter as

$$F = -\iint_A \sigma_{33}(x_1, x_2, 0) dA \tag{4.11}$$

where A is the contact area to be determined.

During the indentation, the contact area monotonically increases with increasing indentation depth. This requires $dF/d\delta > 0$ for $\delta > 0$.

The conditions at infinity require

$$u_1(x_1, x_2, x_3) = u_2(x_1, x_2, x_3) = u_3(x_1, x_2, x_3) = 0 \text{ for } \sqrt{x_1^2 + x_2^2 + x_3^2} \to \infty \tag{4.12}$$

$$\phi(x_1, x_2, x_3) = 0 \text{ for } \sqrt{x_1^2 + x_2^2 + x_3^2} \to \infty \tag{4.13}$$

For the indentation by an insulating indenter, the electric boundary condition on the surface of the piezoelectric materials is

$$D_3(x_1, x_2, 0) = 0 \tag{4.14}$$

4.3 Finite element modeling

3D analysis of the indentation deformation is performed in the ABAQUS finite element code of nonlinear deformation feature. A fixed Cartesian coordinate system (x_1,

$x_{2'}$, $x_{3'}$) is used with the $x_{3'}$ being parallel to the loading direction, and the other Cartesian coordinate system (x_1, x_2, x_3) is used for the piezoelectric material, which can rotate about the x_1-axis with the x_3-axis being the axisymmetric axis of the material. The x_1-axis coincides with the $x_{1'}$-axis, and the angle between the $x_{3'}$-axis and the x_3-axis is θ. At θ= 0º, the coordinate system ($x_{1'}$, $x_{2'}$, $x_{3'}$) coincides with the system (x_1, x_2, x_3).

The Berkovich pyramid indenter of an ideal shape with a sharp tip and a face angle of 65.27º (or inclined angle of 24.73º) is used in the simulation. The reasons for using an ideal shape are: (1) the surface images of the impressions are usually triangular in appearance rather than circular although there is a blunt tip [132]; (2) the surface profile of the blunted tips due to wear is still under debate and effects of tip radii on the indentation response of materials remain uncertain due to their complexities and the inhomogeneous wear of the tip [133]; (3) the effect of the tip rounding or offset on the error of contact area and the measured contact modulus and hardness values becomes insignificant with increasing indentation depth [134], and ideal Berkovich indenter represents the real indenter very well if the indentation depth reaches 1 μm [135].

The piezoelectric material is modeled as a cylinder with a radius of 50 μm and a thickness of 30 μm. The maximum indentation displacement is 1 μm; under this condition the piezoelectric material can be essentially treated as semi-infinite. The bottom surface is fixed and electrically grounded to ensure the far field conditions. Surface-to-surface "hard" contact is defined between the indenter as the master surface and the sample surface as the slave surface. Displacement-controlled indentation is used in the simulation. The finite element mesh, shown in Figure 4.1, consists of 179580 8-node linear piezoelectric bricks with mesh refinement around the contact zone.

Table 4.1 lists the material properties [136,137] used in the simulation, which are referenced to the coordinate system of (x_1, x_2, x_3), in which both elastic constants and piezoelectric constants are presented in the matrix form instead of the tensor form.

4.4 Results and discussion

4.4.1 Electric potential-displacement relationship

To examine the electromechanical interaction during the indentation, the indentation-induced potential at the contact center between the indenter and the piezoelectric half-space is monitored. Figure 4.2 shows the variation of the indentation-induced potential with the indentation depth for various angles between the loading direction and the axisymmetric axis (the poling direction) and frictionless contact ($\mu = 0$). The indentation-induced potential increases with increasing the indentation depth for all the angles shown in the figure, while the proportionality between the indentation-induced potential and the indentation depth is dependent on the angle between the loading direction and the axisymmetric axis (the poling direction).

Figure 4.3 shows the variation of the ratio $\phi(0,0,0)/\delta$ with the angle θ for the indentation of PZT-4 with frictionless contact. The dependence of the electromechanical interaction on the angle θ is obvious. The magnitude of the indentation-induced potential at the contact center reaches the maximum value at θ=0º and 180º, while it reaches the minimum value of 0 at θ=90º and 270º. The sign of the induced electric potential depends on the relative direction between the loading direction and the poling direction (axisymmetric axis). This is because the piezoelectric constants reverse their sign while the elastic and dielectric constants remain unaltered due to polarization switching [2].

The simulation results for the indentation deformation of $(Ba_{0.917}Ca_{0.083})TiO_3$ is also included in Figure 4.3 for the variation of $\phi(0,0,0)/\delta$ with θ. Obviously, the variation of $\phi(0,0,0)/\delta$ with θ follows a similar trend as that for the indentation of PZT-4. It is expected that such behavior might also apply to other transversely isotropic piezoelectric materials. From Figure 4.3, one can express the relationship between the ratio of

$\phi(0,0,0)/\delta$ and θ (in the unit of degree) as

$$\frac{\phi(0,0,0)}{\delta} = \frac{\phi_0}{\delta_0}\cos\frac{\pi\theta}{180} \tag{4.15}$$

for the indentation of a transversely isotropic piezoelectric half-space by a rigid, insulating Berkovich indenter with the frictionless contact. Here, ϕ_0 and δ_0 are the indentation-induced potential at contact center and the indentation depth, respectively, for the indentation with θ=0º. Similar relation also has been obtained for the indentation of transversely isotropic piezoelectric materials by a rigid, conducting or insulating indenter of flat end [138].

To examine the effect of the contact friction on the indentation-induced potential at the contact center, the Coulomb friction law is used. Figure 4.4 shows the variation of the indentation-induced potential at contact center with the indentation depth for two friction coefficients of 0 and 0.5 with the loading being parallel and anti-parallel to the axisymmetric axis (the poling direction). The contact friction does not change the linear dependence of the indentation-induced potential on the indentation depth, while the proportionality depends on the friction coefficient.

Figure 4.5 shows the effect of the contact friction on the ratio of $\phi(0,0,0)/\delta$ for the Berkovich indentation of PZT-4 with the loading direction the same as the poling direction (i.e., θ=0º). The ratio increases from 1.32 for frictionless to 1.40 for the friction coefficient larger than or equal to 0.35. There is about 6% difference, which suggests that the effect of contact friction on the electromechanical interaction for the Berkovich indentation of transversely isotropic piezoelectric materials is negligible. One can use the results from the frictionless contact to approximately calculate the electromechanical behavior during the indentation.

It has been believed that conical indentation is equivalent to pyramidal indentation provided that the volume-to-depth relationship is the same [139]. The indentation deformation created by the Berkovich indenter can be approximated as that by a conical indenter of half included angle of 70.3º for elastic-plastic materials. It is unclear if the

equivalence can also be used to describe the electromechanical behavior occurring in the indentation deformation of transversely piezoelectric materials.

Figure 4.6 shows the variation of the indentation-induced potential at the contact center with the indentation depth for the indentation of PZT-4 with θ=0º by a rigid, insulating conical indenter of half included angle of 70.3º and a rigid, insulating Berkovich indenter. A good coincidence between the Berkovich and its equivalent conical indentations can be seen. The proportionality between the indentation-induced potential at the contact center and the indentation depth is independent of the type of indenters, suggesting that the depth-potential relationship at the contact center for the indentation of PZT-4 with θ=0º by a rigid, insulating conical indenter of 70.3º is equivalent to that by the Berkovich indenter.

For the indentation of a transversely isotropic piezoelectric half-space by a rigid, insulating conical indenter, the indentation-induced potential at the contact center for $\theta = 0^\circ$ can be expressed as [3,12, 24]

$$\phi(0,0,0) = \delta \frac{M_3 M_8 - M_4 M_7}{M_1 M_8 - M_2 M_7} \tag{4.16}$$

where M_i (i=1, 2, …, 8) are dependent on the material properties of the piezoelectric material [3,12, 24]. Substituting Eq. (4.16) in Eq. (4.15) yields

$$\frac{\phi(0,0,0)}{\delta} = \frac{M_3 M_8 - M_4 M_7}{M_1 M_8 - M_2 M_7} \cos\frac{\pi\theta}{180} \tag{4.17}$$

which describes the dependence of the ratio of the indentation-induced potential at the contact center to the indentation depth on the relative angle between the loading direction and the poling direction for the indentation of transversely isotropic piezoelectric materials by a rigid, insulating Berkovich indenter.

4.4.2 Load-displacement relationship

Figure 4.7 shows the indentation load-displacement curves for three different angles of 0º, 45º and 90º between the loading direction and the poling direction. The load-displacement curves are similar to each other. The indentation with the angle of 0º

between the loading direction and the poling direction requires the largest indentation load to produce the same indentation depth.

It is known that the indentation load is proportional to the square of the indentation depth for the indentation of a semi-infinite transversely isotropic piezoelectric material with $\theta=0^{o}$ by a rigid, conical indenter [3,12,24,39]. One would expect that a similar relationship holds for the Berkovich indentation of a semi-infinite transversely isotropic piezoelectric material with $\theta\neq0^{o}$. Using the best curve-fitting to fit the load-displacement curves shown in Figure 4.7, one obtains

$$F = K\delta^2 \tag{4.18}$$

for all three angles. Here, K is a prefactor depending on the material properties and the relative direction between the loading direction and the poling direction. The quadratic dependence of the indentation load on the indentation depth is a natural consequence of the geometric self-similarity of the indenter. Nevertheless, it is worth mentioning that the quadratic dependence is only applicable to linear elastic deformation including linear elasticity, linear piezoelectricity, and linear magnetoelasticity for the indentations by conical and pyramidal indenters. For nonlinear elasticity and elastic-plastic deformation, the indentation load is a power function of the indentation depth with the exponent not equal to 2. For example, two-dimensional and 3D finite element simulations and experiments of the Berkovich indentation of fused silica had showed the exponent of 1.46 [140].

Figure 4.8 depicts the variation of the prefactor K with the angle between the loading direction and the poling direction for the Berkovich indentation of PZT-4. The simulation results for the indentation deformation of $(Ba_{0.917}Ca_{0.083})TiO_3$ is also included in the figure. Larger indentation load for the indentation of $(Ba_{0.917}Ca_{0.083})TiO_3$ is required than that for PZT-4 to produce the same indentation depth, which is consistent with the experimental observation and numerical results for spherical indentation [1,68]. Such behavior is due to higher elastic moduli of $(Ba_{0.917}Ca_{0.083})TiO_3$ than those of PZT-4. Independent of the piezoelectric materials, the prefactor K starts with a maximum value at $\theta=0^{o}$, decreases to a minimum value at $\theta=90^{o}$, and then increases to the maximum

value at θ=180º. The indentation response follows the same behavior for the angle of θ in the range of 180 to 360º. One expects that the prefactor *K* for the conical indentation with a half included angle of 70.3º is the same as that for the Berkovich indentation, since the finite element simulation of the conical indentation of PZT-4 with θ=0º and 90º gives $K(0^\circ)/K(90^\circ)=167.78/152.25\approx 1.10$, the same as $K(0^\circ)/K(90^\circ)\approx 1.10$ for the Berkovich indentation of PZT-4.

From Figure 4.8, one might suggest the dependence of the prefactor *K* on the angle θ should also apply to other transversely isotropic piezoelectric materials. Using the relationship between the indentation load and the indentation depth for the conical indentation of semi-infinite transversely isotropic piezoelectric materials with θ=0º [12,3,24,39], one has

$$\frac{F}{\delta^2}=\frac{4}{\pi}\frac{M_6M_7-M_5M_8}{M_1M_8-M_2M_7}\tan 70.3^\circ\, f(\theta,c_{ij},e_{ij},\in_{ij}) \tag{4.19}$$

with $f(\theta,c_{ij},e_{ij},\in_{ij})$ as

$$f(\theta,c_{ij},e_{ij},\in_{ij})=\alpha+\beta\cos\frac{\pi\theta}{90} \tag{4.20}$$

Here, α is a constant related to the indentation response of the piezoelectric material at θ=45º and β is a constant dependent on material properties.

From Equation (4.20), one can calculate the contact stiffness for the Berkovich indentation of a semi-infinite transversely isotropic piezoelectric material as

$$\frac{dF}{d\delta}=\frac{8\delta\tan 70.3^\circ}{\pi}\frac{M_6M_7-M_5M_8}{M_1M_8-M_2M_7}\left(\alpha+\beta\cos\frac{\pi\theta}{90}\right) \tag{4.21}$$

It is known that the contact area is proportional to the square of the indentation depth (see below for discussion). Thus, the contact stiffness is proportional to the square root of the contact area (or the indentation depth).

Figure 4.9 shows the contact zone between the Berkovich indenter and the semi-infinite PZT-4 at the indentation depth of 1 μm for two angles of 0º and 90º. The

contact edges of the contact zone form a triangle with the characteristics of an equilateral triangle, independent of the relative angle between the loading direction and the poling direction. The zigzag edges at the contact edges are due to the discrete finite element mesh. From Figure 4.9, it is reasonable to assume that the projected contact area for the Berkovich indentation is an equilateral triangle. Thus, the relationship between the projected contact area A_p and the true contact area A can be expressed as [141]

$$A_p = A\cos\left(90^\circ - 65.27^\circ\right) = 3\sqrt{3}\delta_c^2 \tan^2 65.27^\circ \tag{4.22}$$

where δ_c is the contact depth.

The evaluation of the contact area is of paramount importance in characterizing the mechanical properties of materials for the sharp-instrumented indentation. Figure 4.10 shows the variation of the true contact area with the indentation depth for the Berkovich indentation of PZT-4 and $(Ba_{0.917}Ca_{0.083})TiO_3$ with θ=0º, 45 º and 90º. The contact area scales with the square of the indentation depth; and there is no observable effect of the relative direction between the loading direction and the poling direction and the anisotropy of the piezoelectric material.

Using the best curve-fitting and the relation between the projected contact area and the true contact area, one obtains

$$A_p = 9.0\delta^2 \tag{4.23}$$

which is consistent with the result given by Giannakopoulos [142] for the Berkovich indentation of isotropic, linear elastic materials. The contact topology within the realm of elasticity and piezoelectricity is solely dependent on geometrical configuration, including the indenter geometry and the unformed surface profile of materials.

The effect of the angle θ on the dependence of the contact depth on the indentation depth is also examined. The FEM results show that the contact depth is proportional to the indentation depth, as expected, and independent of the angle θ. The proportionality is 0.61, which is slightly smaller than 0.65 for the conical indentation of the same piezoelectric materials.

Substituting Equation (4.23) into Equation (4.21), one has

$$\frac{dF}{d\delta} = \frac{8\sqrt{A_p}\tan 70.3^o}{3\pi}\frac{M_6M_7 - M_5M_8}{M_1M_8 - M_2M_7}\left(\alpha + \beta\cos\frac{\pi\theta}{90}\right) \tag{4.24}$$

4.5 Conclusion

The sharp-instrumented indentation technique has been gradually used to characterize the electromechanical response of piezoelectric materials. A 3D finite element model was built to analyze the indentation behavior of a transversely isotropic piezoelectric half-space by a rigid, insulating Berkovich indenter, aiming at examining the anisotropic effect and establishing the semi-analytical relationship between the indentation load and the indentation depth, and between the indentation-induced potential and the indentation depth.

The finite element results revealed that the indentation load was proportional to the square of the indentation depth. Using the analytical result for the indentation of a transversely isotropic piezoelectric half-space with the loading direction parallel to the poling direction, a semi-analytical relationship between the indentation load and the indentation depth was obtained. The pre-factor for the relationship between the indentation load and the indentation depth depends on the angle and the piezoelectric properties of materials. In contrast to the load-displacement relationship, the indentation-induced potential at the contact center is proportional to the indentation depth. The proportionality is only a function of the angle between the loading direction and the poling direction, independent of the type of indenters. These relationships may be used in the indentation technique to measure the relative direction of the loading axis to the poling direction (axisymmetric axis) of transversely isotropic piezoelectric materials.

Table 4.1 Material properties used in the simulation

	PZT-4	$(Ba_{0.917}Ca_{0.083})TiO_3$
Elastic coefficients (GPa)		
C_{11}	139	158
C_{12}	77.8	69
C_{13}	74.3	67.5
C_{33}	115	150
C_{44}	25.6	45
Piezoelectric coefficients (C/m^2)		
e_{31}	-5.2	-3.1
e_{33}	15.1	13.5
e_{15}	12.7	10.9
Dielectric constants (10^{-9} F/m)		
ε_{11}	6.461	8.850
ε_{33}	5.620	8.054

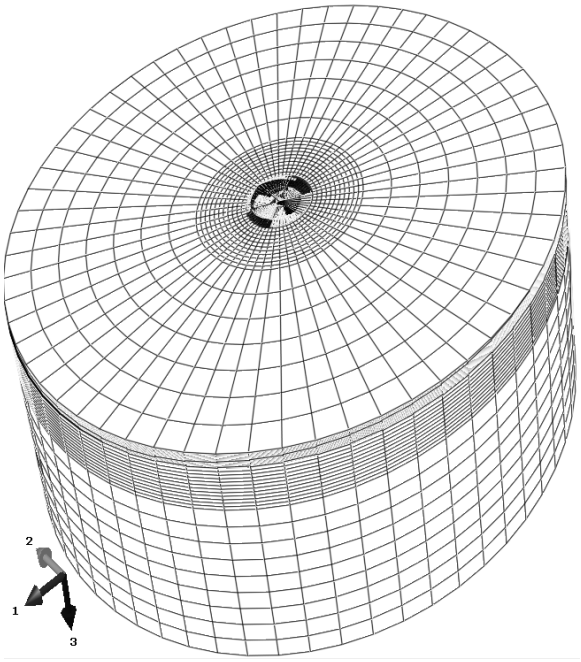

(a)

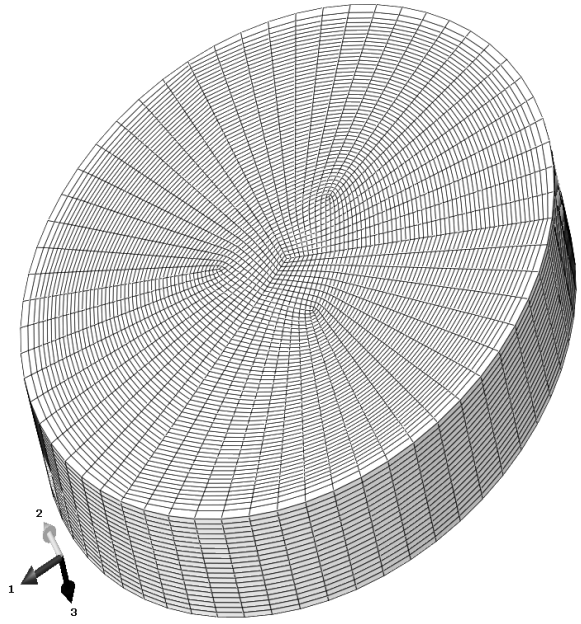

(b)

Figure 4.1 (a) Finite element mesh used in the simulation (b) mesh refinement around the contact zone

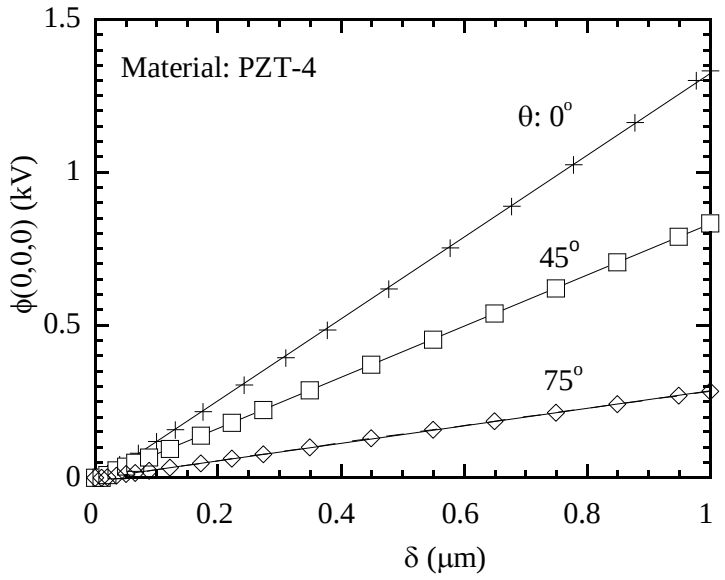

Figure 4.2 Variation of the indentation-induced potential at the contact center with the indentation depth for various angles between the loading direction and the poling direction (material: PZT-4, μ=0)

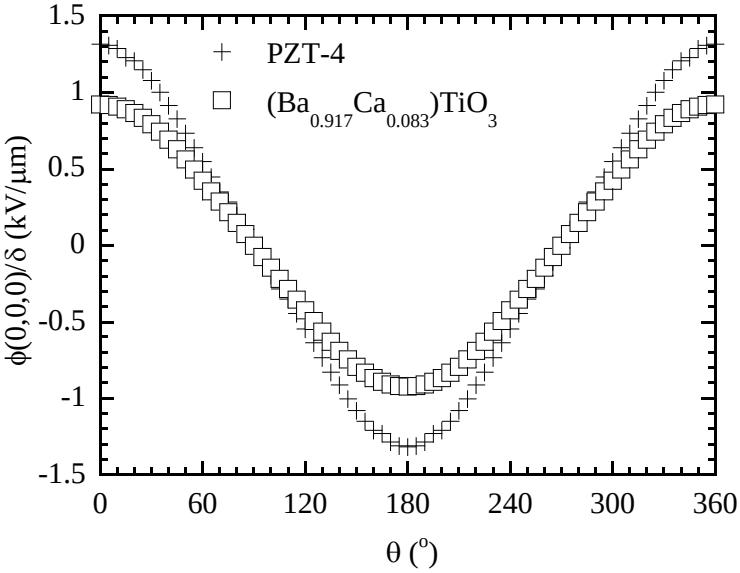

Figure 4.3 Variation of the ratio of $\phi(0,0,0)/\delta$ with the angle θ for PZT-4 and $(Ba_{0.917}Ca_{0.083})TiO_3$, μ=0

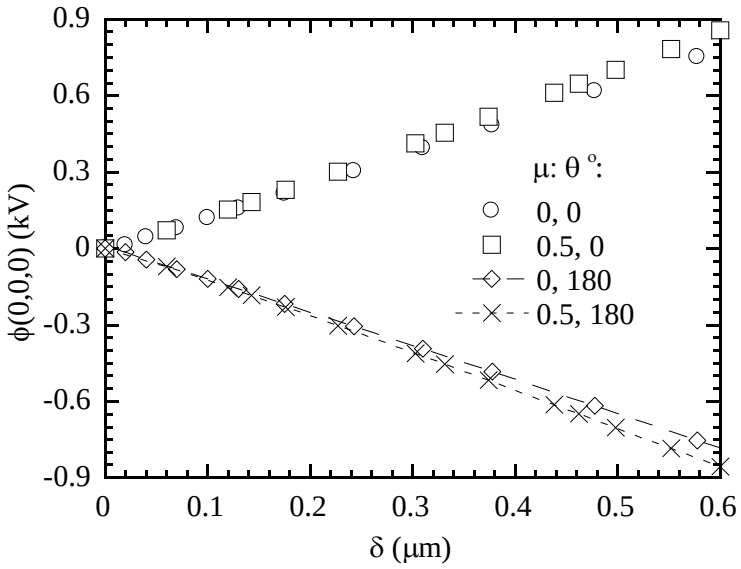

Figure 4.4 Variation of the indentation-induced potential with the indentation depth for the Berkovich indentation of PZT-4 with friction coefficients of 0 and 0.5 and the angles of 0º and 180º

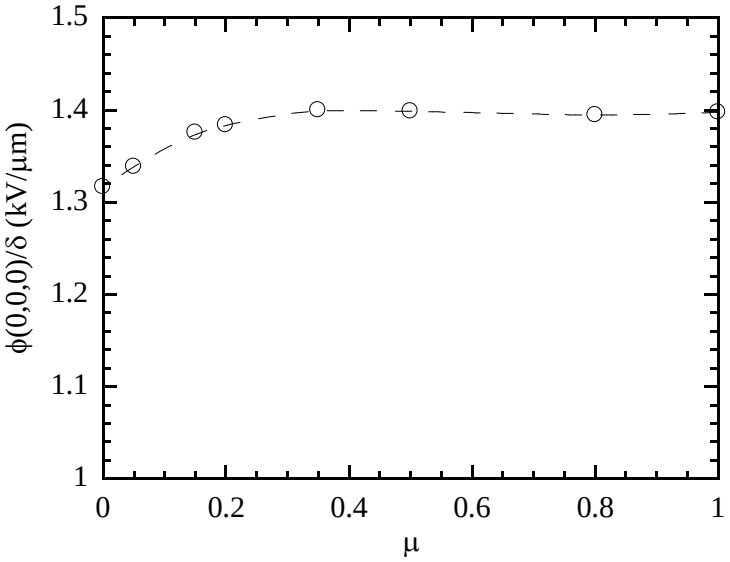

Figure 4.5 Effect of the contact friction on the proportionality between the indentation-induced potential and the indentation depth for the indentation of PZT-4 by a rigid, insulating Berkovich indenter with the loading direction the same as the poling direction

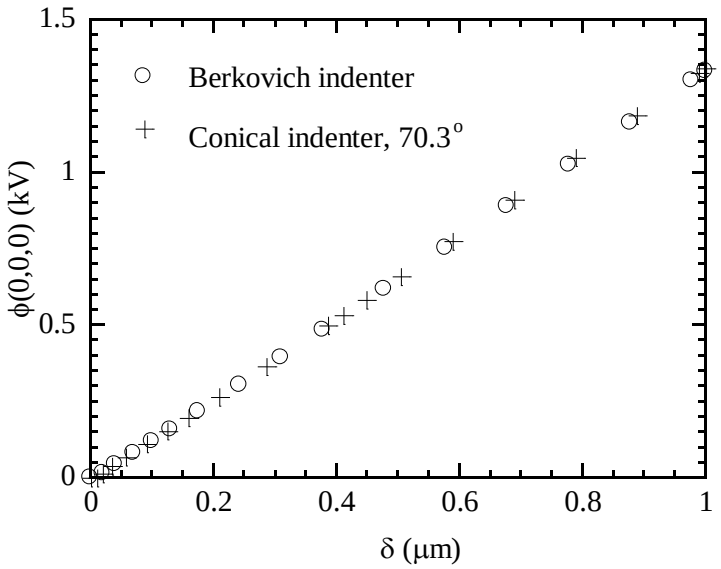

Figure 4.6 Comparison of the indentation-induced potential at the contact center for the indentation of PZT-4 with θ=0˚ by a rigid, insulating Berkovich indenter and a rigid, insulating conical indenter, μ=0

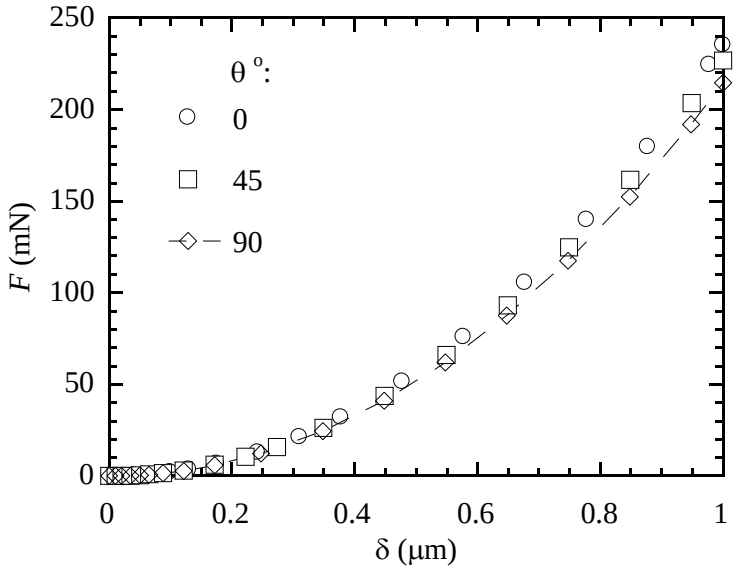

Figure 4.7 Indentation load-displacement curves for the indentation of PZT-4 with three different angles of 0º, 45º and 90º between the loading direction and the poling direction, μ=0

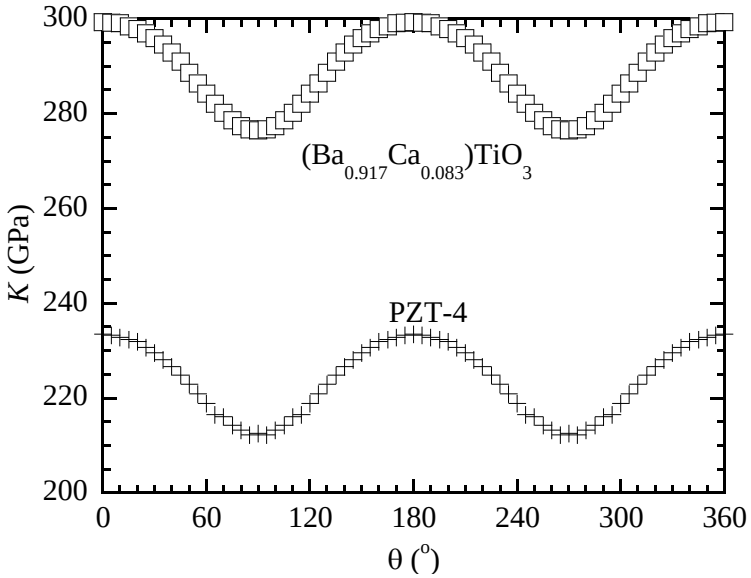

Figure 4.8 Dependence of the pre-factor *K* on the angle θ for PZT-4 and $(Ba_{0.917}Ca_{0.083})TiO_3$, μ=0

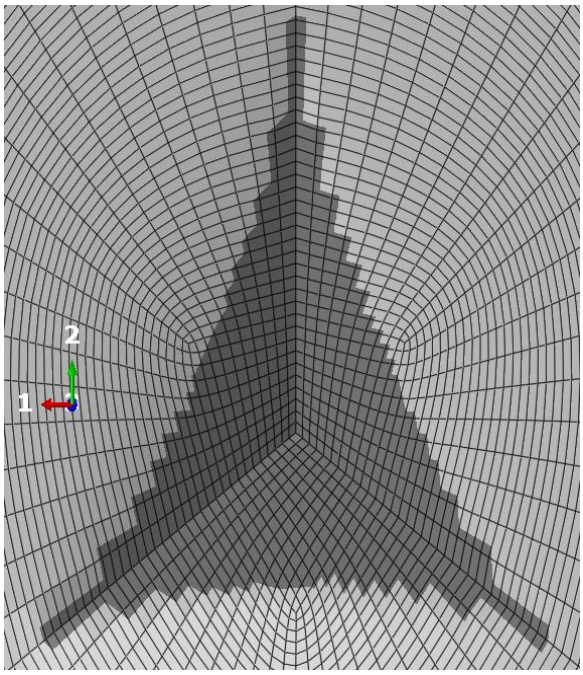

(a)

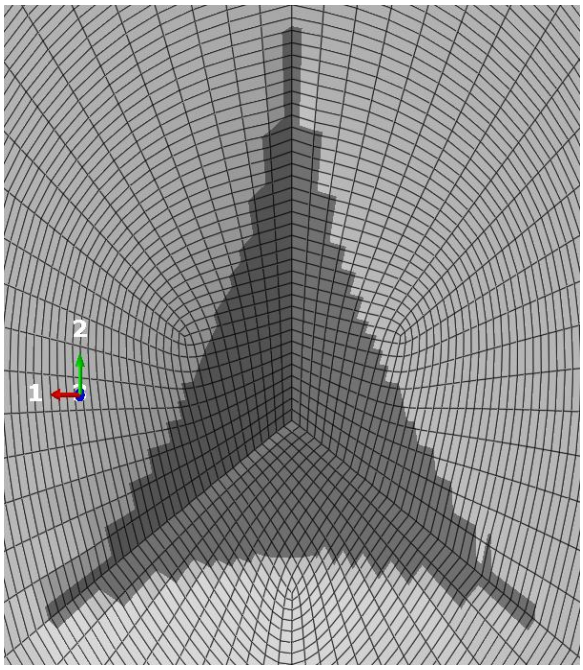

(b)

Figure 4.9 Topology of the contact zone between the indenter and PZT-4 for the Berkovich indentation with the maximal indentation depth of 1 μm (μ=0): (a) θ=0º, and (b) θ=90º

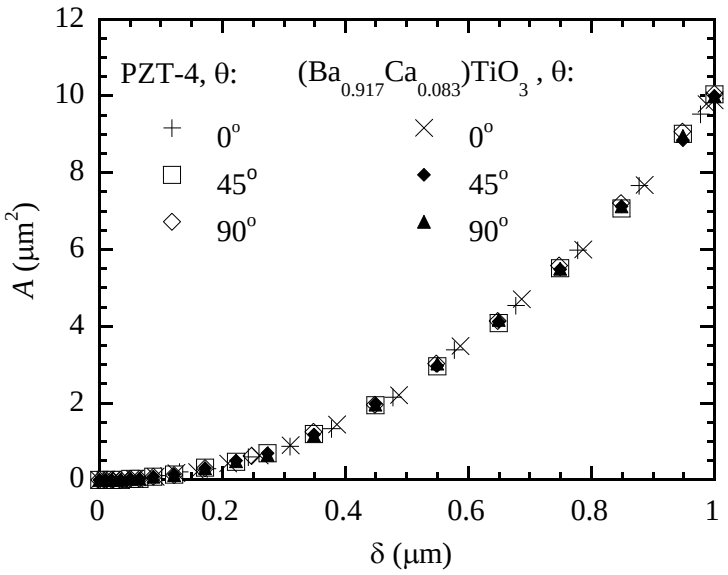

Figure 4.10 Dependence of the true contact area on the indentation depth for the indentation of PZT-4 and $(Ba_{0.917}Ca_{0.083})TiO_3$ with three different angles of 0º, 45º, and 90º between the loading direction and the poling direction

Chapter - 5 Indentation of piezoelectric thin films

5.1 Introduction

Piezoelectric materials with the characteristics of electromechanical coupling are available in a variety of shapes and forms, such as films [143,144,145], multi-layers [146], and fibers [147,148,149,150] for various sensor and actuator applications in functional structures and smart systems [151,152,153,154,155]. Accurate determination of the material behavior of piezoelectric materials at the small scale is vital for the applications in microelectromechanical and nanoelectromechanical systems. The instrumented indentation technique, which has been used to determine the mechanical properties of small structures and thin films, is believed to be capable of characterizing the mechanical as well as electrical properties of piezoelectric materials [2,6,10,11,66].

To date, most analytical and numerical studies have focused on the indentation of a piezoelectric half space [3,4,12,21,39,42,61,63,156,157,158,159]. However, compared to the indenter size and the specimen thickness, piezoelectric films have finite thickness rather than infinite thickness in engineering and biomechanical applications. Simplified solutions can be obtained when the contact radius is much larger than the film thickness [9,24,100,160,161,162]. Thus, it is desirable to probe the material properties of piezoceramics by indenting piezoelectric thin films, in which the contact radius is far greater than the film thickness.

Using the Hankel transform and a conducting indenter, Matysiak [63] was the first to study the axisymmetric contact of a piezoelectric half-space. Following Matysiak's approach [63], Giannakopoulos and Suresh [12] presented a general solution for the axisymmetric indentation of a piezoelectric half-space. Although their analytical solutions have the same structures as those given by Chen et al. [61], Kalinin et al. [4], and Wang at al. [24], they are numerically different. Wang et al. [24] studied the indentation of piezoelectric films and suggested that the expressions given by Giannakopoulos and Suresh [12] are problematic. In addition, the boundary condition with zero normal stress at the edge of contact zone [12] is inapplicable for a flat-ended indenter, since there is stress singularity [163]. Sridhar et al. [66] performed the normal indentation of a transversely isotropic, linear piezoelectric half-space by a conducting sphere with zero potential bias and found that the indentation response of piezoelectric materials depended on electric boundary conditions. Yang [3] derived the contact stiffness, effective piezoelectric constant, and the electric displacement intensity factor for the axisymmetric indentation of a semi-infinite piezoelectric material by a rigid, conducting indenter of arbitrary-axisymmetric profile and found that analytical solutions cannot be obtained for certain combinations of material properties of piezoelectric materials. Ding et al. [39] solved the elastic and electric fields for a series of axisymmetric contact problems, including pressing a spherical indenter, a conical indenter and an upright circular flat indenter onto a transversely isotropic piezoelectric half-space. Yang [23] analyzed the electromechanical interaction between a compliant surface electrode and a semi-infinite piezoelectric material. Wang and Han [42] used frictionless conditions between a piezoelectric layer and a rigid substrate to numerically simulate the deformation of the piezoelectric layer indented by a flat-ended cylindrical indenter. Kamble et al. [2] simulated the spherical indentation of polycrystalline PZT-4 and misused the zero electric potential condition on the axial axis in the finite element analysis. Liu and Yang [75]

carried out finite element simulation of spherical indentation of a transversely isotropic piezoelectric half space under different electrical boundary conditions and found that the electrical boundary condition has significant effects on the induced electric potential and charge, stress distribution, and indentation load.

Motivated by the practical application of piezoelectric films and the need to have a better understanding of the indentation behavior of piezoelectric films, a systematic finite element analysis of the spherical indentation of a piezoelectric film is carried out. The focus is on the effect of electric boundary conditions on the contact deformation of piezoelectric films with the contact radius much larger than the film thickness. The dependence of the electric response on the indentation deformation is also discussed.

5.2 Problem formulation

5.2.1 Equilibrium equations

Consider the indentation of a transversely isotropic piezoelectric film of thickness *t* by a rigid spherical indenter of radius *R*. As shown in Figure 5.1, the piezoelectric film is supported by a rigid substrate with non-slip condition. A cylindrical polar coordinate system $(r,\ \theta,\ z)$ is used with z-axis being parallel to the poling direction. The *r*-axis is perpendicular to the *z*-axis, and θ is the azimuth angle between a reference line and the *r*-axis. In the absence of body and inertia forces, the equilibrium equations for the axisymmetric problem are

$$\frac{\partial \sigma_{rr}}{\partial r} + \frac{\partial \sigma_{rz}}{\partial z} + \frac{\sigma_{rr} - \sigma_{\theta\theta}}{r} = 0 \tag{5.1}$$

$$\frac{\partial \sigma_{rz}}{\partial r} + \frac{\partial \sigma_{zz}}{\partial z} + \frac{\sigma_{rz}}{r} = 0 \tag{5.2}$$

and in the absence of free electric charge in the piezoelectric film, the electrostatic equation is

$$\frac{\partial D_r}{\partial r}+\frac{\partial D_z}{\partial z}+\frac{D_z}{r}=0 \tag{5.3}$$

where σ_{rr}, σ_{zz}, $\sigma_{\theta\theta}$ and σ_{rz} are the components of stress tensor, and D_r and D_z are the components of electric displacement vector.

For linear transversely isotropic piezoelectric materials with poling direction being parallel to the *z*-axis, the constitutive equations in the absence of any thermal or residual polarization strains with conventional notations are

$$\begin{pmatrix} \sigma_{rr} \\ \sigma_{\theta\theta} \\ \sigma_{zz} \\ \sigma_{rz} \\ D_r \\ D_z \end{pmatrix} = \begin{pmatrix} C_{11} & C_{12} & C_{13} & 0 & 0 & -e_{31} \\ C_{12} & C_{11} & C_{13} & 0 & 0 & -e_{31} \\ C_{13} & C_{13} & C_{33} & 0 & 0 & -e_{33} \\ 0 & 0 & 0 & C_{44} & -e_{15} & 0 \\ 0 & 0 & 0 & e_{15} & \in_{11} & 0 \\ e_{31} & e_{31} & e_{33} & 0 & 0 & \in_{33} \end{pmatrix} \begin{pmatrix} \varepsilon_{rr} \\ \varepsilon_{\theta\theta} \\ \varepsilon_{zz} \\ \gamma_{rz} \\ E_r \\ E_z \end{pmatrix} \tag{5.4}$$

where C_{11}, C_{12}, C_{13}, C_{33}, and C_{44} are elastic constants measured in a constant electric field intensity (short circuited condition); e_{15}, e_{31}, and e_{33} are piezoelectric constants measured in possession of a spontaneous electric field; $\in_{11}$ and $\in_{33}$ are dielectric constants measured with no mechanical constraint. The subscript "3" denotes the properties along the poling direction; subscripts "1" and "2" denote those along two-mutually orthogonal directions in the plane perpendicular to the poling direction.

The relationships between the components of strain tensor (ε_{rr}, $\varepsilon_{\theta\theta}$, ε_{zz}, and ε_{rz}) and the components of the displacement vector (u_r and u_z) are

$$\varepsilon_{rr}=\frac{\partial u_r}{\partial r},\ \varepsilon_{\theta\theta}=\frac{u_r}{r},\ \varepsilon_{zz}=\frac{\partial u_z}{\partial z},\ \text{and}\ \gamma_{rz}=2\varepsilon_{rz}=\frac{\partial u_r}{\partial z}+\frac{\partial u_z}{\partial r} \tag{5.5}$$

and the relationships between the components of electric field intensity (E_r and E_z)

and electric potential (ϕ) are

$$E_r = -\frac{\partial \phi}{\partial r}, \text{ and } E_z = -\frac{\partial \phi}{\partial z} \tag{5.6}$$

The indentation load can be determined from the force balance on the indenter as

$$F = -2\pi \int_0^a \sigma_{zz}(r,0) r dr \tag{5.7}$$

During the indentation, the contact radius monotonically increases with the indentation load. This requires $dF/dh > 0$ for $h > 0$.

The conditions at infinity require

$$u_r(r,z) = u_z(r,z) = 0 \text{ and } \phi(r,z) = 0 \text{ for } \sqrt{r^2 + z^2} \to \infty \tag{5.8}$$

5.2.2 Mechanical boundary conditions

For the contact problem of a transversely isotropic piezoelectric film ($-t < z < 0$, t is the film thickness) by a rigid, spherical indenter, the mechanical boundary conditions are

$$u_z(r,0) = h - f(r) \text{ for } 0 \le r < a \tag{5.9}$$

$$\sigma_{zz}(r,0) = 0 \text{ for } r > a \tag{5.10}$$

where h is the indentation depth of the indenter, a is the contact radius, and $f(r)$ is the surface profile of the indenter. For an indentation by a rigid spherical indenter of radius R with $a << R$, there is

$$f(r) \approx \frac{r^2}{2R} \tag{5.11}$$

For frictionless contact between the indenter and the film, the shear stress is zero, i.e.

$$\sigma_{rz}(r,0) = 0 \tag{5.12}$$

The nonslip contact between the film and the rigid substrate gives

$$u_z(r,-t) = u_r(r,-t) = 0 \tag{5.13}$$

The condition determining the contact radius a is

$$\sigma_{zz}(a,0) = 0 \tag{5.14}$$

5.2.3 Electrical boundary conditions

Two types of indenters are used in the finite element analysis. They are:

Case I: Insulating indenter

The electric boundary condition on the surface of the piezoelectric material for the indentation by an insulating indenter is

$$D_z(r,0) = 0 \quad \text{for } r \geq 0 \tag{5.15}$$

Case II: Conducting indenter

For a conducting indenter without prescribed electric potential, the electric potential within the contact region is a constant. The electric boundary condition on the surface of the piezoelectric material becomes

$$D_z(r,0) = 0 \quad \text{for } r > a \tag{5.16}$$

$$\frac{\partial \phi(r,0)}{\partial r} = 0 \quad \text{for } r < a \tag{5.17}$$

For a grounded conducting indenter, one has

$$\phi(r,0) = 0 \quad \text{for } r < a \tag{5.18}$$

which has technological significance for the application of the sharp-instrumentation indentation in characterizing the properties of piezoelectric materials

The indentation-induced electric charge, Q_p, within the contact area on the top surface of the piezoelectric film can be calculated by integrating the vertical component

of the electric displacement, $D_z(r,0)$, within the contact area as

$$Q_p = 2\pi\int_0^a rD_z(r,0)dr \tag{5.19}$$

which gives the total charge accumulated in the conducting indenter as

$$Q_i = -2\pi\int_0^a rD_z(r,0)dr \tag{5.20}$$

For an insulating substrate, there is

$$D_z(r,-t) = 0 \tag{5.21}$$

and for a grounded substrate

$$\phi(r,-t) = 0 \tag{5.22}$$

There are six possible combinations of the electric boundary conditions (II, IG, CI, CG, GI, and GG). The II corresponds to the insulating indenter and the insulating substrate, IG to the insulating indenter and the grounded substrate, CI to the conducting indenter without prescribed electric potential and the insulating substrate, CG to the conducting indenter without prescribed electric potential and the grounded substrate, GI to the grounded indenter and the insulating substrate, and GG to the grounded indenter and the grounded substrate.

It needs to be emphasized that the simulation focuses on the contact radius being much larger than the film thickness, and there is no transfer of free charges between the indenter and the piezoelectric film.

The distribution of electric field depends on the geometrical morphology of a material. Puglisi and Zurlo [164] analyzed the effect of surface curvature on electric field localization in thin dielectric films and obtained an approximate expression for the electric field. Yang and Song [165,166] analyzed the field-induced surface instability of a conducting material with a sinusoidal surface topology by analyzing the effect of the sinusoidal surface on the field and stress distribution. Generally, one needs to include the

effect of local curvature on the electric field in the analysis. However, the analysis of the indentation deformation is based on the linear theory of piezoelectricity, which requires that the boundary conditions, including the electric boundary conditions, be referenced to the undeformed state. In numerical calculations, such as finite element simulation, the electric boundary conditions are actually satisfied at each increment.

5.3 Finite element modeling

To simulate the indentation deformation, the nonlinear deformation feature in the ABAQUS finite element code is used. Transversely isotropic piezoelectric materials, which have axisymmetric features about the poling direction, are used. The material properties of PZT-4 [23] given in Table 5.1 are used in the simulation. The rigid indenter of 500 μm in radius is modeled by a rigid, analytical surface. The dimensions of the piezoelectric material used in the simulation are 200 μm in radius and 0.5 μm in thickness. The maximum indentation depth of 50 nm is only 10% of the film thickness which avoids any severe deformation that may introduce depolarization or cracking during indentation; the indentation depth of 50 nm is believed to be non-destructive to the sample.

Due to the symmetric features, an axisymmetric model is used. Figure 5.2 shows the finite element mesh near the contact zone. The finite element mesh consists of 125,708 four-node axisymmetric piezoelectric elements. Finer meshes are used near the contact region. The surface of the sphere is automatically smoothed to reduce the inaccuracy in calculating the contact stress. Along the interface, the contact elements are used to monitor the change of the contact zone during the indentation. For the conducting indenter or substrate, the nodes within the contact region or on the interface are constrained by the equal electric potential; for the grounded conducting indenter or substrate, the nodes within the contact region or on the interface are constrained with zero electric potential.

A displacement-controlled indentation is used in the simulation. The indenter is

gradually pushed onto the surface of the piezoelectric material to a preset indentation depth, and then it is withdrawn until the load on the indenter becomes zero. During the indentation, the equal-potential condition for indentation by a conducting indenter is checked at each increment to ensure that the nodes in contact with the conducting indenter have the same electric potential.

5.4 Results and discussion

5.4.1 Mechanical response

The contact radius is a function of the indentation depth, and the closed-form solutions of the contact radius for the indentation of thin films with $t \ll a \ll R$ have been obtained for only two cases. Wang et al. [24] obtained the dependence of the contact radius on the indentation depth for the indentation of a transversely isotropic piezoelectric film by an insulating indenter with a grounded, rigid substrate as

$$a = \sqrt{2Rh} \tag{5.23}$$

and for the indentation of a piezoelectric film by a conducting indenter of potential ϕ_0 with a grounded, rigid substrate as

$$a = \sqrt{2R(h + \frac{e_{33}}{C_{33}}\phi_0)} \tag{5.24}$$

Equation (5.24) reduces to Equation (5.23) for a grounded, conducting indenter, i.e., $\phi_0 = 0$. Figure 5.3 shows the variation of the contact radius with the indentation depth for all six different combinations of electrical boundary conditions. The overlap of the curves indicates the variation of the contact radius with the indentation depth for the spherical indentation of a piezoelectric film is independent of the electric boundary conditions given in section 5.2. Under the condition that $h/t \geq 0.01$, the simulation results show that the relationship between the contact radius, *a*, and the indentation depth, *h*, can be well described by Equation (5.23), while for $h/t < 0.01$, Equation (5.23)

overestimates the contact radius due to the constraint of $a \gg t$. At $h/t = 0.01$, $a = 4.78 \times 10^{-3} R = 4.78t$. This result suggests that Equation (5.23) can be used to determine the contact radius from the indentation depth when $a \geq 4.78t$.

For the spherical indentation of a piezoelectric half-space, the relationship between the contact radius and the indentation depth is [3]

$$a = \sqrt{Rh} \tag{5.25}$$

which is independent of the type (i.e., the electrical boundary condition) of the indenter (e.g., insulating, electrically grounded, or conducting). For the purpose of comparison, Equation (5.25) is also included in Figure 5.3. It can be seen that Equation (5.25) describes the indentation depth-contact radius relationship very well for a semi-infinite medium so that $h << t$ and $a << t$.

The indentation load-depth relationship has been used to determine the reduced contact modulus for the instrumentation indentation technique. According to the results given by Wang et al. [24], the relationship between the indentation load and the indentation depth is

$$F = (C_{33} + \frac{e_{33}^2}{\in_{33}}) \frac{\pi R h^2}{t} \tag{5.26}$$

for the indentation of a transversely isotropic piezoelectric film by an insulating indenter with a grounded substrate (i.e. the IG case), and

$$F = C_{33} \frac{\pi R h^2}{t} \tag{5.27}$$

for the indentation by a grounded, conducting indenter with a grounded substrate (i.e. the GG case). Independent of the electric boundary conditions, the indentation load is proportional to the indenter radius and the square of the indentation depth and inversely proportional to the film thickness, which is similar to the results given by Yang [160,161] for the spherical indentation of compressible, elastic films with the contact radius much

larger than the film thickness. The effect of the electric boundary conditions is represented by the coefficients.

Figure 5.4 shows the indentation load-depth curves for all six different combinations of electrical boundary conditions. For comparison, the results calculated from Equations (5.26) and (5.27) are also included. The finite element results are in agreement with the analytical results for the corresponding boundary conditions. The electric boundary conditions have some effect on the dependence of the indentation load on the indentation depth, since the curves slightly differ from one another. The indentation load in general increases with the square of the indentation depth for all six cases under the simulation conditions. To produce the same indentation depth, the smallest indentation load is needed for the indentation by a grounded, conducting indenter with a grounded substrate, while the largest indentation load is needed for the indentation by an insulating indenter with an insulating substrate. Comparison of the dependence of the indentation load on the indentation depth for all six cases reveals that the force responses can be divided into two categories; one is associated with the grounded and conducting indenter, and the other is related to the indentation by an insulating indenter or a conducting indenter without prescribed potential.

It is worth mentioning that the finite element analysis of the spherical indentation of a transversely isotropic piezoelectric half-space by a conducting or an insulating indenter has been performed by using the ABAQUS finite element code [75]. The simulation results are in accord with the results given by the analytical relationships between the indentation load and the indentation depth as summarized by Wang et al. [24] and given by Ding et al. [39], which have validated the finite element code used in this work.

From Equations (5.26) and (5.27) and the simulation results shown in Figure 5.4, one can express the relationship between the indentation load and the indentation depth for all six cases as

$$F = \chi \frac{\pi R h^2}{t} \tag{5.28}$$

where χ is a function of the material properties of piezoelectric materials and the electric boundary conditions. Equation (5.28) gives the contact stiffness, *S*, as

$$S = \frac{dF}{dh} = 2\chi \frac{\pi R h}{t} = \frac{\chi A}{t} \tag{5.29}$$

for the spherical indentation of transversely isotropic piezoelectric films with the contact radius much larger than the film thickness. Here, $\chi = C_{33} + e_{33}^2 / \in_{33}$ for the indentation by an insulating indenter with a grounded substrate and $\chi = C_{33}$ for the indentation by a grounded, conducting indenter with a grounded substrate. The contact stiffness is proportional to the contact area *A* and inversely proportional to the film thickness in contrast to the result for the spherical indentation of semi-infinite piezoelectric materials. Equation (5.29) provides an approach to measure the electromechanical properties of piezoelectric films by controlling the electric boundary conditions.

For the indentation of a transversely isotropic piezoelectric film with the contact size much larger than the film thickness, the distribution of normal stress over the contact area ($0 \le r \le a$) is [24]

$$\sigma_{zz}(r,0) = -(c_{33} + \frac{e_{33}^2}{\in_{33}}) \frac{a^2 - r^2}{2Rt} = -(c_{33} + \frac{e_{33}^2}{\in_{33}}) \frac{2Rh - r^2}{2Rt} \tag{5.30}$$

for the spherical indentation by an insulating indenter with a grounded substrate (i.e. the case of IG), and

$$\sigma_{zz}(r,0) = -\frac{c_{33}(a^2 - r^2)}{2Rt} = -\frac{c_{33}(2Rh - r^2)}{2Rt} \tag{5.31}$$

for the spherical indentation by a grounded indenter with a grounded substrate (i.e. the case of GG). Both the stress distribution in the contact zone is a quadratic function of the

radial variable r. Figure 5.5 shows the finite element results of the distribution of the normal stress in the contact zone for all six cases with the maximum indentation depth of 50 nm. For comparison, the analytical results of Equations (5.30) and (5.31) are also included in Figure 5.5. For the spherical indentation by an insulating indenter or a grounded indenter with a grounded substrate, the magnitudes of the normal stress obtained from the FEM simulation are in accord with the corresponding analytical results for $r/t \geq 7$ and slightly larger than the corresponding analytical results for $r/t < 7$. Such behavior is due to the condition used in deriving Equations (5.30) and (5.31) which requires $a/t >> 1$, even though it has no significant effect on the load-displacement relationship. As shown in Figure 5.5, the piezoelectric material experiences compressive stress, as expected, with the maximum compressive stress being at the contact center. For the same indentation depth and the spherical indenter of the same size, the indentation by an insulating indenter with an insulating, rigid substrate produces the largest compressive stress in the contact zone, while the indentation by a grounded indenter with a grounded, rigid substrate produced the smallest compressive stress. Due to the singularity of electric field, the indentation by the conducting indenter creates a stress singularity at the contact edge, which likely will lead to structure damage.

5.4.2 Electrical response

The dependence of the indentation-induced electric potential at the contact center on the indentation depth is depicted in Figure 5.6. The magnitude of the electric potential at the contact center increases with increasing the indentation depth, which is in accordance with the mechanism of piezoelectric behavior. For the same indentation depth, the indentation by the insulating indenter with a grounded, rigid substrate induces the largest electric potential at the contact center, while the indentation of the piezoelectric film by the conducting indenter with an insulating, rigid substrate induces the smallest electric potential. These results suggest that the electric boundary conditions determine the electric response of the piezoelectric film during indentation. For $h/t \geq 0.2$, the

indentation-induced electric potential at the contact center is a linear function of the ratio h/t for any contact radius larger than the film thickness, i.e.

$$\phi_c = \alpha + \kappa \frac{h}{t} \tag{5.32}$$

where ϕ_c is the electric potential at the contact center, and α and κ are constants depending on the material properties and the electric boundary conditions. Through the best curve-fitting, one can calculate the constants of α and κ from the FEM results. For the indentation by a conducting indenter without a prescribed potential, the indentation-induced potential on the indenter then can be calculated from Equation (5.32) if the constants α and κ have been determined from the numerical calculation or from the indentation test of piezoelectric films by characterizing the variation of the contact potential with the indentation depth.

According to the definition of piezoelectric charge coefficients, d_{ij}, [167], there is

$$d_{ij} = \frac{\partial \varepsilon_j}{\partial E_i} \tag{5.33}$$

in which ε_j is the matrix representation of ε_{ij} with $\varepsilon_1 = \varepsilon_{11}$, $\varepsilon_2 = \varepsilon_{22}$, $\varepsilon_3 = \varepsilon_{33}$, $\varepsilon_4 = 2\varepsilon_{23}$, $\varepsilon_5 = 2\varepsilon_{13}$, and $\varepsilon_6 = 2\varepsilon_{12}$. For the indentation of piezoelectric films by the conducting indenter with the grounded substrate and the contact radius much larger than the film thickness, the compressive strain underneath the indenter can be approximated as

$$\varepsilon_3 \approx -\frac{h}{t-h} \tag{5.34}$$

and the magnitude of the electric field intensity as

$$E_3 \approx \frac{\phi_c}{t-h} = \frac{\alpha}{t-h} + \frac{\kappa}{t}\frac{h}{t-h} = \frac{\alpha}{t-h} + \frac{\kappa}{t}\varepsilon_3 \tag{5.35}$$

Substituting Equations (5.34) and (5.35) into Equation (5.33) and using the condition

of $h << t$, the piezoelectric charge coefficient, d_{33}, can be determined by

$$d_{33} \approx -\frac{t}{\kappa} \approx -\left(\frac{d\phi_c}{dh}\right)^{-1} \tag{5.36}$$

The nominal piezoelectric charge coefficients as determined from the indentation of a piezoelectric film by a conducting indenter with a grounded, rigid substrate and the contact radius much larger than the film thickness is inversely proportional to the derivative of the electric potential with respect to the indentation depth.

Due to the electromechanical coupling in piezoelectric materials, the indentation deformation by the conducting indenter will polarize the piezoelectric material and lead to an accumulation of electric charges on the conducting indenter. The total charge accumulated on the surface of the conducting indenter can be calculated from Equation (5.20).

Figure 5.7 shows the variation of the total charge on the indentation depth for the indentation by the conducting indenter. The total electric charge increases with increasing the indentation depth due to the piezoelectric coupling. For the same indentation depth, the largest total charge accumulated on the conducting indenter is induced when the indenter is electrically grounded, while the smallest total charge is induced for the indentation with a perfectly insulating substrate. It can be seen that the electric boundary conditions play an important role in controlling the accumulation of electric charges on the conducting indenter.

For the indentation of the piezoelectric film with a grounded substrate, the simulation results shown in Figure 5.7 suggests that, for $h/t \geq 10^{-3}$, the total charge accumulated on the conducting indenter is a power function of the ratio of h/t. Using the best curve-fitting, one obtains

$$Q_i = \beta\left(\frac{h}{t}\right)^n \tag{5.37}$$

with n=2 for the indentation by a grounded indenter with a grounded substrate and n=1.5 for the indentation by a conducting indenter without prescribed potential and with a grounded substrate. Here β is a constant depending on the material properties and the electric boundary conditions.

Using the result given by Wang et al. [24] for the grounded indenter and the grounded substrate with the poling direction being anti-parallel to the loading direction, the total charge is found to be

$$Q = \frac{e_{33}\pi R}{t} h^2 \tag{5.38}$$

For comparison, the calculated results from Equation (5.38) are also included in Figure 5.7. Obviously, the simulation results are in agreement with those calculated from Equation (5.38) for $h/t \geq 10^{-2}$. For the spherical indentation of piezoelectric films by a grounded, conducting indenter with a grounded substrate and the contact radius much larger than the film thickness, Equation (5.38) can be used to determine the piezoelectric constant e_{33}.

For the indentation by a grounded indenter with a grounded, rigid substrate and a>>t, one can use the result given by Wang et al. [24] to obtain the distribution of the normal component of the electric displacement in the contact zone as

$$D_z(r,0) = \mp \frac{\left(a^2 - r^2\right) e_{33}}{2Rt} \text{ for } 0 \leq r \leq a \tag{5.39}$$

in which the sign of ± depends on the relative direction between the loading direction and the poling direction (axisymmetric axis). For the current configuration with the loading direction anti-parallel to the poling direction, the "–" is used in Equation (5.39). The normal component of the electric displacement is quadratic function of the radial variable r. Figure 5.8 depicts the distribution of the normal component of the electric

displacement for all the six different boundary conditions with the maximum indentation depth of 50 nm. For comparison, the results obtained from Equation (5.39) are also included in Figure 5.8, which is slightly less than the FEM results near the contact center, while there is good agreement in the region away from the contact center.

For the indentation by an insulating, rigid indenter, the normal component of the electric displacement is zero, as expected. There exists a transition of the normal component of the electric displacement from negative value to positive value for the other four types of electric boundary conditions of CI, CG, GI, and GG. The field singularity is observable for the indentation by a conducting indenter due to non-zero potential on the indenter, which leads to the stress singularity at the contact edge as shown in Figure 5.5. It is worth mentioning that the field singularity has not been reported for the indentation of piezoelectric films, even though the same behavior has been observed from the finite element simulation of semi-infinite piezoelectric materials by Liu and Yang [75].

Figure 5.9 shows the distribution of electric potential on the contact surface between the indenter and the piezoelectric film for all the six electric boundary conditions with the maximum indentation depth of 50 nm. The electric potential for the grounded indenter is zero in the contact zone, as expected. The distribution of electric potential depends on the electrical boundary conditions. The indentation by the conducting indenter produces uniform, non-zero electric potential on the contact surface. The magnitude of the indentation-induced potential is a function of the electric condition of the rigid substrate with the grounded substrate generating larger magnitude of electric potential than that by the insulating substrate. Non-uniform electric potential is created for the indentation by the insulating indenter, which is relatively independent of the electric condition of the substrate.

The above analyses have established the rationale of using the sharp-instrumented indentation to characterize the complicated electromechanical interaction of piezoelectric

films. The load-displacement relationship and the load-potential relationship can be used to quantify the piezoelectric behavior of piezoelectric films similar to the work by Kollosche and Kofod [168] in using the contact technique to examine the dependence of the breakdown strength of soft elastomers on Young's modulus. Careful comparison between the FEM results and experimental results will be explored in the future.

5.5 Conclusion

Finite element analysis of the indentation deformation of piezoelectric films with the properties of PZT-4 by a rigid spherical indenter revealed the effects of different electric boundary conditions on the mechanical and electrical responses of piezoelectric thin films. When the contact radius is much larger than the film thickness, six different combinations of the electric boundary conditions between the indenter and the film, and between the film and the substrate, were used to investigate the effect of electric boundary conditions on the electrical and mechanical responses of the piezoelectric film.

The indentation load was found to be proportional to the square of the indentation depth for all six cases. The indentation by a grounded conducting indenter and a grounded substrate produces the smallest indentation load, while the indentation under an insulating indenter and an insulating substrate produces the largest indentation load, under the same indentation depth. For $h/t \geq 0.01$, the contact radius is proportional to the square root of the indentation depth and is independent of the electric boundary conditions. A simple formula was established to calculate the contact stiffness, which is proportional to the contact area and inversely proportional to the film thickness, unlike the spherical indentation of semi-infinite piezoelectric materials.

For $h/t \geq 0.02$, the indentation-induced electric potential at the contact center is a linear function of the ratio of h/t, when the contact radius is larger than the film thickness, with the slope κ dependent on the electric conditions. For the indentation by a conducting indenter with a grounded substrate and $h/t \geq 10^{-3}$, the total charge

accumulated on the indenter is a power function of the ratio of h/t. The nominal piezoelectric charge coefficient d_{33} is inversely proportional to the derivative of the electric potential with respect to the indentation depth for the indentation of piezoelectric films by a conducting indenter with a grounded rigid substrate.

Table 5.1 Material properties of PZT-4 piezoceramics

Elastic constant (10^{10} Nm^{-2})					Piezoelectric constant (Cm^{-2})			Dielectric constant (10^{-10} CV^{-1} m^{-1})	
C_{11}	C_{12}	C_{13}	C_{33}	C_{44}	e_{31}	e_{33}	e_{15}	$\in_{11}$	$\in_{33}$
13.9	7.78	7.43	11.3	2.56	-6.98	13.84	13.44	60.0	54.7

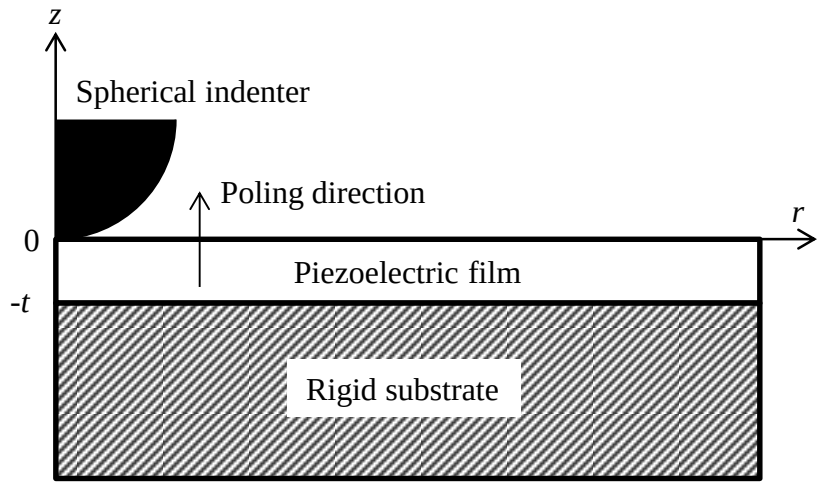

Figure 5.1 Schematic of the spherical indentation of a piezoelectric film on a rigid substrate

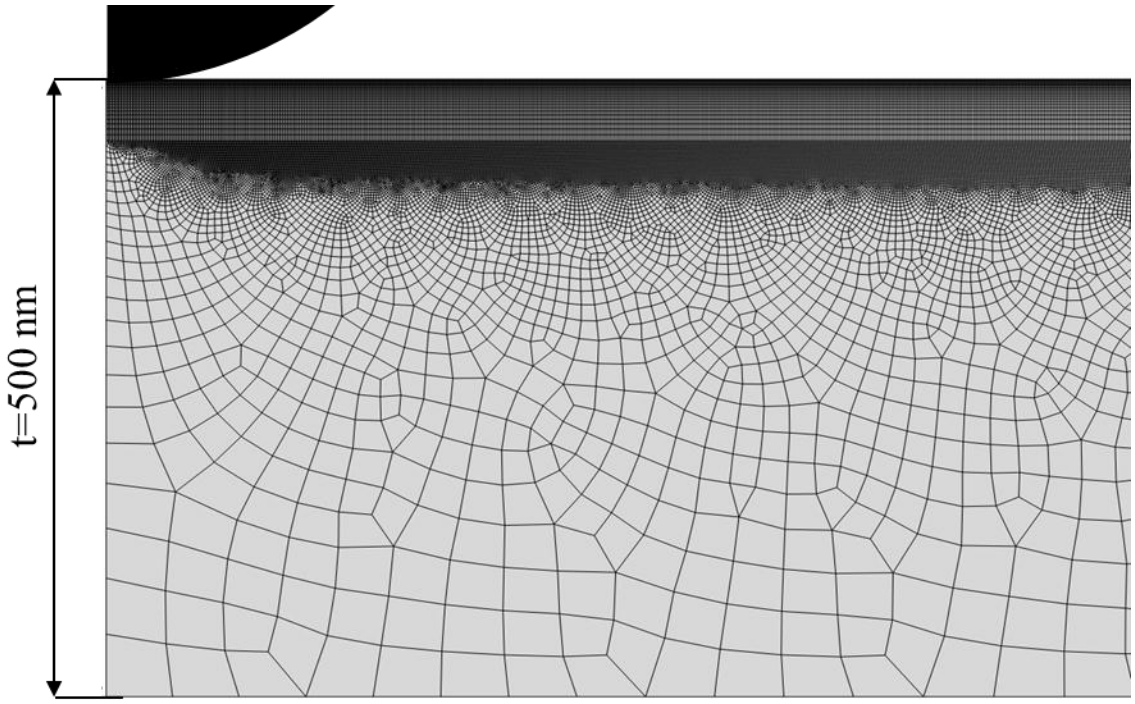

Figure 5.2 Finite element mesh of the spherical indentation

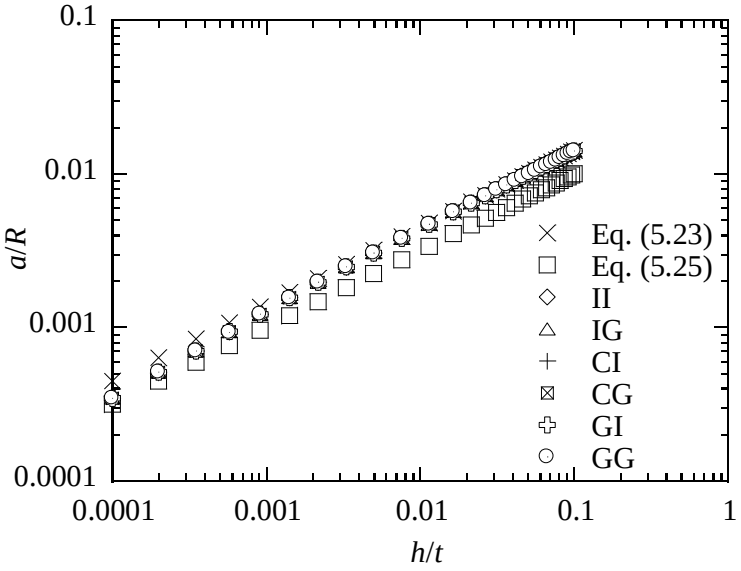

(a)

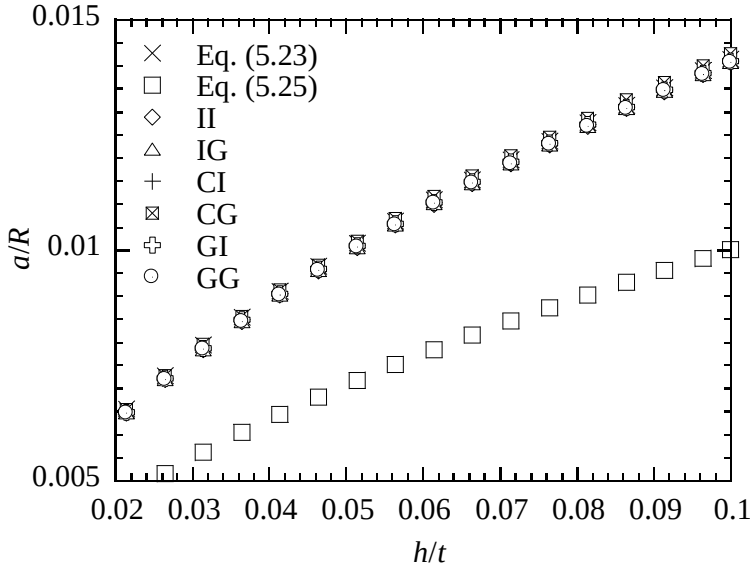

(b)

Figure 5.3 (a) Variation of the contact radius with the indentation depth for six different electric boundary conditions; (b) enlarged view of the contact radius-indentation depth curves for $0.02 \leq h/t \leq 0.1$

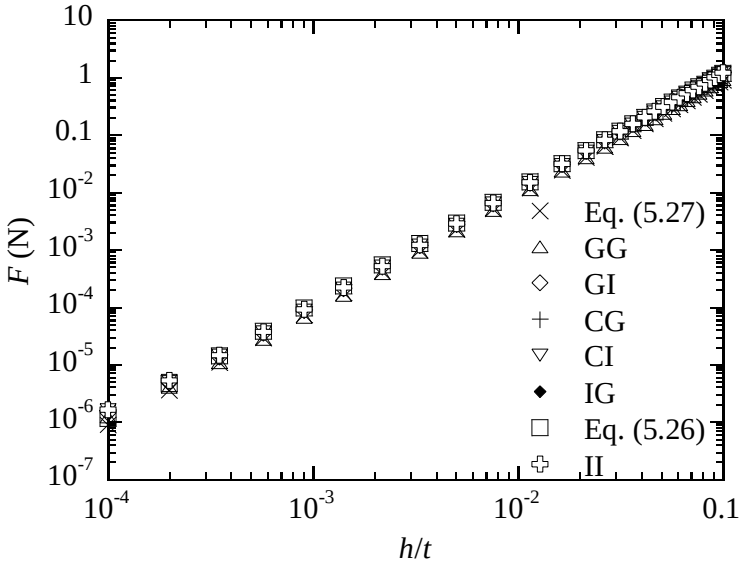

Figure 5.4 The dependence of the indentation load on the indentation depth for six different electric boundary conditions

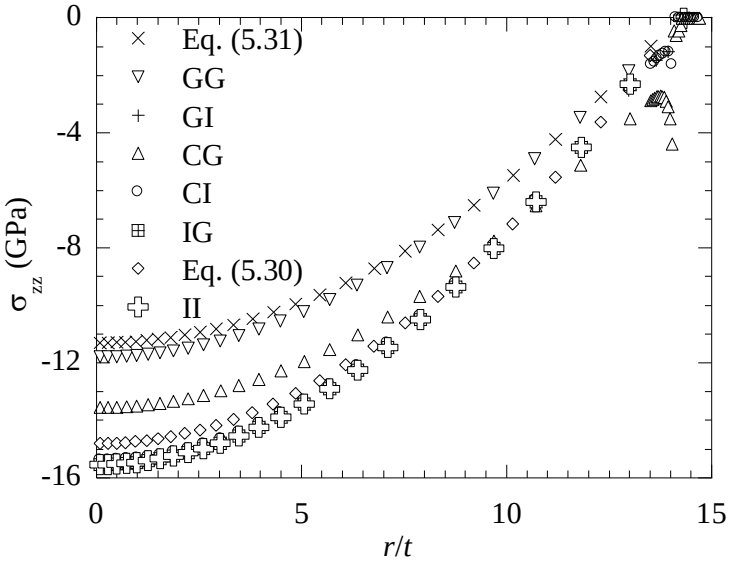

Figure 5.5 The distribution of the normal stress on the top surface of the piezoelectric materials for six different electric boundary conditions with an indentation depth of 50 nm

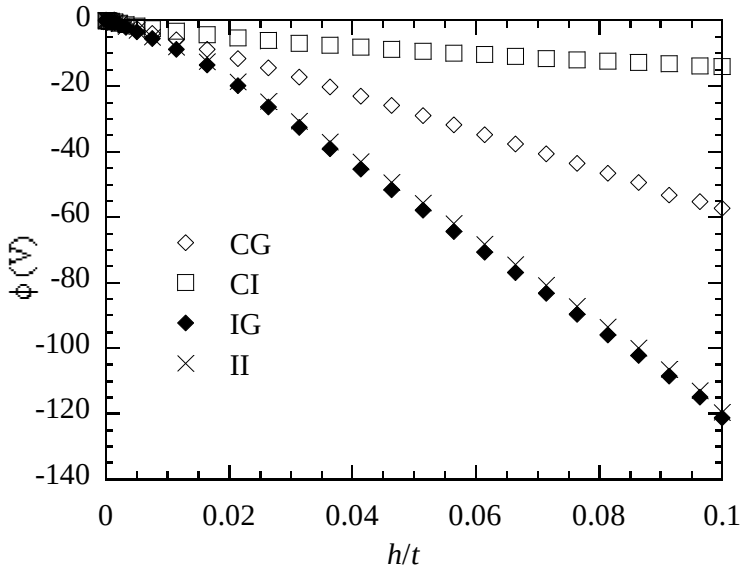

Figure 5.6 The dependence of the electric potential at the contact center on the indentation depth for four different electric conditions

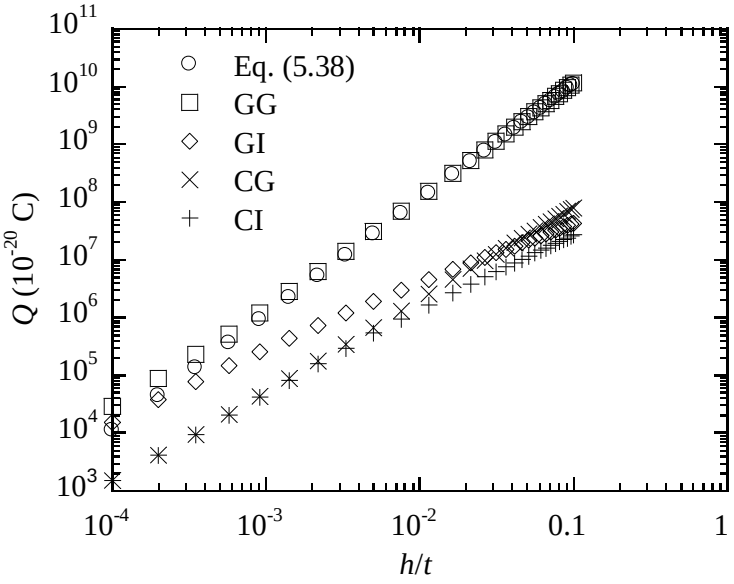

Figure 5.7 The variation of the total electric charges accumulated on the conducting indenter with the indentation depth for four different electric boundary conditions

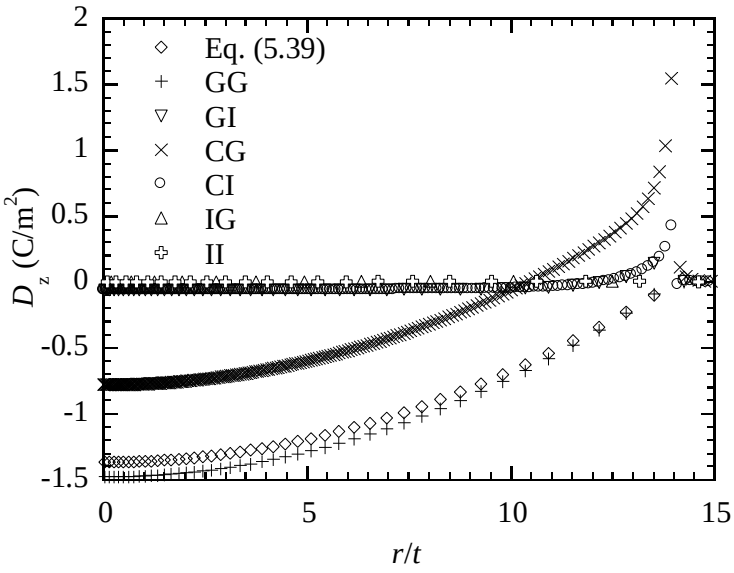

Figure 5.8 The distribution of the normal component of the electric displacement on the top surface of the piezoelectric material for six different electric boundary conditions with an indentation depth of 50 nm

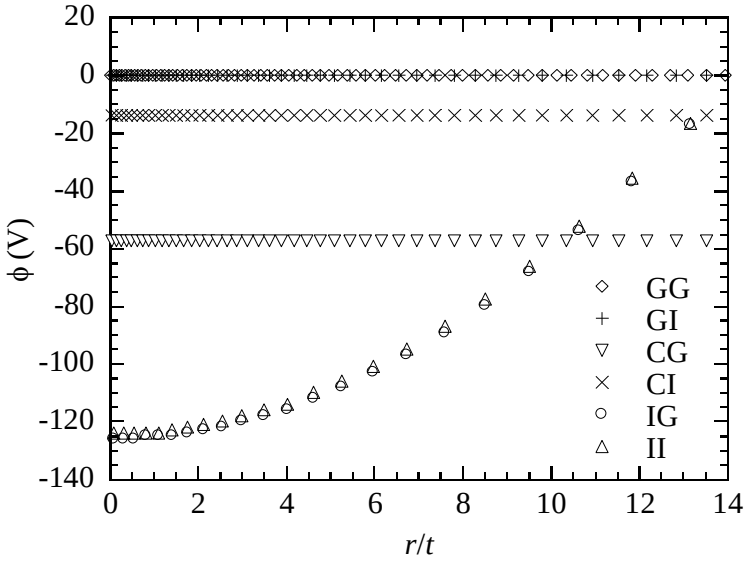

Figure 5.9 The distribution of the electric potential on the top surface of the piezoelectric material for six different electric boundary conditions with an indentation depth of 50 nm

Chapter - 6 Indentation-induced interfacial decohesion between a piezoelectric film and an elastic substrate

6.1 Introduction

Piezoelectric thin films have proliferated in a variety of applications such as energy harvesting devices, adaptive structures, sensors, and actuators due to their strong electromechanical coupling [169,170]. The interface strength between a piezoelectric film and substrate is of practical importance, and determines the reliability and durability of devices and structures. Various techniques such as blister tests [171], peeling tests [172], and instrumented indentation techniques [173] have been developed to investigate the interface strength between films and substrates. Instrumented indentation techniques offer unique and effective advantages in characterizing the interaction between films and substrates, as it provides a quick and reproducible method to determine the initiation of interfacial crack from a pop-in event at a critical indentation load [114,174].

In general, numerical analysis is indispensable to interpret indentation results of thin films of a finite thickness adhesively bonded to a substrate [175]. Zhang et al. [176] used a plane strain finite element model to investigate the propagation of an interface crack for a ductile film adhesively bonded to a ductile substrate by a rigid microwedge indenter and found the load drop corresponded to delamination. Li and Siegmund [108] used a cohesive zone model to study the indentation-induced interfacial delamination under the condition of a rigid conical indenter for a ductile coating on an elastic substrate with a weak interface. Li and Siegmund [177] numerically studied the mechanics of the indentation-induced delamination of a ductile film on an elastic substrate with a strong interface characterized by a traction-separation formulation, and proposed a calibration chart for determining cohesive parameters from two critical indentation loads. Liu et al. [178] focused on the indentation-induced buckling of a ductile thin film by a microwedge indenter using a two-dimensional finite element model with a traction-separation law and discussed the effect of interfacial parameters and film thickness on crack length. Xia et al.

[179] numerically conducted a detailed parametric study to investigate delamination mechanism maps and the influence of material and interface properties on the critical indentation depth and load corresponding to the crack nucleation, using an interfacial law for a stiff elastic coating on an elastic-plastic substrate. Chen et al. [180] simulated a two-dimensional indentation-induced delamination using a traction-separation law for the interfacial adhesion behavior and found that the initiation of interfacial delamination was dependent on interfacial strength and energy. Using a simplified traction-separation law, Liu and Yang [115] studied the delamination behavior of a film-substrate structure with elastic-plastic film and substrate. They examined the effects of indentation depth and film thickness on the size of delamination zone. Few studies have been done on the indentation-induced interfacial failure of piezoelectric film structures. Yan and Shang [181] carried out numerical simulation to investigate the interfacial delamination of a sandwiched-cantilever-type piezoelectric structure by a point load, which was applied to the edge of the cantilever. They found that the bilinear cohesive model was more appropriate than the exponential and trapezoidal cohesive models in describing interfacial delamination for brittle structures. However, they did not give the electrical boundary condition in their finite element model.

Application of the indentation technique to the characterization of piezoelectric films is in an embryonic stage. The mechanics of the contact-induced interfacial decohesion in piezoelectric film structures necessitates a systematic study before the indentation tests can be applied extensively in measurement of interfacial behavior and material properties of piezoelectric structures. In this chapter, a detailed finite element analysis is conducted to investigate the effects of interface properties, substrate properties, and film thickness on the indentation behavior of a transversely isotropic piezoelectric film—weakly bonded to an elastic and conducting substrate. Specifically the critical variables corresponding to the discontinuities in the indentation response curves are discussed.

6.2 Problem formulation

Consider a piezoelectric film weakly bonded to an elastic isotropic substrate. A traction-separation law [178,182,183,184,185,186] is used to model the interface interaction between the film and the substrate to analyze the separation of the film from the substrate. The interface is the only site where cracks or failure can occur. A pressure overclosure relationship governing the compressive behavior of contact surfaces is used to ensure that surfaces are impenetrable. The interfacial mechanism takes effect only when surfaces do not contact.

The traction-separation law used is the same as the one referenced in [180], and is described briefly as below. For simplicity, the interfacial constraint in normal and tangential directions is assumed to be uncoupled (i.e. pure normal separation with zero shear slip by itself does not introduce interfacial force in the shear directions, nor does pure shear slip with zero normal separation by itself introduce interfacial force in the normal direction). The initial traction-separation behavior before damage initiation is linearly elastic as

$$T = K\delta \tag{5.40}$$

where T is the traction stress, K is the interfacial stiffness, and δ is its corresponding contact separation along the normal or shear direction. Contact separations are the relative displacements between the nodes on the slave surface and their corresponding projection points on the master surface along the contact normal and shear directions. Before initiation of delamination, the traction-separation law remains reversible.

A quadratic stress criterion is used for damage initiation as

$$\left\langle T_n \right\rangle^2 + T_s^2 + T_t^2 = T_0^2 \tag{5.41}$$

where T_n, T_s and T_t are the normal and the two shear tractions respectively, and T_0 is the interface strength representing the peak value of the interaction stress between two surfaces when the separation is either purely normal to the interface, or solely in the first

or the second shear direction. The symbol $< >$ represents the Macaulay bracket with its usual interpretation as

$$\langle x \rangle = \begin{cases} 0, x < 0 \\ x, x \geq 0 \end{cases} \tag{5.42}$$

which ensures that a purely compressive stress does not cause separation.

The delamination at the interface is characterized by progressive degradation of the interfacial stiffness, which is described by the damage evolution law. After the damage initiation, the component of the contact stresses changes according to

$$\begin{aligned} T_n &= (1-D) K \langle \delta_n \rangle \\ T_s &= (1-D) K \delta_s \\ T_s &= (1-D) K \delta_t \end{aligned} \tag{5.43}$$

where δ_n, δ_s, δ_t are the normal and the two shear separations respectively, and D is the overall damage at the separation point. Before the damage initiation, D is 0. With the damage initiation, D evolves monotonically from 0 to 1 upon further loading. The moment that D reaches 1 is considered a threshold failure, which is the initiation of the interfacical decohesion between the film and the substrate.

Damage evolution is defined based on the fracture energy that is dissipated as a result of the damage process. It is assumed that the critical fracture energies purely along the normal direction are the same as that purely along the first or the second shear direction. A linear mixed-mode fracture energy criterion, which is independent of the cracking mode, is used when complete failure occurs [180,187]

$$G_n + G_s + G_t = G_c \tag{5.44}$$

where G_n, G_s, G_t are the work done by the surface tractions and their conjugate separations in the normal, the first and the second shear directions, respectively. G_c is the critical fracture energy required to cause the failure during separation purely along the normal direction or the first or second shear direction. The use of the fracture energy as a criterion for complete failure is reasonable since a fracture criterion based on the

maximum mechanical strain energy release rate for piezoelectric media under mechanical and electrical loading is proposed and verified by Park and Sun [188].

After the damage initiation, the degradation of D is calculated by

$$D = \frac{\delta_{eff}^{f}\left(\delta_{eff}^{m} - \delta_{eff}^{0}\right)}{\delta_{eff}^{m}\left(\delta_{eff}^{f} - \delta_{eff}^{0}\right)} \tag{5.45}$$

with

$$\delta_{eff} = \sqrt{\langle \delta_n \rangle^2 + \delta_s^2 + \delta_t^2} \tag{5.46}$$

$$\delta_{eff}^{f} = 2G_c / T_0 \tag{5.47}$$

where δ_{eff} is the effective separation, δ_{eff}^{m} is the maximum effective separation attained during the loading history, δ_{eff}^{f} is the effective separation at complete failure, and δ_{eff}^{0} is the effective separation at damage initiation. When total failure occurs, there is [187]

$$\langle \delta_n \rangle^2 + \delta_s^2 + \delta_t^2 = \delta_{eff}^{f} \tag{5.48}$$

Unloading after damage initiation is assumed to occur linearly toward the origin of the traction-separation plane, as described by

$$T_{eff} = \frac{\delta_{eff}^{0}\left(\delta_{eff}^{f} - \delta_{eff}^{m}\right)}{\delta_{eff}^{m}\left(\delta_{eff}^{f} - \delta_{eff}^{0}\right)} K\delta_{eff} \quad \text{for } 0 \le \delta_{eff} \le \delta_{eff}^{m} \text{ and } \delta_{eff}^{0} < \delta_{eff}^{m} < \delta_{eff}^{f} \tag{5.49}$$

where T_{eff} is the effective traction. The unloading path after decohesion initiation makes healing of decohesion excluded, since only part of the cohesive energy is recovered.

Figure 6.1 shows the schematic of the traction-separation law in terms of traction vs. separation. A bilinear traction-separation law is used in the analysis. Reloading subsequent to unloading also occurs along the same linear path until the softening envelope (line *AB*) is reached.

6.3 Finite element modeling

An axisymmetric finite element model in a cylindrical coordinate system (r, θ, z) is established in the ABAQUS software package to describe the indentation of the piezoelectric film-elastic substrate structure by a rigid sphere. The traction-separation law as discussed in the above section is used to define the interface between the piezoelectric film and the elastic substrate. The poling direction of the piezoelectric film, which is along axis-*oz* (i.e., positive *z*-axis), is anti-parallel to the loading direction. The piezoelectric film can be approximated as a single crystal, since there is a perfect orientation along *c*-axis or (001) for PZT thin films [189]. A piezoelectric lead zirconate titanate material, PZT-4 [188], is used for the film and its properties are listed in Table 6.1. The thickness of the film, t, is 10 nm. The elastic substrate of 2 μm thickness is conducting and electrically grounded. A conical indenter of semi-conical angle of 40.28° (equivalent to the cube-corner indenter) is used, and a tip radius of 5 nm is used to avoid stress singularity in the simulation. The maximum indentation depth is no more than half of the film thickness, which substantiates the assumption that the substrate is elastic [180,190,191]. The radial dimension is 5 μm and large enough to have negligible edge effect.

Figure 6.2 shows the finite element mesh used in the simulation. Mesh refinement is accomplished near the contact region where there is a large stress gradient. The size of the element increases gradually with the distance away from the contact zone. There are 15500 and 26660 elements for the film and the substrate, respectively. Finite sliding, node-to-surface formulation is used for substrate to film contact, with substrate as slave surface and film as master surface. Finite sliding, surface-to-surface formulation is used for indenter to film contact, with indenter as master surface and film as slave surface. The contact is frictionless. A zero electric potential constraint is applied on the bottom nodes of the piezoelectric film when the opening between the film and the substrate is smaller than 0.01 nm. No zero electric potential constraint is applied on the bottom nodes of the

piezoelectric film when the separation between the film and the substrate is larger than 0.01 nm. The indenter is electrically grounded with zero electric potential. The indenter is rigid and represented by an analytical surface. The nodes on the outer circumferential edge of the piezoelectric film are electrically grounded to ensure the zero electric potential condition at infinity. An axisymmetric condition of zero radial displacement is applied at the axisymmetric axis. The indenter is gradually pushed into the film in a displacement-controlled way. The nodes of the piezoelectric film that are in contact with the indenter are constrained with zero electric potential.

The simulation is performed step by step due to the change of the electrical boundary condition caused by the contact change. The effect of the electric field on the fracture criterion for piezoceramics is neglected, since the mechanical strain energy release rate accounts for the effect of the electric field very well [188].

The indentation load, *F*, can be determined from the force balance as [75]

$$F = -2\pi \int_0^a r\sigma_{zz} dr \tag{5.50}$$

where *a* is the contact radius, and σ_{zz} is the contact stress within the contact region.

For the indentation by a grounded, rigid indenter, the total charge, *Q*, induced on the surface of the indenter can be calculated as [75]

$$Q = -2\pi \int_0^a r D_z dr \tag{5.51}$$

where D_z is the normal electric displacement within the contact region.

6.4 Results and discussion

Three parameters are needed to define the traction-separation law: (1) *K*, which controls reversible elastic stiffness; (2) T_0, which represents the interfacial strength for damage initiation; and (3) G_c, which represents the energy consumed by interface separation. Two parameters are needed to characterize the linear elastic solid: (1) elastic modulus *E*; and (2) Poisson's ratio *v*. In the default conditions, film thickness is 10 nm,

and interfacial parameters listed in Table 6.2 and mechanical properties listed in Table 6.3 are used for the interface and the linear elastic substrate. The interfacial strength, T_0, is within the experimentally measured range [192,181,193]. In this study a brittle interface is assumed due to the brittle nature of piezoelectric film structures [189], and the work of adhesion is small to represent weak bonding between the film and the substrate.

In the simulation, the variable *D*, which represents the overall damage, is directly monitored. The point when *D* just reaching 1 is used as a criterion for the decohesion initiation. At the instant of the cohesion failure, the indentation variables such as the indentation displacement, indentation load, and indentation-induced charge are regarded as the critical variables.

Figure 6.3 shows the indentation responses including the load-displacement (*F*-*h*) and the induced-charge-displacement (*Q*-*h*) curves for a representative case for a weakly bonded interface. For comparison purposes, the results of a perfectly bonded contact are also included in Figure 6.3. There is no "pop-in" or "kink" event in the loading curve for a perfectly bonded contact. Both the indentation load and the indentation-induced charge increase with increasing indentation displacement. The loading and unloading responses are reversible for the perfectly bonded contact as expected for elastic deformation. Before decohesion occurs, the indentation responses are the same for weakly and perfectly bonded contact. For the piezoelectric film weakly bonded to the elastic substrate, there is a "pop-in" event at the indentation depth of ~0.9 nm in the loading curve, representing local decohesion failure. Both the load-displacement curve and the charge-displacement deviate from those of the perfectly bonding contact. These results reveal the dependence of the indentation behavior on the interfacial behavior of the film-substrate structure. It is interesting to note that the unloading behavior is different from the loading behavior once local decohesion failure occurs.

Figure 6.4 shows the depth dependence of the derivatives of *dF/dh* and *dQ/dh* (*h* is the indentation depth). A sudden drop of the derivatives around the indentation depth of

0.9 nm is observed. Such a drop is associated with local interface decohesion created by the indentation, and is a salient feature of a weakly bonded interface. This behavior offers a viable technique to characterize the initiation of interfacial decohesion between a piezoelectric film and a substrate by using the derivatives of *dF/dh* and *dQ/dh* as well as the load-displacement and charge-displacement curves for the load-controlled indentation.

Figure 6.5 shows the overall damage parameter of *D* on the interface between the film and the substrate for the loading phase. For small indentation depth, *D* is zero along the interface when the interface is intact. With increasing the indentation depth, *D* becomes nonzero and local damage initiates at the position of ~7.5 nm on the interface. The magnitude of *D* increases while increasing the indentation depth and reaches the value of 1 at the indentation depth of 0.9 nm, indicating the initiation of local decohesion on the interface. Further indentation causes the expansion of the decohesion zone. The decohesion initiates at a distance from the axisymmetric axis and grows both inwardly and outwardly along the interface.

Using the results shown in Figure 6.5, the dependence of decohesion zone size on the indentation depth is depicted in Figure 6.6. Decohesion zone size increases with the indentation depth after the initiation of local decohesion on the interface. The larger the indentation, the larger the local decohesion zone size is. For indentation depth larger than 2 nm, decohesion zone size is proportional the indentation depth. The unloading process has no effect on enlarging interfacial failure for the weak bonding between a piezoelectric film and an elastic substrate. The decohesion initiates and expands only during the loading process.

Under the condition that *D* is smaller than 1, local damage can be “healed”, and the interface restores to the undeformed state after final unloading. For the portion of the interface, on which $D=1$, permanent failure occurs, and the decohesion remains unchanged after the final unloading. The “healing” on the interface, on which $D<1$, leads

to a slight decrease of the indentation load required for the same indentation depth during the unloading process, as shown in Figure 6.3.

In general, the critical indentation depth/deformation to initiate interface decohesion is a function of material and interfacial properties. The following is focused on the parametric study to evaluate the influence of the interface and substrate properties on the critical indentation depth. Effect of film thickness is also discussed.

Figure 6.7 shows dependence of the critical indentation depth, h_c, for the onset of decohesion on the effect of interface energy. The interface stiffness and strength remain unchanged. The critical indentation depth increases with increasing the interface energy, as expected. Larger interfacial adhesion energy certainly makes the interfacial failure more difficult and requires a larger indentation depth for the initiation of local decohesion. An approximately linear relationship between interface energy and the critical indentation depth is observed for $G_c \geq 0.7\times10^{-3}$ J/m^3. Note there is a constraint among K, T_0 and G_c, that is $G_c \geq T_0^2/(2K)$. G_c cannot be arbitrarily small.

Figure 6.8 shows the dependence of the critical indentation depth on the interface strength. The interface stiffness and interface energy remain unchanged. Note that there is a constraint among K, T_0 and G_c, that is $T_0 \leq \sqrt{2KG_c}$. T_0 cannot be arbitrarily large. For $T_0 \leq 60$ MPa, the critical indentation depth decreases with increasing the interfacial strength. There is a slight increase in the critical indentation depth for $T_0 > 60$ MPa. Such behavior is associated with the constraint of constant interface energy and interface stiffness. Under the condition of constant interface energy and interface stiffness, the relative displacement between atoms decreases with increasing the interface strength to cause local decohesion. This is similar to the simple spring model for the atomic bonding. For a given bonding strength, the maximum separation between atoms decreases with the increase of the spring stiffness. The normal indentation onto the surface of the piezoelectric film causes radial displacement and the difference of the radial displacement

between the atoms in the piezoelectric film and the elastic substrate, which monotonically increases with increasing the indentation depth until reaching the maximum separation for the decohesion. For $T_0 \leq 60$ MPa, interfacial decohesion is dominantly controlled by the relative motion between the film and the substrate along the radial direction on the interface. The mechanism for the slight increase of the critical indentation depth for $T_0 >$ 60 MPa is unclear. It is likely due to the transition from the shear-controlled decohesion to the mix-mode-controlled decohesion. Such behavior had been reported by Xia et al. [179] for the indentation-induced delamination between an elastic substrate and an elastic-plastic substrate.

Figure 6.9 shows the dependence of the critical indentation for the occurrence of local decohesion on the interface stiffness. Note that there is a constraint among K, T_0 and G_c, that is $K \geq T_0^2/(2G_c)$. Hence, K cannot be arbitrarily small. The effect of K on the indentation deformation of near-surface material is negligible for shallow indentation. The critical indentation depth decreases with increasing the interface stiffness, following similar trends to the effect of the interface strength and the spring model of atomic bonding. The relative displacement between the film and the substrate for local decohesion decreases with the increase of the interface stiffness under the condition of constant interface energy and interface strength.

It is known that the mechanical properties of substrate play an important role in determining the indentation response of the film-substrate structure. The failure behavior of a hard-film-soft-substrate is distinct from that for a soft-film-hard-substrate. The elastic modulus of the substrate determined whether a film-substrate system is hard-film-soft-substrate or soft-film-hard-substrate [180].

Figure 6.10 shows the effect of the elastic modulus of substrate, E, on the critical indentation depth. The critical indentation depth increases with the increase of the elastic modulus of the substrate. The higher the elastic modulus of the substrate, the smaller the deformation of the substrate is. The relative displacement between the film and the

substrate decreases with the increase of the elastic modulus of the substrate due to less deformation in the substrate. For the PZT-4 film-elastic substrate system, the system can be approximated as a hard-film-soft-substrate system when E<50 GPa and as soft-film-hard-substrate when E≥100 GPa. For large elastic modulus of the substrate, the critical indentation depth becomes relatively independent of the mechanical properties of the elastic substrate due to small deformation and the decrease of the maximum interface stress.

It is worth noting that the contact size between the indenter and the film is dependent on the elastic properties of the substrate. For example, the contact area for the indentation depth of 0.9 nm is about 13.8 nm^2 for E=100 GPa and 16.7 nm^2 for E=200 GPa. The "pop-in" or "kink" event is not always recognizable. For small E, the "pop-in" event is more prominent. The reason for such behavior is that local decohesion is not always perceptible during indentation since the film may separate smoothly from the substrate without the snap-back instability as determined by the material and interface properties [179].

Figure 6.11 shows the effect of Poisson's ratio of the substrate, v, on the critical indentation depth. The increase of the Poisson ratio causes a slight increase in the indentation depth. This result is because a large Poisson's ratio causes more radial displacement of the substrate near the interface for the same indentation depth, which reduces the magnitude of the relative displacement between the film and the substrate. The effect of Poisson's ratio on the critical indentation depth is less prominent than the elastic modulus of substrate, and the effect of Poisson's ratio on contact radius is negligible under small indentation depth.

The thickness effect on the contact deformation of piezoelectric material has become a primary interest to researchers recently, since the properties of thin-film PZTs are superior to those of bulk solids. The recent trend in the miniaturization of piezoelectrically active devices is driving research on the size-effect of these functional

materials under reduced length scales. Effect of film thickness, which is crucial for the design and fabrication of smart structures, on the contact behavior of piezoelectric materials needs to be examined.

Figure 6.12 shows the effect of the thickness of the piezoelectric film, *t*, on the critical indentation depth. The critical indentation depth increases approximately linearly with increasing the film thickness. For a large film thickness, stresses distribute more uniformly near the interface in both the film and the substrate, which reduces the magnitude of stresses. This leads to small relative displacement between the film and the substrate for the same indentation depth and reduces the potential of local decohesion. The smaller the film thickness, the easier it is to induce local decohesion by the sharp-instrumented indentation for the same indentation depth. The confinement to the lateral displacement of thin films causes the indentation-induced interface failure for ultra-thin films.

6.5 Conclusion

Piezoelectric materials, which are of innate brittleness and susceptible to fracture, are usually subjected to a highly localized load by surface contact with electrodes in service, since contact stress concentration is a common form of loading for thin film structures. Finite element analysis of the linear electro-elastic indentation of monolithic piezoelectric thin films is expected to offer some desirable features and thus renders indentation of piezoelectric film structures great potential for becoming a new and fast method for the characterization of properties of both piezoelectric materials and interfaces.

In this work, a traction-separation law is used for investigating the indentation-induced interfacial decohesion of a transversely piezoelectric film weakly bonded to an elastic and electrically grounded substrate. Under the condition of shallow indentation, the interface failure is predominantly by the shear decohesion. The measureable critical indentation depth for the onset of decohesion during indentation,

which corresponds to a threshold failure at the interface between the film and the substrate, can be used as a comparative method for determining the interface and material properties.

The finite element results show that the two interfacial quantities of the traction-separation law can be determined from the indentation load and indentation-induced charge at the onset of failure at the film/substrate interface for the piezoelectric film-elastic substrate system. The “pop-in” event during indentation is only expected for certain interface behavior, since under some conditions, films can delaminate smoothly from substrate without the snap-back instability. The findings necessitate further probing into the complexities and detailed mechanics of the indentation of thin films constituted of smart materials. Films of larger thickness and substrates of large elastic modulus and Poisson’s ratio are desirable to prevent the initiation of interface crack for film-substrate structures. The results obtained from the finite element analysis of the indentation-induced interface decohesion of the PZT-4 film can be applicable to other transversely isotropic piezoelectric films. However, the effects of material properties of various piezoelectric films remain to be fully explored.

.

Table 6.1 Material properties of PZT-4

	Elastic constant (10^{10} N/m^2)					Piezoelectric constant (C/m^2)			Dielectric constant (10^{-10} C/V m)	
	C_{11}	C_{12}	C_{13}	C_{33}	C_{44}	e_{31}	e_{33}	e_{15}	$\in_{11}$	$\in_{33}$
PZT-4	13.9	7.78	7.43	11.3	2.56	-6.98	13.84	13.44	60.0	54.7

Table 6.2 Parameters for an interfacial model

K (GPa/nm)	T_0 (MPa)	G_c (10^{-3} J/m^2)
2	50	1.25

Table 6.3 Material properties for the elastic substrate

Elastic modulus, E (GPa)	Poisson's ratio, v
100	0.25

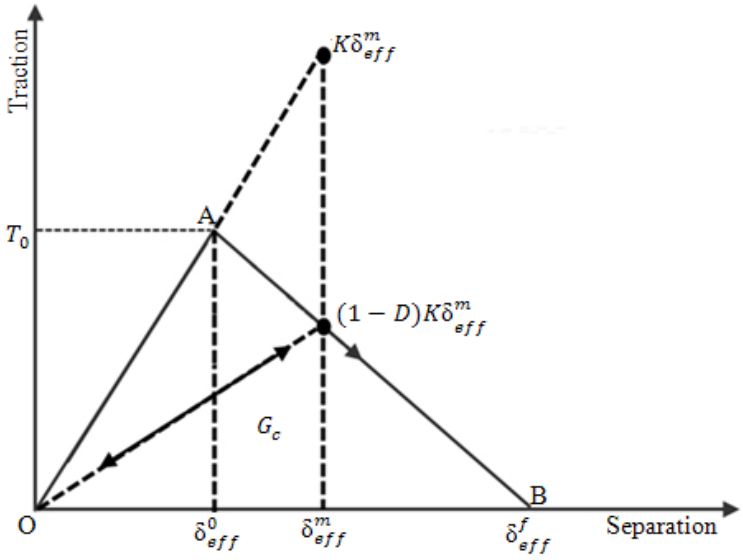

Figure 6.1 Schematic of the traction-separation law

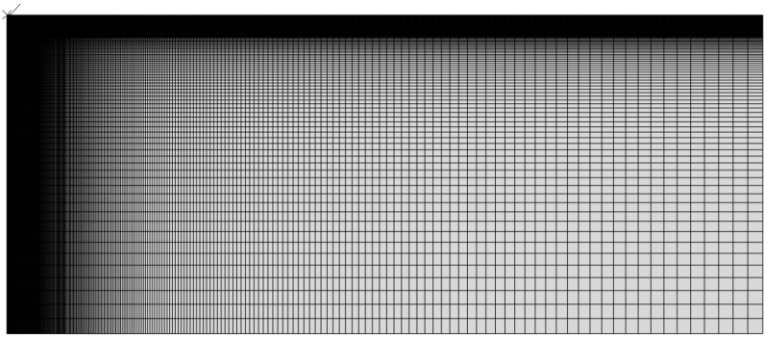

(a)

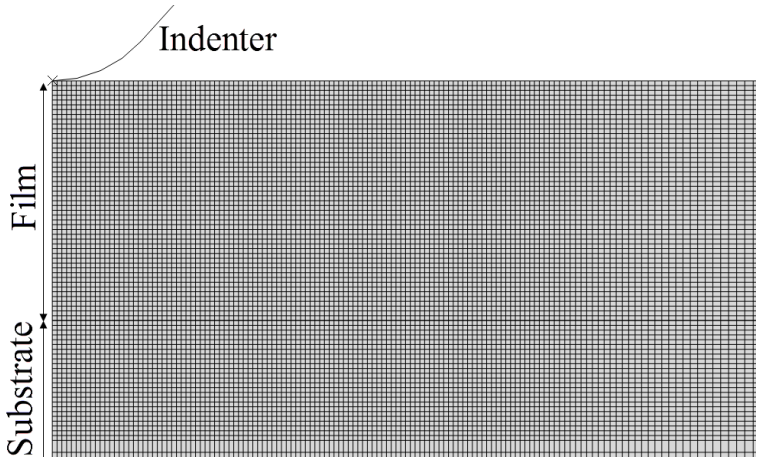

(b)

Figure 6.2 Finite element mesh for the film/substrate structure: (a) overview; and (b) enlarged view near the indenter

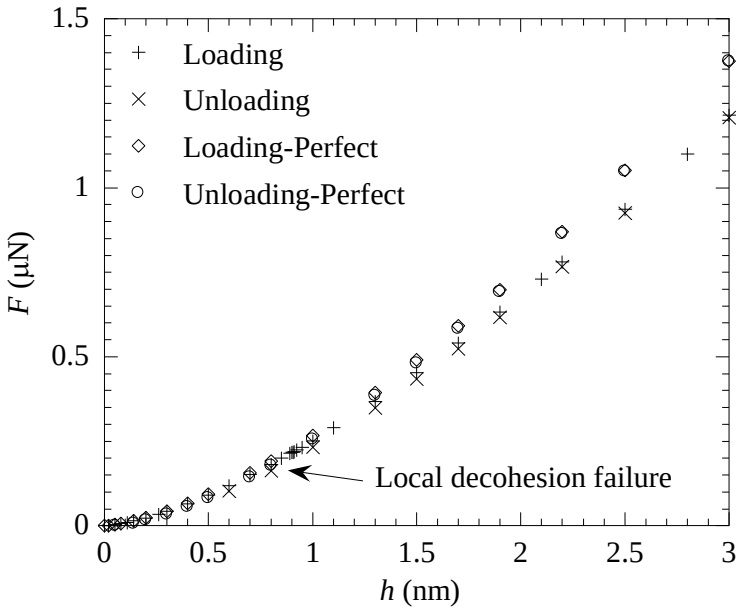

(a)

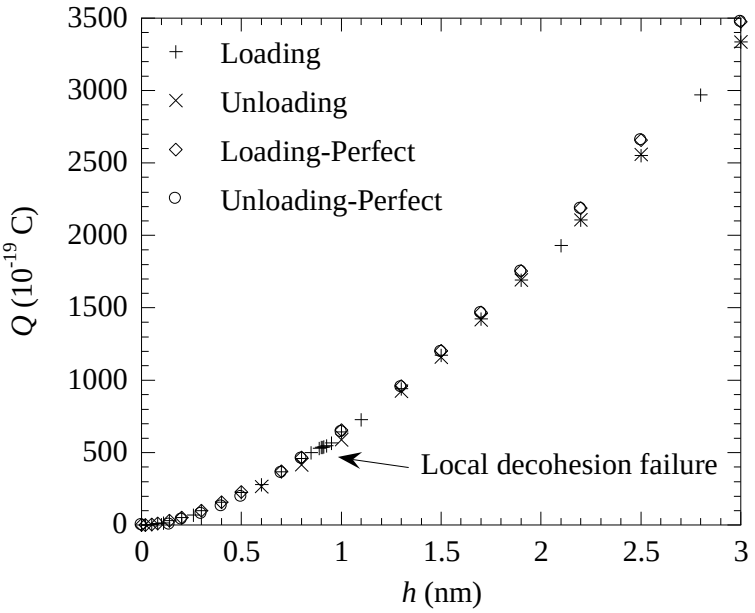

(b)

Figure 6.3 Indentation responses of the piezoelectric film-elastic substrate structure: (a) indentation load (F) vs. indentation depth (h); and (b) electric charge (Q) accumulated on the conducting indenter vs. indentation depth (h) (interfacial parameters: K=2 GP/nm, G_c=1.25×10^{-3} J/m^2, T_0=50 MPa; substrate's parameters: E= 100 GPa, ν=0.25; film thickness, t=10 nm)

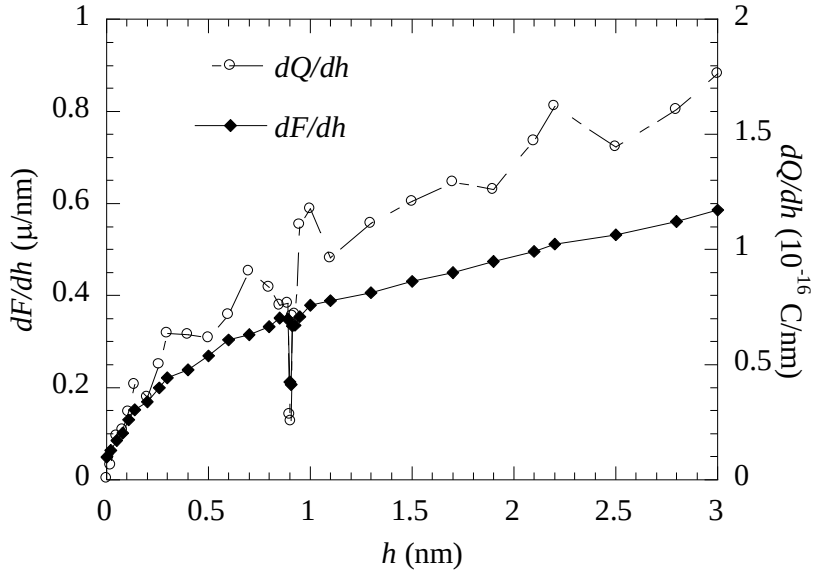

Figure 6.4 Variation of the derivatives of dF/dh and dQ/dh with the indentation depth for the piezoelectric film-elastic substrate structure with a weakly bonded interface (interfacial parameters: K=2 GP/nm, G_c=1.25×10^{-3} J/m^2, T_0=50 MPa; substrate's parameters: E= 100 GPa, ν=0.25; film thickness, t=10 nm

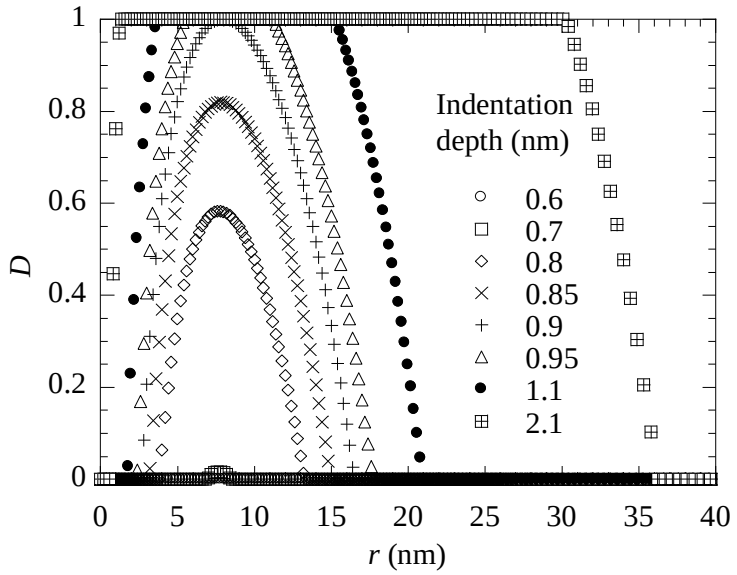

Figure 6.5 Evolution of the overall damage parameter, D, on the interface during the loading phase (interfacial parameters: K=2 GP/nm, G_c=1.25×10^{-3} J/m^2, T_0=50 MPa; substrate's parameters: E= 100 GPa, ν=0.25; film thickness, t=10 nm)

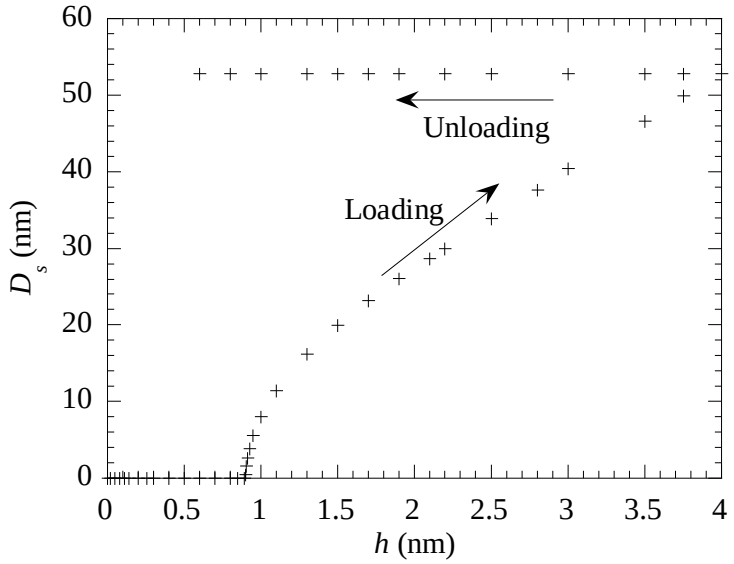

Figure 6.6 Variation of the decohesion zone size (D_s) with the indentation depth during loading and unloading (interfacial parameters: K=2 GP/nm, G_c=1.25×10^{-3} J/m^2, T_0=50 MPa; substrate's parameters: E= 100 GPa, v=0.25; film thickness, t=10 nm)

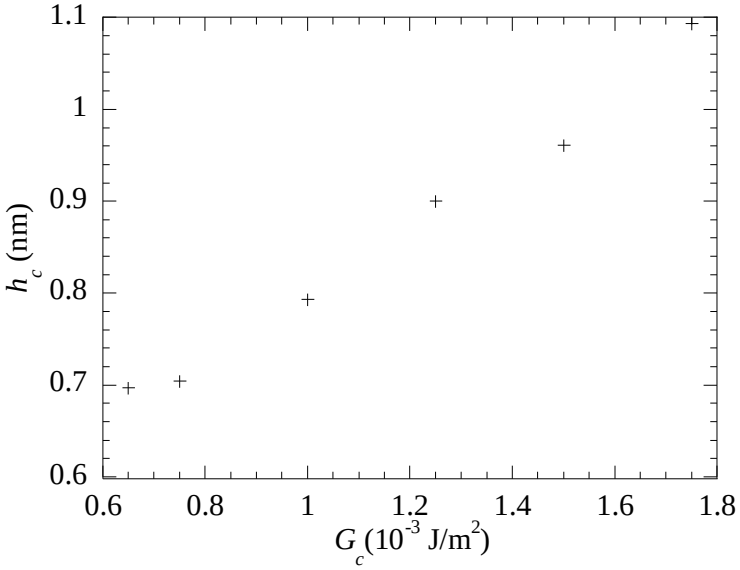

Figure 6.7 Dependence of the critical indentation depth (h_c) on the work of adhesion for the initiation of local decohesion (interfacial parameters: K=2 GP/nm, T_0=50 MPa; substrate's parameters: E= 100 GPa, v=0.25; film thickness, t=10 nm)

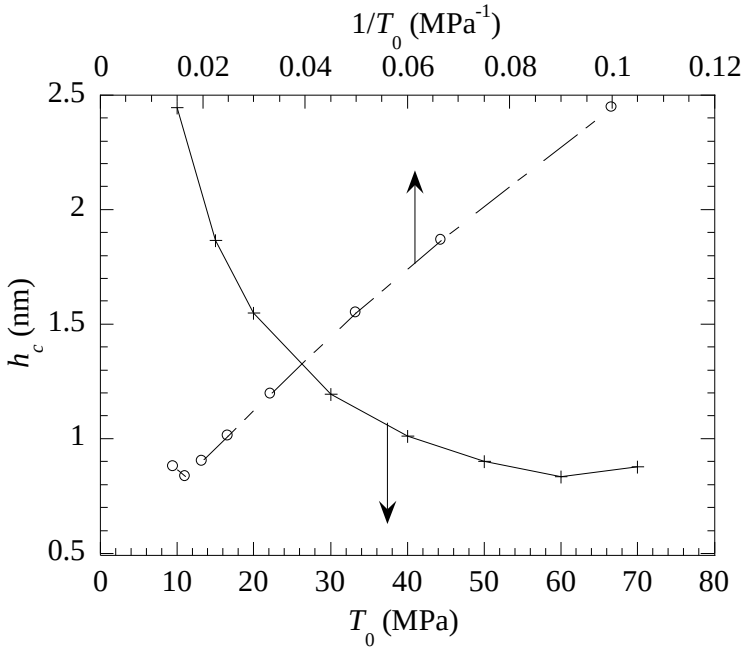

Figure 6.8 Effect of interfacial strength on the critical indentation depth for the initiation of local decohesion (interfacial parameters: K=2 GP/nm, G_c=1.25×10^{-3} J/m^2; substrate's parameters: E= 100 GPa, v=0.25; film thickness, t=10 nm)

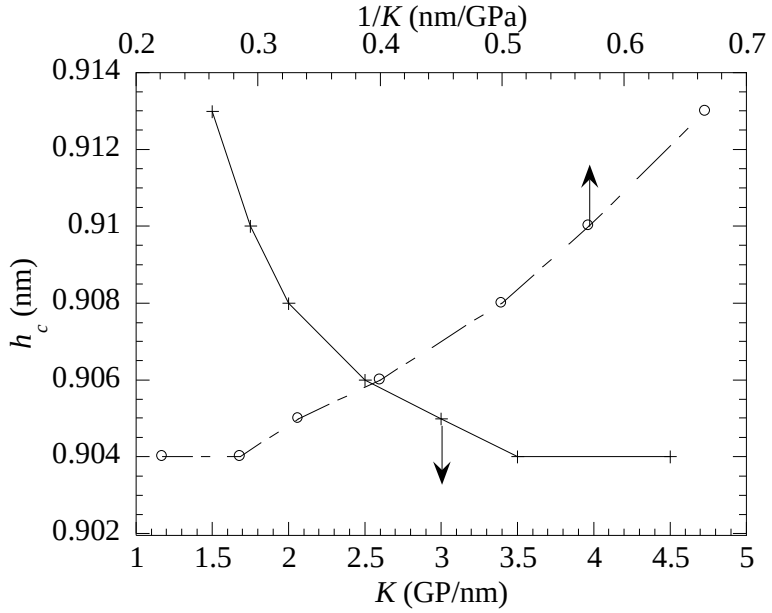

Figure 6.9 Influence of cohesion stiffness on the critical indentation depth for the initiation of local decohesion (interfacial parameters: T_0=50 MPa, G_c=1.25×10^{-3} J/m^2; substrate's parameters: E= 100 GPa, v=0.25; film thickness, t=10 nm)

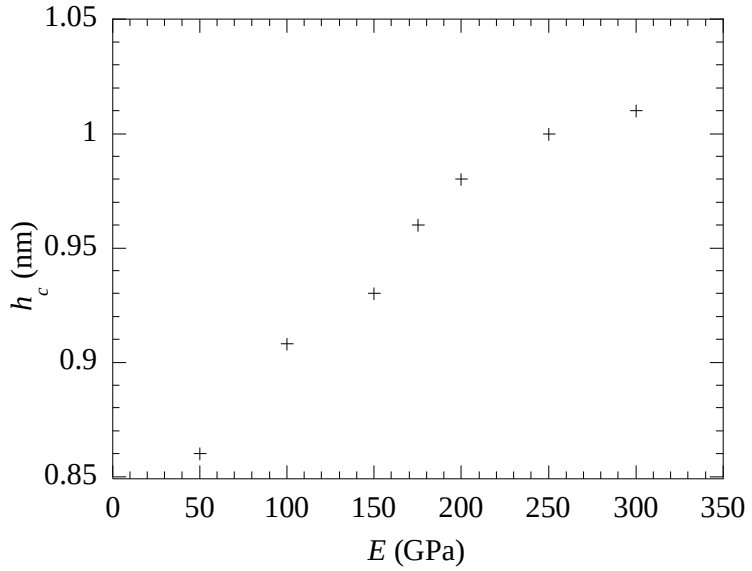

Figure 6.10 Effect of elastic modulus of the substrate on the critical indentation depth for the initiation of local decohesion (interfacial parameters: K=2 GPa/nm, T_0=50 MPa, G_c=1.25×10^{-3} J/m^2; substrate's parameters: ν=0.25; film thickness, t=10 nm)

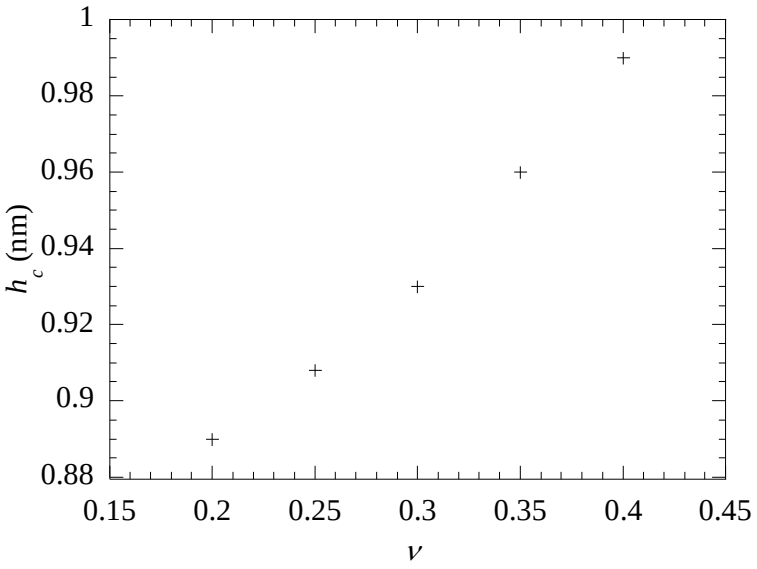

Figure 6.11 Influence of Poisson's ratio of the substrate on the critical indentation depth for the initiation of local decohesion (interfacial parameters: K=2 GPa/nm, T_0=50 MPa, G_c=1.25×10^{-3} J/m^2; substrate's parameters: E=100 GPa; film thickness, t=10 nm)

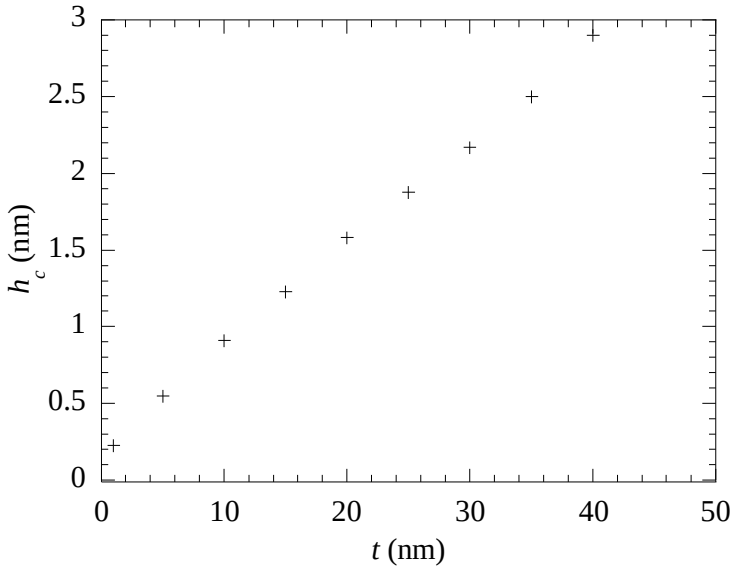

Figure 6.12 Effect of the film thickness (t) on the critical indentation depth for the initiation of local decohesion (interfacial parameters: K=2 GPa/nm, T_0=50 MPa, G_c=1.25×10^{-3} J/m^2; substrate's parameters: E=100 GPa, v=0.25)

.

Chapter - 7 Conclusions and prospective of future work

7.1 Conclusion

In this dissertation, the indentation deformation of transversely isotropic piezoelectric materials is investigated by recourse to finite element analysis. The focus is placed on effects of material orientation (i.e., angle between the indentation loading direction and the polarization direction). Both semi-infinite and thin-film piezoelectric materials are analyzed with different electrical and mechanical boundary conditions.

In Chapter - 3, a 3D finite element model, which can be regarded as semi-infinite, was developed to investigate the frictionless indentation of homogeneous, transversely isotropic linear piezoelectric materials by a flat-ended indenter with different angles between the polarization direction and the indentation loading direction. Two types of indenters were considered: an insulating indenter, and a conducting indenter without prescribed electric potential. The finite element results revealed that both the indentation load and the magnitude of the indentation-induced potential linearly increased with increasing the indentation depth. The proportionality for the linear relationship between the indentation load and the indentation depth depends on the angle, type of indenters, and piezoelectric properties of materials. In contrast to the load-displacement relationship, the proportionality for the linear relationship between the indentation-induced potential and the indentation depth is only a function of the angle between the loading direction and the poling direction, independent of the type of indenters. Semi-analytical relationships as a function of the angle were established between the indentation load and the indentation depth and between the indentation-induced potential and the indentation depth. These relationships may be used in the indentation technique to measure the relative direction of the loading axis to the poling direction (axisymmetric axis) of transversely isotropic piezoelectric materials.

In Chapter - 4, the Berkovich indentation of piezoelectric materials by an insulating indenter was studied by recourse to the 3D finite element analysis. The finite element results revealed that the indentation load was proportional to the square of the indentation depth. Using the analytical results for the indentation of a transversely isotropic

piezoelectric half-space with the loading direction parallel to the poling direction, a semi-analytical relationship between the indentation load and the indentation depth was obtained. The pre-factor for the relationship between the indentation load and the indentation depth depends on the angle and the piezoelectric properties of materials. In contrast to the load-displacement relationship, the indentation-induced potential at the contact center is proportional to the indentation depth. The proportionality is only a function of the angle between the loading direction and the poling direction, independent of the type of indenters. These relationships may be used in the indentation technique to measure the relative direction of the loading axis to the poling direction (axisymmetric axis) of transversely isotropic piezoelectric materials.

In Chapter - 5, finite element analysis was carried out for the spherical indentation of transversely isotropic piezoelectric thin films perfectly bonded to a rigid substrate under different electrical boundary conditions. Six different combinations of the electric boundary conditions between the indenter and the film and between the film and the substrate were used to investigate the effect of electric boundary conditions on the electrical and mechanical responses of the piezoelectric film when the contact radius is much larger than the film thickness. The indentation load was found to be proportional to the square of the indentation depth for all six cases, with the smallest indentation load being required to produce the same indentation depth for the indentation by a grounded, conducting indenter with a grounded substrate and the largest indentation load for the indentation by an insulating indenter with an insulating substrate. For $h/t \geq 0.01$, the contact radius is proportional to the square root of the indentation depth and is independent of the electric boundary conditions. A simple formula was established for the calculation of the contact stiffness which is proportional to the contact area and inversely proportional to the film thickness in contrast to the result for the spherical indentation of semi-infinite piezoelectric materials. For $h/t \geq 0.2$, the indentation-induced electric potential at the contact center is a linear function of the ratio of h/t for the contact radius being much larger than the film thickness with the slope κ being dependent on

the electric boundary conditions. For the indentation by a conducting indenter with a grounded substrate and $h/t \geq 10^{-3}$, the total charge accumulated on the indenter is a power function of the ratio of h/t. The nominal piezoelectric charge coefficient d_{33} is inversely proportional to the derivative of the electric potential with respect to the indentation depth for the indentation of piezoelectric films by a conducting indenter with a grounded, rigid substrate.

In Chapter - 6, an interfacial traction-separation law was used for investigating the indentation-induced interfacial decohesion of a transversely isotropic piezoelectric film weakly bonded to a conducting and elastic substrate. For the displacement-controlled indentation, the finite element results showed that the two interfacial quantities of the traction-separation law can be determined from the indentation load and indentation-induced charge at the onset of failure at the film/substrate interface for the piezoelectric film-elastic substrate system. The "pop-in" event during indentation is only expected for certain interface behaviors since, under some conditions, the film can delaminate smoothly from the substrate without the snap-back instability. The findings necessitate further probing into the complexities and detailed mechanics of the indentation of thin films constituted of smart materials. Films of a larger thickness, substrates of large elastic modulus and Poisson's ratio are desirable to prevent the initiation of interface crack for film-substrate structures. The results obtained from the finite element analysis of the indentation-induced interfacial decohesion of the PZT-4 film can be applicable to other transversely isotropic piezoelectric films. However, the effects of the material properties of various piezoelectric films remain to be fully explored.

The results obtained in this dissertation, which provide quantitative information of the indentation response of piezoelectric structures under different mechanical and electrical boundary conditions as well as different material orientations, are intended to

be helpful in gaining a better understanding of the contact mechanics of piezoelectric materials, and in facilitating the development of piezoelectricity-related research. For example, the results can be used for characterizing piezoelectric films and the poling direction of piezoelectric materials by indentation techniques.

Although finite element results are in agreement with analytical solutions for the cases with closed-form solutions, comparison between simulation results and experimental data show significant difference. The indentation load in the simulation is much larger than that in experiments under the same indentation depth. The difference between simulation and experiments can be attributable to many factors such as the dynamic responses, non-linear and hysteresis behavior of piezoceramics, effects of defect (e.g., porosity and cracks), effects of microstructure features (e.g., grain size), effects of processing, depolarization and fracture of piezoelectric materials. It is a challenge to quantitatively predict the experimental results of indentation of piezoelectric materials based on the existing theoretical models.

7.2 Prospects of future work

7.2.1 Effect of materials and material orientation

Only transversely isotropic piezoelectric materials are considered in this work. For a transversely isotropic piezoelectric material, there are 10 independent constants: namely, 5 elastic, 3 piezoelectric, and 2 dielectric constants. However, there are many types of piezoelectric materials, which could be more anisotropic than transversely isotropic piezoelectric materials and have different features of the indentation response. Future research needs to consider the most general case of piezoelectric materials, which have 45 independent constants, including 21 elastic, 18 piezoelectric, and 6 dielectric constants.

7.2.2 Other piezoelectric materials

For indentation by a flat-ended cylindrical indenter, the indenter considered is either

insulating or conducting without prescribed electric potential. The conducting indenter could be electrically grounded or prescribed a certain electric potential in experiments. Prominent effects of non-zero electric potential applied on the conducting indenter on indentation load, contact radius, and electric charge were found in reference [26]. It follows that a conducting indenter with a certain prescribed electric potential should also be considered in the future work. For the Berkovich indentation, only insulating indenter is considered. Conducting indenters, which require a rather laborious task, need to be investigated.

7.2.3 Effect of mechanical boundary conditions

For the indentation of a piezoelectric half space, only two indenters (i.e., flat-ended cylindrical and Berkovich indenters) are considered. The analytical solutions of the contact deformation of piezoelectric materials have been limited to axisymmetric geometries, and approximate solutions might not be easily generalized. Other indenters such as Vickers, wedge and cubic-corner indenters will be considered in the following work.

The effect of friction between indenter and indented surface is only considered for the Berkovich indentation by an insulating indenter. It is desirable to explore the effect of the friction between indenter and indented surface for different indenters and electrical boundary conditions.

Adhesive contact between indenter and indented surface is not considered in the present work. However, adhesive contact between indenter and coated material like that between film and substrate in Chapter - 6 is desirable to be taken into account especially under the condition of shear loading. Theory of adhesive contact has recently been extended to the case of a rigid sphere onto an elastic film perfectly bonded to a rigid substrate [194]. The work on adhesive contact of piezoelectric materials needs to be performed.

The indenter considered is rigid. However, elastic deformation of the tip material should be accounted to modify the ideally rigid displacement. For tips coated by conductive metals such as Au (E_{Au}=78 GPa) or Pt (E_{Pt}=168 GPa), the contribution of tip material to effective Young's modulus E^* is considerable, resulting in substantial increase of contact area [4]. An indentation load larger than a critical value can also cause yielding of the indenter. Total compliance should take into account the compliance between indenter and back surface as well as the compliance between indenter and specimen [2]. In addition, tip flattening due to wear and rough surface contact [195] is inevitable under realistic conditions. A sufficiently obtuse apex is highly preferable [68]. Hence, the influences of indenter tip geometry as well as surface roughness are worth of studying in the future.

For the indentation of piezoelectric thin films, only spherical indenter and a bi-layer structure were considered. The substrate considered was purely isotropic elastic. A detailed analysis requires investigation of effects of different indenters (e.g., conical, and flat-ended cylindrical indenters), different substrates (elastic-plastic substrates, anisotropic substrates, and substrates with electromechanical coupling). In addition, multilayer structures should also be considered, since indentation of multilayer structures has become a primary interest to researchers recently, and crack might be suppressed in a multilayer structure if the layers are sufficiently thin [196].

References

1 A.E. Giannakopoulos. Strength analysis of spherical indentation of piezoelectric materials. Journal of Applied Mechanics 67 (2000) 409-416.

2 S.N. Kamble, D.V. Kubair and U. Ramamurty. Indentation strength of a piezoelectric ceramic: Experiments and simulations. Journal of Materials Research 24 (2009) 926-935.

3 F.Q. Yang, Analysis of the axisymmetric indentation of a semi-infinite piezoelectric material: The evaluation of the contact stiffness and the effective piezoelectric constant, Journal of Applied Physics 103 (2008) 074115.

4 S.V. Kalinin, E. Karapetian and M. Kachanov, Nanoelectromechanics of piezoresponse force microscopy, Physical Review B 70 (2004) 18401.

5 N. Nakamura, H. Ogi and M. Hirao, Elastic, anelastic, and piezoelectric coefficients of GaN, Journal of Applied Physics 111 (2012) 013509.

6 U. Ramamurty, S. Sridhar, A. E. Giannakopoulos and S. Suresh. An experimental study of spherical indentation on piezoelectric materials. Acta Materialia 47 (1999) 2417-2430.

7 H. Hertz, in: H. Hartz, et al. (Eds.), Miscellaneous Papers, Macmillan, London, 1863.

8 I.N. Sneddon, The relation between load and penetration in the axisymmetric Boussinesq problem for a punch of arbitrary profile, International Journal of Engineering Science 3 (1965) 45-57.

9 K.L. Johnson, Contact Mechanics, Cambridge University Press, Cambridge, 1985.

10 L. Lefki and G.J. M. Dormans, Measurement of piezoelectric coefficients of ferroelectric thin films, Journal of Applied Physics 76 (1994) 1764-1767.

11 D. Fu, K. Ishikawa, M. Minakata and H. Suzuki, Observation of piezoelectric relaxation in ferroelectric thin films by continuous charge integration, Japanese Journal of Applied Physics Part I 40 (2001) 5683.

12 A.E. Giannakopoulos and S. Suresh, Theory of indentation of piezoelectric materials, Acta Materialia 47 (1999) 2153-2164.

13 A.J. Ishlinskii, The axi-symmetric problem in plasticity and the Brinell test, Journal of Applied Mathematics and Mechanics 8 (1944) 201-224.

14 R. Hill, E.H. Lee and S.I. Tupper, The theory of combined plastic and elastic deformation with particular reference to a thick tube under internal pressure,

Proceedings of the Royal Society of London A188 (1947) 273-290.

15 R.T. Shield, Plastic flow of metals under conditions of axial symmetry, Proceedings of the Royal Society of London A233 (1955) 267-287.

16 D. Tabor, The average pressure of solids, Physics Review 1 (1970) 145-179.

17 K.L. Johnson, The correction of indentation experiments, Journal of the Mechanics and Physics of Solids 18 (1970) 115-126.

18 W.C. Oliver and G.M. Pharr, An improved technique for determining average pressure and elastic modulus using load and displacement sensing indentation experiments, Journal of Material Research 7 (1992) 1564-1583.

19 H. Bei, E.P. George, J.L. Hay and G.M. Pharr, Influence of indenter tip geometry on elastic deformation during nanoindentation, Physical Review Letters 95 (2005) 045501.

20 S. Shim, H. Bei, E.P. George and G.M. Pharr, A different type of indentation size effect, Scripta Materialia 59 (2008) 1095-1098.

21 W.Q. Chen, T. Shioya and H.J. Ding, The elasto-electric field for a rigid conical punch on a transversely isotropic piezoelectric half-space, Journal of Applied Mechanics 66 (1999) 764-771.

22 S. Matysiak, Axisymmetric problem of punch pressinginto a piezoelectroelastic half space, Bulletin of the Polish Academy of Sciences, Technical Sciences 33 (1985) 25-34.

23 F.Q. Yang, Electromechanical interaction of linear piezoelectric materials with a surface electrode, Journal of Materials Science 39 (2004) 2811-2820.

24 J.H. Wang, C.Q. Chen and T.J. Lu, Indentation responses of piezoelectric films, Journal of the Mechanics and Physics of Solids 56 (2008) 3331-3351.

25 J.H. Wang and C.Q. Chen, Indentation responses of piezoelectric films ideally bonded to an elastic substrate, International Journal of Solids and Structures 48 (2011) 2743-2754.

26 Y.F. Wu, H.Y. Yu and W.Q. Chen, Mechanics of indentation for piezoelectric thin films on elastic substrate, International Journal of Solids and Structures 49 (2012) 95-110.

27 Y.F. Wu, H.Y. Yu and W.Q. Chen, Indentation on piezoelectric films in smooth contact with an elastic substrate, 2010 IEEE 221-225.

28 H.M. Dang and F.Q. Yang, Nanoindentation behavior of advanced materials (thesis

master degree), Department of Chemical and Materials Engineering, University of Kentucky (2009).

29 B.R. Lawn, K.S. Lee, H. Chai, A. Pajares, S. Wuttiphan, I.M. Peterson and X. Hu, Damage-resistant brittle coatings, Advanced Engineering Materials 2 (2000) 745-748.

30 M. Ohring, Materials Science of Thin Films, 2nd edn., Academic Press, San Diego, California (2002), 203.

31 R.K. Singh, Z.F. Zhou, L.K.Y. Li, P. Munroe, M. Hoffman and Z.H. Xie, Design of functionally graded carbon coatings against contact damage, Thin Solid Films 518 (2010) 5769-5776.

32 R.W. Hoffman, Overview of the solid-solid interface: mechanical stability, Materials Science and Engineering 53 (1982) 37-46.

33 V. Piefort, Finite Element Modelling of Piezoelectric Active Structures, Doctoral Dissertation (2000-2001), University Libre De Bruxelles, Active Structures Laboratory, Department of Mechanical Engineering and Robotics.

34 Y. Shoko and S. Thomas, Multilayer piezoelectric actuators – structures and reliability, in: AIAA/ASME/ASCE/AHS/ASC Structures, Structural Dynamics, and Materials Conference, 34th and AIAA/ASME Adaptive Structures Forum 19-22 (1993) 3581-3586.

35 K. Uchino, Manufacturing technology of multilayered transducers, Ceramic Transactions 49 (1995) 81-93.

36 D. Damjanovic and R.E. Newnham, Electrostrictive and piezoelectric materials for actuator applications, Journal of Intelligent Material Systems and Structures 3 (1992) 190-209.

37 K. Uchino and S. Takahashi, Multilayer ceramic actuators, Current Opinion in Solid State & Materials Science 1 (1996) 698-705.

38 W. Zhu, K. Yao, and Z. Zhang, Design and fabrication of a novel piezoelectric multilayer actuator by thick-film screen printing technology, Sensors and Actuators 86 (2000) 149-153.

39 H.J. Ding, P.F. Hou and F.L. Guo, The elastic and electric fields for three-dimensional contact for transversely isotropic piezoelectric materials, International Journal of Solids and Structures 37 (2000) 3201-3229.

40 S.M. Xiong, G.Z. Ni and P.F. Huo, The Reissner-Sagoci problem for transversely isotropic piezoelectric half-space, Journal of Zhejiang University Science 9 (2005)

986-989.

41 D. Diamond, S. Coyle, S. Scarmagnani and J. Hayes, Wireless sensor networks and chemo-/biosensing, Chemical Reviews 108 (2008) 652-879.

42 B.L. Wang and J. C. Han, A circular indenter on a piezoelectric layer, Archive of Applied Mechanics 76 (2006) 367-379.

43 B.B.L. Wang, J.C. Han, S.Y. Du, H.Y. Zhang and Y.G. Sun, Electromechanical behaviour of a finite piezoelectric layer under a flat punch, International Journal of Solids and Structures 45 (2008) 6384-6398.

44 F.Q. Yang, Piezoelectric Response in the contact deformation of piezoelectric materials, in Micro and Nano Mechanical Testing of Materials and Devices, edited by F.Q. Yang and J.C.M. Li, Springer (2008) 155-178.

45 T.L. Jordan and Z. Ounaies, Piezoelectric Ceramics Characterization, ICASE NASA Langley Research Center, Hampton, Virginia, NASA/CR-2001-211225. ICASE Report No. 2001-28.

46 Y. Kagawa and T. Yamabuchi, Finite element simulation of two-dimensional electromechanical resonators, IEEE Transactions on Sonics and Ultrasonnics, SU-21 (1974) 275-283.

47 R. Lerch, Modern techniques in electroacoustic transducer development, Proceedings of the 9th Conference on Acoustics, Budapest, Hungary, 1988.

48 D.F. Ostergaard and T.P. Pawlak, Three-dimensional finite elements for analyzing piezoelectric structures, Proceedings of IEEE Ultrosound Symposium, Williamsburg, VA, (1986) 639-642.

49 R. Lerch, Simulation of piezoelectric devices by two- and three-dimensional finite elements, IEEE Transactions on Ultrasonics, Ferroelectrics, and Frequency Control 37 (1990) 233-247.

50 M.S. Zarnik, D. Belavic, H. Ursic and S. Macek, Numerical modeling of ceramic mems structures with piezoceramic thick films, Journal of Electroceramics 20 (2008) 3-9.

51 D.T. Detwiler, M.H.H. Shen and V.B. Venkayya, Finite element analysis of laminated composite structures containing distributed piezoelectric actuators and sensors, Finite Elements in Analysis and Design 20 (1995) 87-100.

52 R.L. Goldberg, M.J. Jurgens, D.M. Mills, G.S. Henriquez, D. Vaughan and S.W. Smith, Modeling of piezoelectric multilayer ceramics using finite element analysis, IEEE Transactions on Ultrasonics, Ferroelectrics, and Frequency Control 44 (1997)

1204-1214.

53 A. Benjeddou, Advances in piezoelectric finite element modeling of adaptive structural elements: a survey, Computers and Structures 76 (2000) 347-363.

54 H.S. Zhou and C.I. Tseng, Distributed piezoelectric sensor/actuator design for dynamic measurement/control of distributed parameter systems: a piezoelectric finite element approach, Journal of Sound and Vibration 138 (1990) 17-34.

55 K.Y. Lam, X.Q. Peng, G.R. Liu and J.N. Reddy, A finite-element model for piezoelectric composite laminates, Smart Materials and Structures 6 (1997) 583-591.

56 A. Mannini and P. Gaudenzi, Multi-layer higher-order finite elements for the analysis of free-edge stresses in piezoelectric actuated laminates, Composite Structures 61 (2003) 271-278.

57 M. Kögl and M.L. Bucalem, Analysis of smart laminates using piezoelectric MITC plate and shell elements, Computers and Structures 82 (2005) 1153-1163.

58 O.O. Evtushenko, S.I. Matysiak and V.I. Pauk, On a homogenized model of periodically layered piezoelectric composites, Materials Science 32 (1996) 359-367.

59 M. Kögl and E.C.N. Silva, Topology optimization of smart structures: design of piezoelectric plate and shell actuators, Smart Material Structure 14 (2005) 387-399.

60 C.Y.K. Chee, L.Y. Tong, and G.P. Steven, A review on the modeling of piezoelectric sensors and actuators incorporated in intelligent structures, Journal of Intelligent Material Systems and Structures 9 (1998) 3-19.

61 W.Q. Chen and H.J. Wang, Indentation of a transversely isotropic piezoelectric half-space by a rigid sphere, Acta Mechanica Solida Sinica 12 (1999) 114-120.

62 J.H. Wang, C.Q. Chen and T.J. Lu, Indentation responses of piezoelectric films, Journal of the Mechanics and Physics of Solids 56 (2008) 3331-3351.

63 S. Matysiak, Axisymmetric problem of punch pressing into a piezoelectro-elastic half space, Bulletin of the Polish Academy of Sciences 33 (1985) 25-34.

64 Z.K. Wang and B.L. Zheng, The general solution of three-dimensional problems in piezoelectric media, International Journal of Solids and Structures 32 (1995) 105-115.

65 H.J. Ding, B. Cheng and J. Lian, General solutions for coupled equations for piezoelectric media, International Journal of Solids and Structures 33 (1996) 2283-298.

66 A. Saigal, A.E. Giannakopoulos, H.E. Pettermann and S. Suresh, Electrical response

during indentation of a 1-3 piezoelectric ceramic-polymer composite. Journal of Applied Physics 86 (1999) 603-606.

67 S. Sridhar, A.E. Giannakopoulos, S. Suresh and U. Ramamurty, Electrical response during indentation of piezoelectric materials: A new method for material characterization, Journal of Applied Physics 85 (1999) 380-387.

68 S. Sridhar, A.E. Giannakopoulos and S. Suresh, Mechanical and electrical responses of piezoelectric solids to conical indentation, Journal of Applied Physics 87 (2000) 8451-8456.

69 X.Y. Li and M.Z. Wang, On the anisotropic piezoelectric contact problem for an elliptical punch, Acta Mechanica 186 (2006) 87-98.

70 Z.Y. Huang, R.H. Bao and Z.G. Bian, The potential theory method for a half-plane crack and contact problems of piezoelectric materials, Composite Structures 78 (2007) 596-601.

71 A. Makagon, M. Kachanov, S.V. Kalinin and E. Karapetian, Indentation of spherical and conical punches into piezoelectric half-space with frictional sliding: Applications to scanning probe microscopy, Physical Review B 76 (2007) 064115.

72 S.V. Kalinin, B. Mirman and E. Karapetian, Relationship between direct and converse piezoelectric effect on a nanoscale electromechanical contact, Physical Review B 76 (2007) 212102.

73 F.Q. Yang, General solutions of a penny-shaped crack in a piezoelectric material under opening mode loading, The Quarterly Journal of Mechanics & Applied Mathmatics 57 (2004) 529-550.

74 E. Karapetian, M. Kachanov and S.V. Kalinin, Stiffness relations for piezoelectric indentation of flat and non-flat punches of arbitrary platform: Applications to probing nanoelectromechanical properties of materials. Journal of the Mechanics and Physics of Solids 57 (2009) 673-688.

75 M. Liu and F.Q. Yang, Finite element analysis of the spherical indentation of transversely isotropic piezoelectric materials, Modelling and Simulation in Materials and Engineering 20 (2012) 045019.

76 V.S. Kirilyuk and O.I. Levehuk, Indentation of punches into a piezoceramic body: two-dimensional contact problem of electroelasticity, International Applied Mechanics, 44 (2008) 1244-1258.

77 L.L. Ke, J. Yang, S. Kitipornchai and Y.S. Wang, Frictionless contact analysis of a functionally graded piezoelectric layered half-plane, Smart Materials and Structures 17 (2008) 025003.

78 L.L. Ke, J. Yang, S. Kitipornchai and Y.S. Wang, Electro-mechanical frictionless contact behavior of a functionally graded piezoelectric layered half-plane under a rigid punch, International Journal of Solids and Structures 45 (2008) 3313-3333.

79 L.L. Ke, Y.S. Wang, J. Yang and S. Kitipornchai, Sliding frictional contact analysis of functionally graded piezoelectric layered half-plane, Acta Machanica 209 (2010) 249-268.

80 X. Guo and F. Jin, A generalized JKR-model for two-dimensional adhesive contact of transversely isotropic piezoelectric half-space, International Journal of Solids and Structures 46 (2009) 3607-3619.

81 M.F. Wong and K. Zeng, Deformation behavior of PZN-6%PT single crystal during nanoindentation, Philosophyical Magazine 88 (2008) 3105-3128.

82 B. Zhao, Determination of mechanics properties of a piezoelectric material using indentation method with a cylindrical indenter, Advanced Materials Research 335-336 (2011) 1014-1020.

83 G. Cheng and T.A. Venkatesh, Nanoindentation response of anisotropic piezoelectric materials, Philosophical Magazine Letters 92 (2012) 278-287.

84 X.D. Wang, J.H. Song, J. Liu and Z.L. Wang, Direct-current nanogenerator driven by ultrasonic waves, Science 316 (2007) 102-105.

85 L.P. Qin, J.Q. Xu, X.W. Dong and Q.Y. Pan, The template-free synthesis of square-shaped SnO_2 nanowires; the temperature effect and acetone gas sensors, Nanotechnology 19 (2008) 185705.

86 X.D. Wang, J. Zhou, J.H. Song, J. Liu, N.S. Xu and Z.L. Wang, Piezoelectric field effect transistor and nanoforce sensor based on a single ZnO nanowire, Nano Letters 6 (2006) 2768-2772.

87 M.S. Arnold, P. Avouris, Z.W. Pan and Z.L. Wang, Field-effect transistors based on single semiconducting oxide nanobelts, The Journal of Physical Chemistry B 107 (2003) 659-663.

88 J.H. Duan, S.G. Yang, H.W. Liu, J.F. Gong, H.B. Huang, X.N. Zhao, R. Zhang and Y.W. Du, Single crystal SnO_2 zigzag nanobelts, Journal of American Chemical Society 127 (2005) 6180-6181.

89 I. Vrejoiu, M. Alexe, D. Hesse and U. Gösele, Functional perovskites – from epitaxial films to nanostructured arrays, Advanced Functional Materials 18 (2008) 3892-3906.

90 X.D. Wang, E. Graugnard, J.S. King, Z.L. Wang and C.J. Summers, Large-scale

fabrication of ordered nanobowl arrays, Nano Letters 4 (2004) 2223-2226.

91 I.T. Tang, H.J. Chen, W.C. Hwang, Y.C. Wang, M.P. Houng and Y.H. Wang, Applications of piezoelectric ZnO film deposited on diamond-like carbon coated onto Si substrate under fabricated diamond SAW filter, Journal of Crystal Growth 262 (2004) 461-466.

92 X.Y. Zhang, C.W. Lai, X. Zhao, D.Y. Wang, and J.Y. Dai, Synthesis and ferroelectric properties of multiferroic $BiFeO_3$ nanotube arrays, Applied Physics Letters 87(2005) 143102.

93 H.S. Tzhou and S. Pandita, A multi-purpose dynamic and tactile sensor for robot manipulators, Journal of Robotic Systems 4 (1987) 719-741.

94 B. Ren, S. Wing Or, F.F. Wang, X.Y. Zhao, H.S. Luo, X.B. Li, Q.H. Zhang, W.N. Di and Y.Y. Zhang, Piezoelectric energy harvesting based on shear mode $0.71Pb(Mg_{1/3}Nb_{2/3})O_3$-$0.29PbTiO_3$ single crystals, IEEE Transactions on Ultrasonics, Ferroelectrics, and Frequency Control 57 (2010) 1419-1425.

95 H. Chen, M. Liu, C. Jia and Z.H. Wang, Power harvesting using PZT ceramics embedded in orthopedic implants, IEEE Transactions on Ultrasonics Ferroelectrics and Frequency Control 56 (2009) 2010-2014.

96 J. Nuffer and T. Bein, Application of piezoelectric materials in transportation industry, Global Symposium on Innovative Solutions for the Advancement of the Transport Industry 4 (2006) San Sebastian, Spain.

97 J. K. Durr, U.S. Schmidt, H.W. Zaglauer and F.J. Arendts, On the integration of piezoelectric actuators in composite structures for aerospace applications, Journal of Intelligent Material Systems and Structures 10 (1999) 880-889.

98 W.W. Yang and A. Miao, Two-dimensional modeling of the effects of external vibration on the PZT impedance signature, Smart Materials & Structures 19 (2010) 065031.

99 V. Koval, M.J. Reece and A.J. Bushby, Ferroelectric/ferroelastic behavior and piezoelectric response of lead zirconate titanate thin films under nanoindentation. Journal of Applied Physics 97 (2005) 074301.

100 X.G. Ning, M. Lovell and W.S. Slaughter, Asymptotic solutions for axisymmetric contact of a thin, transversely isotropic elastic layer, Wear 260 (2006) 693-698.

101 S.T. Song, X.J. Zheng, H. Zheng and W. Liu, Evaluation of engineering/piezoelectric constants of piezoelectric thin film by combining nanoindentation test with FEM, Computational Materials Science 63 (2012) 134-144.

102 J.Q. Zhang, B.N. Zhang and J.H. Fan, A coupled electromechanical analysis of a piezoelectric layer bonded to an elastic substrate: Part I, development of governing Equations. International Journal of Solids and Structures 40 (2003) 6781-6797.

103 A. Bagchi and A.G. Evans, Measurement of the bonded energy for thin metallization lines on dielectrics, Thin Solid Films 286 (1996) 203-212.

104 M.D. Kriese, W.W. Gerberich and N.R. Moody, Quantitative adhesion measurements of multilayer films: Part I. Indentation mechanics, Journal of Materials Research 14 (1999) 3007-3018.

105 M.D. Kriese, W. W. Gerberich and N.R. Moody, Quantitative adhesion measures of multilayer films: Part II. Indentation of W/Cu, W/W, Cr/ W, Journal of Materials Research 14 (1999) 3019-3026.

106 O. Borrero-López, M. Hoffman, A. Bendavid, and P.J. Martin, Contact damage of tetrahedral amorphous carbon thin films on silicon substrates, Journal of Materials Research 24 (2009) 3286-3293.

107 A. Abdul-Baqi and E. Van der Giessen, Delamination of a strong film from a ductile substrate during indentation unloading, Journal of Materials Research 16 (2001) 1396-1407.

108 W.Z. Li and T. Siegmund, An analysis of the indentation test to determine the interface toughness in a weakly bonded thin film coating-substrate system, Acta Materialia 52 (2004) 2989-2999.

109 C.M. She, Y.W. Zhang and K.Y. Zeng, A three-dimensional finite element analysis of interface delamination in a ductile film/hard substrate system induced by wedge indentation, Engineering Fracture Mechanics 76 (2009) 2272–2280.

110 X.P. Xu and A. Needleman, Numerical simulations of fast crack growth in brittle solids, Journal of Mechanics and Physics Solids 42 (1994) 1397–1434.

111 X.J. Zheng, T.C. Zhou, J.M. Liu and A.D. Li, Interfacial adhesion analysis of Pb(Zr0.52Ti0.48)O3(PZT) thin films by nano-indentation test, Physics Letters A 304 (2002) 110-113.

112 B. Huang, M.H. Zhao and T.Y. Zhang, Indentation fracture and indentation delamination in ZnO film/Si substrate systems, Philosophical Magazine 84 (2004) 1233-1256.

113 A.G. Evans and J.W. Hutchinson, On the Mechanics of Delamination and Spalling in Compressed Films, International Journal of Solids Structures 20 (1984) 455-466.

114 D.B. Marshall and A.G. Evans, Measurement of adherence of residually stressed thin

films by indentation. I. Mechanics of Interface delamination, Journal of Applied Physics 56 (1984) 2632-2638.

115 M. Liu and F.Q. Yang, Finite element analysis of the indentation-induced delamination of bi-layer structures, Journal of Computational and Theoretical Nanoscience 9 (2012) 851-858.

116 M. Alguero, A.J. Bushby, P. Hvizdos, M.J. Reece, R.W. Whatmore and Q. Zhang, Mechanical and electromechanical properties of PZT sol-gel thin films measured by nanoindentation, Integrated Ferroelectrics 41 (2001) 1705-1714.

117 G.F. Zhao, M. Liu and F.Q. Yang, The effect of an electric current on the nanoindentation behavior of tin, Acta Materialia 60 (2012) 3773-3782

118 F.Q. Yang and H.M. Dang, Effect of electric field on the nanoindentation of Zinc Sulfide, Journal of Applied Physics 105 (2009) 056110.

119 F.Q. Yang, K. Geng, P.K. Liaw, G.J. Fan and H. Choo, Deformation in a $Zr_{57}Ti_5Cu_{20}Ni_8Al_{10}$ bulk metallic glass during nanoindentation, Acta Materialia 55 (2007) 321-327.

120 G.A. Schneider, T. Scholz, J. Munoz-Saldana and M.V. Swain, Domain rearrangement during nanoindentation in single-crystalline barium titanate measured by atomic force microscopy and piezoresponse force microscopy, Applied Physics Letters 86 (2005) 192903.

121 Dunn and R.W. Whatmore, Transformation dependence of lead zirconate titanate (PZT) as shown by PiezoAFM surface mapping of Sol-gel produced PZT on various substrates, Integrated Ferroelectrics 38 (2001) 683-691.

122 H. Zeng, P. Wu, D.X. Dong and P. Zhang, Investigation on preparation and properties of $Pb(Zr_{0.95}Ti_{0.05})O_3$ thin films, Infrared Physics & Technology 54 (2011) 21-24.

123 B.N. Cox, W.C. Carter and N.A. Fleck, A binary model of textile composites - I. Formulation, Acta Metallurgica et Materialia 42 (1994) 3463-3479.

124 J. Whitcomb, K. Woo and S. Gundapaneni, Macro finite element for analysis of textile composites, Journal of Composite Materials 28 (1994) 607-617.

125 F.Q. Yang, J.C. M. Li and C.W. Shih, Computer simulation of impression creep using the hyperbolic sine stress law, Materials Science and Engineering A201 (1995) 50-57.

126 F.Q. Yang, Impression creep: effects of slip, stick and cavity depth, International Journal of Mechanical Sciences 40 (1998) 87-96.

127 D.Y. Zhou, Experimental Investigation of Non-linear Constitutive Behavior of PZT Piezoceramics, Dissertation for Master Degree of Engineering, Forschungszentrum Karlsruhe GmbH, Karlsruhe (2003).

128 R.M. McMeeking, A J-integral for the analysis of electrically induced mechanical stress at cracks in elastic dielectrics, International Journal of Engineering Science 28 (1990) 605-613.

129 Y.E. Park, Crack extension force in a piezoelectric material, Transactions ASME Journal of Applied Mechanics 57 (1990) 647-653.

130 P. Delobelle, O. Guillon, E. Fribourg-Blanc, C. Soyer, E. Cattan and D. Remiens, True Young modulus of $Pb(Zr,Ti)O_3$ films measured by nanoindentation, Applied Physics Letters 85 (2004) 5185-5187.

131 A. Rar, G.M. Pharr and W.C. Oliver, Piezoelectric nanoindentation, Journal of Materials Research 21 (2006) 552-556.

132 H. Bei, E.P. George, J.L. Hay and G.M. Pharr, Influence of indenter tip geometry on elastic deformation during nanoindentation, Physics Review Letters 95 (2005) 045501.

133 A.W. Warrn and Y.B. Guo, Mechanical surface properties determined by nanoindentation: experimental and FEA studies on the effects of surface integrity and tip geometry, Surface and Coatings Technology 201 (2006) 423-433.

134 J.M. Antunes, L.F. Menezes and J.V. Fernandes, Three-dimensional numerical simulation of Vickers indentation tests, International Journal of Solids and Structures 43 (2006) 784-806.

135 D.J. Munoz-Paniagua, M.T. McDermott, P.R. Noton and S.M. Tadayyon, Direct tip shape determination of a Berkovich indenter: effect on nanomechanical property measurement and description of a worn indenter, IEEE Transactions on Nanotechnology 4 (2010) 487-493.

136 R.J. Wang, Acoustic Materials Manual, Science Press (1983), China, (in Chinese).

137 B. Jaffe, W.R. Cook and H. Jaffe, Piezoelectric Ceramics, Academic Press, New York, 1971.

138 M. Liu and F.Q. Yang, Orientation effect on the Boussinesq indentation of a transversely isotropic piezoelectric material, to be submitted.

139 M. Lichinchi, C. Lenardi, J. Haupt and R. Vitali, Simulation of Berkovich nanoindentation experiments on thin films using finite element method, Thin Solid Films 312 (1998) 240-248.

140 S. Swaddiwudhipong, J. Hua, K.K. Tho and Z.S. Liu, Equivalency of Berkovich and conical load-indentation curves, Modelling and Simulation in Materials Science and Engineering 14 (2006) 71-82.

141 P.-L. Larsson, A.E. Giannakopoulos, E. Söderlund, D.J. Rowcliffe and R. Vestergaard, Analysis of Berkovich indentation, International Journal of Solids and Structures 33 (1996) 221-248.

142 A.E. Giannakopoulos, Elastic and visoelastic indentation of flat surfaces by pyramid indenters, Journal of the Mechanics and Physics of Solids 54 (2006) 1305-1332.

143 J.H. Han, K.H. Rew and I. Lee, An experimental study of active vibration control of composite structures with a piezo-ceramic actuator and a piezo-film sensor, Smart Materials and Structures 6(1997) 549-558.

144 T. Tunkasiri, Y. Qin and W. Thamjarree, Structure and electrical properties of RF-sputtering deposited thin ferroelectric $Pb(Zr_{0.52}Ti_{0.48})O_3$ films, Journal of Materials Science Letters19(2000) 1913-1916.

145 E.G. Lee, J.K. Lee, W.Y. Jang, J.G. Lee and J.Y. Kim, Domain switching characteristics of preferentially oriented lead zirconate titanate thin films, Journal of Materials Science Letters 19(2000) 1917-1919.

146 B.L. Wang, J.C. Han and S.Y. Du, Electroelastic fracture dynamics for multilayered piezoelectric materials under dynamic anti-plane shearing, International Journal of Solids and Structures 37(2000) 5219-5231.

147 S.S. Livneh, V.F. Janas and A. Safari, Development of fin scale PZT ceramic fiber/polymer shell composite transducers, Journal of the American Ceramic Society 78(1995) 1900-1906.

148 D.N. Fang, A.K. Soh and K.C. Hwang, Nonlinear electric-mechanical behavior of PZT-5 fiber reinforced composite with epoxy resin matrix, Journal of Materials Science Letters 19(2000) 1579-1581.

149 E.K. Akdogan, M. Allahverdi and A. Safari, Piezoelectric composites for sensor and actuator applications, IEEE Transactions on Ultrasonics, Ferroelectrics and Frequency Control 52(2005) 746-775.

150 C.N. Dellan and D.W. Shu, The performance of 1-3 piezoelectric composites with a porous non-piezoelectric matrix, Acta Materialia 56(2008) 754-761.

151 W.P. Mason, Piezoelectric crystals and their application to ultrasonics, Van Nostrand Reinhold, New York, USA (1950).

152 R.C. Pohanka and P.L. Smith, Electronic Ceramics, Properties, Devices and

Applications, Chapter 2, Marcel Dekker, New York (1988).

153 K. Uchino, Piezoelectric actuators and ultrasonic motors, Kluwer Academic Publishers, Boston, Dordrecht, London (1997).

154 P. Luginbuhl, S.D. Collins, G.-A. Racine, M.-A. Gretillat and N.F. de Rooij, Ultrasonic flexural lamb-wave actuators based on PZT thin film, Sensors Actuators A 64(1998) 41-49.

155 P. Muralt, Recent progress in materials issues for piezoelectric mems, Journal of the American Ceramic Society 91(2008) 1385-1396.

156 H. Fan, K.Y. Sze and W. Yang, Two dimensional contact on a piezoelectric half-space, International Journal of Solids and Structures 33(1996) 1305-1315.

157 J.G. Wang, S.S. Fang and L.F. Chen, The state vector methods for space axisymmetric problems in multilayered piezoelectric media, International Journal of Solids and Structures 39 (2002) 3959-3970.

158 C.F. Gao and N. Noda, Green's functions of a half-infinite piezoelectric body: exact solutions, Acta Mechanica 172(2004) 169-179.

159 L.L. Ke, J. Yang, S. Kitipornchai and Y.S. Wang, Electro-mechanical frictionless contact behavior of a functionally graded piezoelectric layered half-space under a rigid punch, International Journal of Solids and Structures 45(2008).

160 F.Q. Yang, Thickness effect on the indentation of an elastic layer, Materials Science and Engineering A 358(2003) 226-2323313-3333.

161 F.Q. Yang, Asymptotic solution to axisymmetric indentation of a compressible elastic thin film, Thin Solid Films 515(2006) 2274-2283.

162 F.Q. Yang, Axisymmetric indentation of an incompressible Elastic Thin Film, Journal of Physics D: Applied Physics 36(2003) 50-55.

163 E. Karapetian, M. Kachanov and S.V. Kalinin, Nanoelectromechanics of piezoelectric indentation and applications to scanning probe microscopies of ferroelectric materials, Philosophical Magazine 85(2005) 1017-1051.

164 G. Puglisi and G. Zurlo, Electric field localizations in thin dielectric films with thickness non-uniformities, Journal of Electrostatics 70 312-316.

165 F.Q. Yang and W. Song, The influence of electromechanical interaction on morphological instability of an elastic conducting half-space, Phys. Rev. B 72 (2005) 165417.

166 F.Q. Yang and W. Song, Morphological instability of elastic thin films—effect of

electromechanical interaction, Applied Physics Letters 87 (2005) 111912.

167 R. Holland and E.P. Eernissen, Design of Resonant Piezoelectric Devices, The Colonial Press Inc. (1969).

168 M. Kollosche and G. Kofod G, Electrical failure in blends of chemically identical, soft thermoplastic elastomers with different elastic stiffness, Applied Physics Letters 96(2010) 071904.

169 A. Arnau (ed.), Piezoelectric Transducers and Applications, Spring, New York, 2004.

170 S. Priya and D.J. Inman (eds.) Energy Harvesting Technologies, Springer, New York, 2009.

171 M.L. Williams, The fracture threshold for an adhesive interlayer, Applied Polymer Science 14 (1970) 1121-1126.

172 Y.G. Wei and J.W. Hutchinson, Interface strength, work of adhesion and plasticity in the peel test, International Journal of Fracture 93 (1998) 315-333.

173 F.P. Ganneau, G. Constantinides and F.-J. Ulm, Dual-indentation technique for the assessment of strength properties of cohesive-frictional material, International Journal of Solids and Structures 43 (2006) 1727-1745.

174 C. Kocer and R.E. Collins, Angle of Hertzian cone racks, Journal of the American Ceramic Society 81 (1998) 1736-1742.

175 R. Narasimhan and S.K. Biswas, A finite element study of the indentation mechanics of an adhesively bonded layered solid, International Journal of Mechanical Sciences 40 (1998) 357-370.

176 Y.W. Zhang, K.Y. Zeng and R. Thampurun, Interface delamination generated by indentation in thin film systems— a computational mechanics study, Materials Science Engineering A 319-321 (2001) 893-897.

177 W. Li and T. Siegmund, Numerical study of indentation delamination of strongly bonded films by use of a cohesive zone model, Computer Modeling in Engineering and Structures 5 (2004) 81-90.

178 P. Liu, Y.W. Zhang, K.Y. Zeng, C. Lu and K.Y. Lam, Finite element analysis of interface delamination and buckling in thin film systems by wedge indentation, Engineering Fracture Mechanics 74 (2007) 1118-1125.

179 S.M. Xia, Y.F. Gao, A.F. Bower, L.C. Lev and Y.-T. Cheng, Delamination mechanism maps for a strong elastic coating on an elastic-plastic substrate subjected to contact loading, International Journal of Solids and Structures 44 (2007) 3685-3699.

180 L. Chen, K.B. Yeap, K.Y. Zeng and G.R. Liu, Finite element simulation and experimental determination of interfacial adhesion properties by wedge indentation, Philosophical Magazine 89 (2009) 1395-1413.

181 Y.B. Yan and F.L. Shang, Cohesive zone modeling of interfacial delamination in PZT thin films, International Journal of Solids and Structures 46 (2009) 2739-2749.

182 V. Tvergaard, Effect of fibre debonding in a whisker-reinforced metal, Materials Science Engineering A 125 (1990) 203-213.

183 X.P. Xu and A. Needleman, Numerical simulations of fast crack growth in brittle solids, Journal of the Mechanics and Physics and Solids 42 (1994) 1397-1434.

184 V. Tvergaard and J.W. Hutchinson, Toughness of an interface along a thin ductile layer joining elastic solids, Philosophical Magazine A 70 (1994) 641-656.

185 V. Tvergaard and J.W. Hutchinson, Effect of strain-dependent cohesive zone model on predictions of crack growth resistance, International Journal of Solids and Structures 33 (1996) 3297-3308.

186 E.A. Repetto, R. Radovitzky and M. Ortiz, Finite element simulation of dynamic fracture and fragmentation of glass rods, Computer Methods in Applied Mechanics Engineering 183 (2000) 3-14.

187 L. Chen, K.B. Yeap, K.Y. Zeng, C.M.She and G.R. Liu, Interfacial delamination cracking shapes and stress states during wedge indentation in a soft-film-on-hard-substrate system—Computational simulation and experimental studies, Journal of Materials Research 26 (2011) 1-13.

188 S. Park and C.T. Sun, Fracture criteria for piezoelectric ceramics, Journal of the American Ceramic Society 78 (1995) 1475-1480.

189 F. Shang, T. Kitamura and H. Hirakata, Delamination test and the effect of free edge on interface strength of PZT thin films, Integrated Ferroelectrics 73 (2005) 67-74.

190 K.B. Yeap, K.Y. Zeng and D.Z. Chi, Determining the interfacial toughness of low-K films on Si substrate by wedge indentation: further studies, Acta Materialia 56 (2008) 977.

191 K.B. Yeap, K.Y. Zeng, H.Y. Jiang, L. Shen and D.Z. Chi, Determining interfacial properties of submicron low-k films on Si substrate by using wedge indentation technique, Journal of Applied Physics 101 (2007) 123531.

192 K.L. Mittal, Adhesion measurement of thin films, Electrocomponents Science and Technology 3 (1976) 21-42.

193 R. Jacobsson and B. Kruse, Measurement of adhesion of thin evaporated films on glass substrates by means of direct pull off method, Thin Solid Films 15 (1973) 71-77.

194 S.T. Choi, Extended JKR theory on adhesive contact of a spherical tip onto a film on a substrate, Journal of Materials Research 27 (2012) 113-121.

195 V.A. Yastrebov, J. Durand, H. Proudhon and G. Cailletaud, Rough surface contact analysis by means of the finite element method and of a new reduced model, Comptes Rendus Mecanique 339 (2011) 473-490.

196 W. Yang and Z. Suo, Cracking in ceramic actuators caused by electrostriction, Journal of the Mechanics and Physics of Solids 42 (1994) 649-663.

Vitae

Ming Liu was born on June 17th, 1985 in the city of Harbin, the capital of Heilongjiang Province, P.R. China.

Education

Master of Engineering, Materials Processing Engineering
Department of Materials Science and Engineering
Harbin Institute of Technology (HIT), Harbin, P.R. China
August, 2007 - July, 2009

- Admitted to HIT Graduate Institute without Normally Mandatory Entrance Examinations
- The Third Prize of the Fifth National Postgraduate Mathematic Model Competition, November, 2008
- The First Prize of 2008 Northeast Three Provinces Mathematic Model Competition, May, 2008
- The Second Prize of the Fourth National Postgraduate Mathematic Model Competition, December, 2007
- Gold Medal of 2007 Chorus Competition of Harbin Institute of Technology, September, 2007
- The Special Scholarship for the first postgraduate year, 2007
- The First Rank Scholarship for the second postgraduate year, 2008

Bachelor of Engineering, Materials Shaping and Controlling Engineering, Department of Materials Science and Engineering
Harbin Institute of Technology (HIT), Harbin, P.R. China
August, 2003 - July, 2007

- Outstanding Graduate, 2007
- The Second Prize of 2007 HIT Mathematic Model Competition, June, 2007
- National Scholarship, 2007
- People Scholarship: The First Prize once, The Second Prize thrice, The Third Prize twice
- Honor for Triple A Student of HIT, 2006
- Honor for Outstanding Student Leader of HIT, 2005
- Honor for All-around Students thrice

Publications in refereed, archival journals

1. **Ming Liu** and Fuqian Yang, Finite element simulation of the effect of electric boundary conditions on the spherical indentation of transversely isotropic piezoelectric films, *Smart Materials and Structures* 21 (2012) 105020 (10pp).
2. **Ming Liu** and Fuqian Yang, Finite element analysis of the indentation-induced delamination of bi-layer structures, *Journal of Computational and Theoretical Nanoscience* 9 (2012) 851-858.
3. **Ming Liu** and Fuqian Yang, Finite element analysis of the spherical indentation of transversely isotropic piezoelectric materials, *Modelling and Simulation in Materials Science and Engineering* 20 (2012) 045019 (15pp).
4. Guangfeng Zhao, **Ming Liu** and Fuqian Yang, The effect of an electric current on the nanoindentation behavior of tin, *Acta Materialia* 60 (2012) 3773-3782.
5. **Ming Liu** and Fuqian Yang, Finite element analysis of current-induced thermal stress in a conducting sphere, *Journal of Electronic Materials* 41 (2012) 352-361.

Conference Presentation

1. **Ming Liu** and Fuqian Yang, Finite element analysis of current-induced thermal stress in a tin ball, Materials Science & Technology 2011, Columbus Ohio.

Professional Affiliations

Student Member in Materials Advantage, 2011 – present

Skills

- Finite element analysis: Abaqus, Comsol
- Numerical analysis: Matlab, Maple, Mathematica, Excel, C++
- Data analysis: KaleidaGraph, Origin, Golden Software Surfer, GetData Graph Digitizer
- Heat treatment: cyclic heat treatment of γ-TiAl
- Microstructure observation: grinding, polishing, and etching
- Material analysis and characterization: X-ray, SEM, TEM, thermal analysis, indentation, tensile test, fracture test

Research Experience

Ph.D.: finite element analysis of the contact deformation of piezoelectric materials

including half-space and thin-film cases under various mechanical and electrical boundary conditions in 3D and axisymmetric models.
Supervisor: Dr. Fuqian Yang.

- Investigated influences of different mechanical boundary conditions (e.g., various indenter geometries, different interfacial behavior between the film and the substrate), and different electrical boundary conditions (e.g., electrically conducting or insulating indenter or substrate) on indentation responses of piezoelectric half–space and thin films of a finite thickness
- Established 3D finite element models to investigate effects of material orientation on indentation behavior of anisotropic materials
- Performed electro-thermal-mechanical simulation for a spherical ball normally pressed by two punches with electric current passing through
- Numerically analyzed the indentation-induced delamination in a bi-layer structure with parametric studies
- Investigated effects of electric current on indentation behavior of tin in a two-dimensional model

M.S.: Directional Solidification γ-TiAl Shot Peening Process (Master Thesis).
Supervisor: Dr. Bin Guo.

- Achieved composite structures with fine grains on the surface and coarse grains in the interior by cyclic heat treatment of γ-TiAl after surface treatment that is shot peening
- Analyzed shot peening process with finite element method, and performed stress and strain analysis with focus on surface plastic deformation, residual stress, and work hardening
- Observed microstructures of γ-TiAl by optical microscopy, and dislocation with twin grains by transmission electron microscopy (TEM)
- Investigated influences of combination of surface treatment and subsequent heat treatment on surface grain refinement

B.S.: Study on preparation, structure and mechanical behavior of SiC_p、Al_2O_{3sf}/AZ91D Magnesium-based composite material (Bachelor Thesis).
Supervisor: Dr. Shoujing Luo.

- Manufactured a short fiber (Al_2O_3) and particle (SiC) reinforced composite material with matrix of AZ91D magnesium by liquid infiltration technique
- Performed tensile and hardness tests for comparison of tensile stress, elastic modulus and hardness between manufactured composite material and original matrix material
- Conducted fracture analysis based on observation of the fracture morphology by scanning electron microscopy (SEM)